INSTITUTE OF PHYSICS PUBLISHING REPORTS ON PROGRESS IN PHYSICS

Rep. Prog. Phys. **69** (2006) 2259–2321 doi:10.1088/0034-4885/69/8/R01

Gamma-ray bursts

P Mészáros

Department of Astronomy & Astrophysics and Department of Physics, Pennsylvania State University, 525 Davey Laboratory, University Park, PA 16802, USA

Received 25 January 2006, in final form 2 May 2006
Published 5 July 2006
Online at stacks.iop.org/RoPP/69/2259

Abstract

Gamma-ray bursts are the most luminous explosions in the Universe, and their origin and mechanism are the focus of intense research and debate. More than three decades after their discovery, and after pioneering breakthroughs from space and ground experiments, their study is entering a new phase with the recently launched Swift satellite. The interplay between these observations and theoretical models of the prompt gamma-ray burst and its afterglow is reviewed.

(Some figures in this article are in colour only in the electronic version)

This article was invited by Professor C Jarlskog.

 © 2006 IOP Publishing Ltd Printed in the UK

Contents

	Page
1. Introduction	2262
2. Observational progress up to 2005	2264
2.1. Progenitor candidates	2266
2.2. Light curve breaks and jets	2267
2.3. Optical flashes	2267
2.4. Association with supernovae	2267
2.5. X-ray flashes	2268
2.6. Empirical correlations and distance estimators	2268
3. Recent results from Swift and follow-up observations	2269
4. Theoretical framework	2271
4.1. The relativistic fireball model	2271
4.2. Reference frames and timescales in relativistic flows	2273
4.3. Relativistic dynamics	2274
4.4. Optical depth and photosphere	2276
4.5. Thermal versus dissipative fireballs and shocks	2277
4.6. Duration, reverse shocks, thin and thick shells	2279
4.7. Spectrum of the prompt GRB emission	2281
4.8. Alternative prompt emission models	2283
5. Afterglow radiation models	2284
5.1. The standard model	2284
5.2. Prompt flashes and reverse shocks	2288
5.3. Dependence on external density, injection variability and anisotropy	2289
5.4. Equal arrival time surface and limb brightening effect	2290
5.5. Jets	2290
6. Current theoretical issues in afterglow models	2292
6.1. Early steep decay	2292
6.2. Shallow decay	2294
6.3. X-ray flares	2294
6.4. Late steep decay and jet breaks	2295
6.5. Prompt optical flashes and high redshift afterglows	2296
7. Short GRB in the Swift era	2297
7.1. Short GRB observations	2297
7.2. Short GRB prompt and afterglow emission	2298
7.3. Short burst hosts and progenitors	2299
7.4. Short burst redshifts and progenitor lifetimes	2300
8. Long GRB progenitors in light of Swift	2301
8.1. Long GRB hosts and progenitors	2301
8.2. Supernova connection	2301
8.3. Jet dynamics, cocoons and progenitors	2302
9. Very high energy photons and non-electromagnetic emission	2304
9.1. UHE photons from GRB	2305

9.2. Cosmic rays from GRB 2306
9.3. UHE neutrinos contemporary with gamma-rays 2307
9.4. Precursor neutrinos 2308
9.5. Gravitational waves 2309
Acknowledgments 2312
References 2312

1. Introduction

Gamma-ray bursts (GRB) are brief events occurring at an average rate of a few per day throughout the universe, which for a brief period of seconds completely flood with their radiation an otherwise almost dark gamma-ray sky. While they are on, they outshine every other source of gamma-rays in the sky, including the Sun. In fact, they are the most concentrated and brightest electromagnetic explosions in the Universe. Until recently, they were undetected at any wavelengths other than gamma-rays, which provided poor directional information and hence there were no direct clues about their site of origin.

This changed in early 1997 when the Beppo-SAX satellite succeeded in detecting them in x-rays, which after a delay of some hours yielded sufficiently accurate positions for large ground-based telescope follow-up observations. These proved that they were at cosmological distances, comparable to those of the most distant galaxies and quasars known in the Universe. Since even at these extreme distances (up to Gigaparsecs, or $\sim 10^{28}$ cm) they outshine galaxies and quasars by a very large factor, albeit briefly, their energy needs must be far greater. Their electromagnetic energy output during tens of seconds is comparable to that of the Sun over $\sim$few $\times 10^{10}$ years, the approximate age of the universe or to that of our entire Milky Way over a few years. The current interpretation of how this prodigious energy release is produced is that a correspondingly large amount of gravitational energy (roughly a solar rest mass) is released in a very short time (seconds or less) in a very small region (tens of kilometres or so) by a cataclysmic stellar event (the collapse of the core of a massive star or the subsequent mergers of two remnant compact cores). Most of the energy would escape in the first few seconds as thermal neutrinos, while another substantial fraction may be emitted as gravitational waves. This sudden energy liberation would result in a very high temperature fireball expanding at highly relativistic speeds, which undergoes internal dissipation leading to gamma-rays, and it would later develop into a blast wave as it decelerates against the external medium, producing an afterglow which gets progressively weaker. The resulting electromagnetic energy emitted appears to be of the order of a per cent or less of the total energy output, but even this photon output (in γ-rays) is comparable to the total kinetic energy output leading to optical photons by a supernova over weeks. The remarkable thing about this theoretical scenario is that it successfully predicts many of the observed properties of the bursts. This fireball shock scenario and the blast wave model of the ensuing afterglow have been extensively tested against observations and have become the leading paradigms for the current understanding of GRB.

Historically, GRBs were first discovered in 1967 by the Vela satellites, although they were not publicly announced until 1973 [233]. These spacecrafts, carrying omnidirectional gamma-ray detectors, were flown by the US Department of Defense to monitor nuclear explosions which might violate the Nuclear Test Ban Treaty. When these mysterious gamma-ray flashes were first detected, and it was determined that they did not come from the Earth's direction, the first suspicion (quickly abandoned) was that they might be the product of an advanced extraterrestrial civilization. Soon, however, it was realized that this was a new and extremely puzzling cosmic phenomenon [233]. For the next 25 years, only these brief gamma-ray flashes were observed, which could be only roughly localized and which vanished too soon, leaving no traces, or so it seemed. Gamma-rays are notoriously hard to focus, so no sharp gamma-ray 'images' exist to this day: they are just diffuse pin-pricks of gamma-ray light. This mysterious phenomenon led to a huge interest and to numerous conferences and publications on the subject, as well as to a proliferation of theories. In one famous review paper at the 1975 Texas Symposium on Relativistic Astrophysics, no fewer than 100 different possible theoretical models of GRB were listed [428], most of which could not be ruled out by the observations then available.

The first significant steps in understanding GRBs started with the 1991 launch of the Compton Gamma-Ray Observatory, whose results were summarized in [132]. The all-sky survey from the BATSE instrument showed that bursts were isotropically distributed, strongly suggesting a cosmological or possibly an extended galactic halo distribution, with essentially zero dipole and quadrupole components [124]. At cosmological distances the observed GRB fluxes imply enormous energies, which, from the fast time variability, must arise in a small volume in a very short time. This leads to the formation of an $e^{\pm} - \gamma$ fireball [173, 353, 457], which expands relativistically. The main difficulty with this scenario was that a smoothly expanding fireball would convert most of its energy into kinetic energy of accelerated baryons (rather than into photon energy) and would produce a quasi-thermal spectrum, while the typical timescales would not explain events much longer than milliseconds. This difficulty was addressed by the 'fireball shock scenario' [309, 416], based on the realization that shocks are likely to arise, e.g. when the fireball ejecta runs into the external medium, after the fireball has become optically thin, thus reconverting the expansion kinetic energy into non-thermal radiation. The complicated light curves can also be understood, e.g. in terms of internal shocks [236, 417, 450] in the outflow itself, before it runs into the external medium, caused by velocity variations in the outflow from the source.

The next major developments came after 1997, when the Italian–Dutch satellite Beppo-SAX succeeded in detecting fading x-ray images which, after a delay of 4–6 h of processing, led to positions [76], allowing follow-ups at optical and other wavelengths, e.g. [484]. This paved the way for the measurement of redshift distances, the identification of candidate host galaxies and the confirmation that they were indeed at cosmological distances [104, 249, 252, 304]. The detection of other GRB afterglows followed in rapid succession, sometimes extending to radio [137, 139] and over timescales of many months [483], and in a number of cases resulted in the identification of candidate host galaxies, e.g. [50, 351, 441]. The study of afterglows has provided strong confirmation for the generic fireball shock model of GRB. This model led to a correct prediction [313], in advance of the observations, of the quantitative nature of afterglows at wavelengths longer than γ-rays, which were in substantial agreement with the data [411, 475, 496, 509, 530].

A consolidation of the progress made by Beppo-SAX was made possible through the HETE-2 satellite [203], after the demise of CGRO and Beppo-SAX. It provided a continuing stream of comparable quality afterglow positions, after typical delays of hours, and contributed to the characterization of a new class of sources called x-ray flashes or XRF [202] resembling softer GRBs, which had been earlier identified with Beppo-SAX. It also localized GRB 030329, which resulted in the first unambiguous association with a supernova (SN2003dh) [204, 467].

The third wave of significant advances in the field is due to the Swift multi-wavelength afterglow satellite, launched in November 2004, which achieved the long-awaited goal of accurately localized afterglows starting a minute or so after the burst trigger, at gamma-ray, x-ray and optical wavelengths [162, 472]. This revealed the hitherto unexplored afterglow behaviour between minutes and hours, enabling a study of the transition from the prompt emission and the subsequent long term afterglow and revealing a rich range of x-ray early behaviour. It also achieved the long-awaited discovery of the afterglows of 'short' gamma-ray bursts (whose hard gamma-ray emission is briefer than 2 s). It furthermore broke through the symbolic redshift $z = 6$ barrier, beyond which very few objects of any kind have been measured.

On the theoretical side, a major issue raised by the large redshifts, e.g. [249, 253], is that the measured γ-ray fluences (the flux integrated over time) imply a total energy of the order of a solar rest mass, $M_{\odot}c^2 \sim 2 \times 10^{54}$ ergs, if it is emitted isotropically. In contrast, the total radiant (and the associated kinetic expansion energy) of supernovae (SN), which

is detected over timescales of weeks to months, is of the order of a thousandth of a solar rest mass, 10^{51} ergs. A GRB emission which is concentrated in a jet, rather than isotropically, significantly alleviates the energy requirements. There is now extensive observational evidence for such collimated emission from GRBs, provided by breaks in the optical/IR light curves of their afterglows [65, 145, 253]. The inferred total amount of radiant and kinetic energy involved in the explosion is in this case comparable to that of supernovae (except that in GRBs the energy is mostly emitted in a jet in γ-rays over tens of seconds, whereas in supernovae it is emitted isotropically in the optical over weeks). While the luminous (electromagnetic) energy output of a GRB is thus 'only' of the same order of magnitude as that of supernovae, the explosion is much more concentrated, both in time and in direction, so its specific brightness for an observer aligned with the jet is many orders of magnitude more intense and appears at much higher characteristic photon energies. Including the collimation correction, the GRB electromagnetic emission is energetically quite compatible with an origin in, say, either compact mergers of neutron star-neutron star (NS–NS) or black hole-neutron star (BH–NS) binaries [109, 341, 353, 320] or with a core collapse (hypernova or collapsar) model of a massive stellar progenitor [292, 356, 389, 528, 529], which would be related to but much rarer than core-collapse supernovae. While in both cases the outcome could be, at least temporarily, a massive fast-rotating ultra-high magnetic field neutron star (a magnetar), the high mass involved is expected to inevitably lead to the formation of a central black hole, fed through a brief accretion episode from the surrounding disrupted core stellar matter, which provides the energy source for the ejection of relativistic matter responsible for the radiation.

A stellar origin of GRB leads to two predictions which are similar to those for core-collapse supernovae, albeit in so far unobserved aspects. In both GRB (whether from compact mergers or from collapsar scenarios) and in core-collapse SN, the central material is compressed to nuclear densities and heated to virial temperatures characteristically in the multi-MeV range, leading to 5–30 MeV thermal neutrinos. And in both cases, the merging or collapsing core material acquires a time-varying quadrupole mass moment (which may be smaller in the SN not related to GRB), which leads to gravitational wave emission. In both GRB and supernovae, the total neutrino emission is of the order of a fraction of a solar rest mass, $\sim$several $\times\, 10^{53}$ ergs. The gravitational wave emission is of the same order for compact mergers, probably less than that for collapsars, and much less in normal core collapse SNe. Experiments currently planned or under construction will be able to probe these new channels.

2. Observational progress up to 2005

Before reviewing, in the next section, the latest observational advances achieved with Swift, the observational progress made up to that time is briefly surveyed. More extensive discussion and references on observations previous to 2004 are, for example, in [132, 385, 483, 541].

The γ-ray phenomenology of GRB was extensively studied and characterized by the BATSE instrument on the Compton GRO satellite [132]. The γ-ray spectra are non-thermal, typically fitted in the MeV range by broken power laws whose energy per decade peak is in the range 50–500 KeV [20], sometimes extending to GeV energies [213]. GRB appeared to leave no detectable traces at other wavelengths, except in some cases briefly in x-rays. The gamma-ray durations range from 10^{-3} s to about 10^{3} s, with a roughly bimodal distribution of long bursts of $t_{\rm b} \gtrsim 2$ s and short bursts of $t_{\rm b} \lesssim 2$ s [246], and substructure sometimes down to milliseconds. The gamma-ray light curves range from smooth, fast-rise and quasi-exponential decay (FREDs), through curves with several peaks, to highly variable curves with many peaks [132, 247] (figure 1). The pulse distribution is complex [377], and the time histories can provide clues for the geometry of the emitting regions [126, 127].

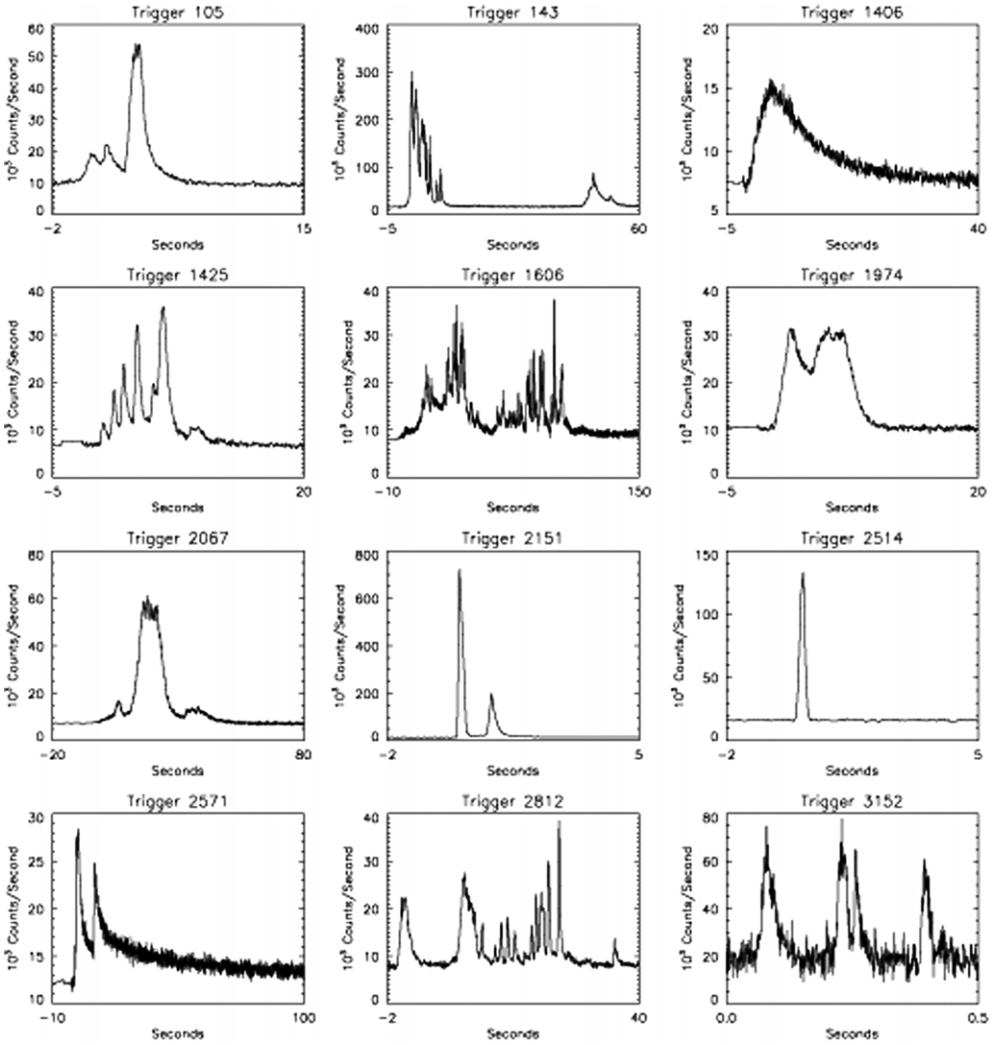

Figure 1. Diversity of gamma-ray light curves observed by BATSE [132].

GRB were conclusively shown to be at cosmological distances following Beppo-SAX localizations of their x-ray afterglows in 1997 [76], followed by optical host galaxy identification and redshift determinations [484]. The afterglows decay as a power law in time in a manner predicted by pre-existing models [313], softening in time from x-rays to optical to radio (e.g. figure 2). The energy needed to explain the total (mainly gamma-ray) energy fluence can be as large as $10^{54}(\Omega_\gamma/4\pi)$ ergs, where $\Delta\Omega_\gamma$ is the solid angle into which the gamma-rays are beamed. This is for the highest fluences seen in some of the most distant bursts, although for many bursts the energy budget problem is not as extreme. If the emission is assumed to be emitted isotropic (isotropic equivalent luminosity or energy) this energy ranges up to a solar rest mass in gamma-rays. This would strain a stellar origin interpretation, since from basic principles and experience it is known that, even for the most efficient radiation conversion schemes, a dominant fraction of the energy should escape in the form of thermal neutrinos and gravitational waves. The energy

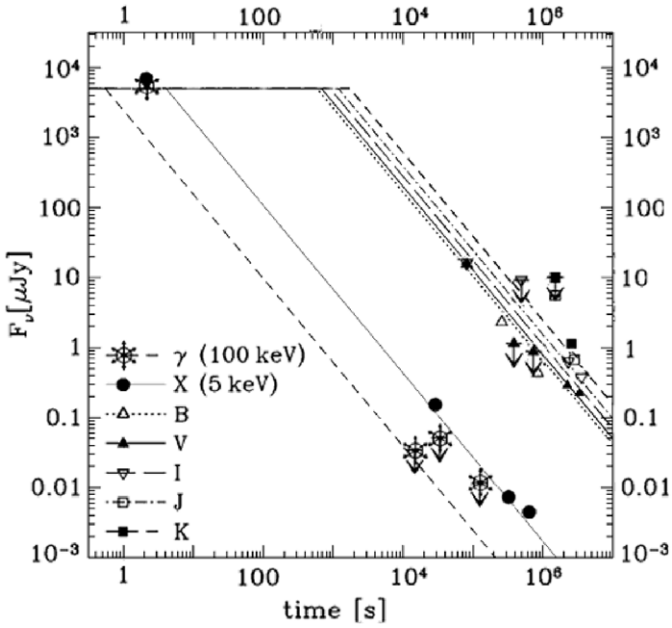

Figure 2. The afterglow light curves of GRB 970228 [530].

requirements are, however, much less severe in the case when the emission is collimated (section 2.2).

GRB afterglow light curves such as those shown in figure 2 have been followed up starting several hours after the trigger in x-rays by Beppo-SAX and subsequently by HETE-2, and in the optical/IR from ground-based telescopes (or in some cases with HST), and have been explained in terms of forward shock emission (for discussions of the pre-Swift data interpretation see, e.g. [307, 385, 483, 541]). Afterglows have been followed up at radio wavelengths in some cases over months, and the analysis and interpretation of the radio spectra and light curves [40, 141, 482] provides important clues for the calorimetry and the multi-waveband model fits discussed in section 5.1.

2.1. Progenitor candidates

There is now strong observational evidence [483] that GRB result from a small fraction ($\sim 10^{-6}$) of stars which undergo a catastrophic energy release event towards the end of their evolution. For the class of long GRB the candidates are massive stars whose core collapses [146, 356, 529] to a black hole, either directly or after a brief accretion episode, possibly in the course of merging with a companion. This scenario is referred to as the collapsar or hypernova scenario, which received strong support through the secure spectroscopic detection in some cases of an associated supernova event (e.g. [156, 204, 467]; also see sections 2.4 and 8.2). For short bursts the most widely speculated candidates are mergers of neutron star (NS) binaries or neutron star-black hole (BH) binaries [109, 173, 314, 353, 320, 267, 427, 268], which lose orbital angular momentum by gravitational wave radiation and undergo a merger. This second progenitor scenario has only now begun to be tested thanks to the Swift detection of short burst afterglows (see sections 3 and 7). Both of these progenitor types are expected to have as an end result the formation of a few solar mass black holes, surrounded by a temporary debris torus

whose accretion can provide a sudden release of gravitational energy, sufficient to power a burst. An important point is that the overall energetics from these various progenitors need not differ by more than about one order of magnitude [317]. The duration of the burst in this model is related to the fall-back time of matter to form an accretion torus around the BH [146,389] or the accretion time of the torus [342]. Other related scenarios include the formation of a fast-rotating ultra-high magnetic field neutron star from a stellar collapse [429,465,477,480,523].

2.2. Light curve breaks and jets

An important subsequent development was the observation, in many of the well-sampled afterglows, of a break or steepening of the x-ray and optical light curves [140,253], which can be interpreted as being due to the outflow being jet-like and the break occurs when the edge of the jet becomes visible, as the jet slows down [315,413,414,453]. The typical (long burst) inferred jet opening angles are $\theta_j \sim 5^\circ$–20°, which reduces the total energy requirements from 10^{53}–10^{54} erg to $\sim 10^{51}$ ergs [140,362], with a dispersion of a factor $\sim$ 10. The details are dependent on assumptions about the jet geometry and whether one addresses the gamma-ray energy [140] or the jet kinetic energy [362], with a somewhat larger dispersion in the latter. Variable optical linear polarization is expected at the time of a jet break [171,425,446], which can provide additional constraints, also on the jet structure. Light curve break determinations continued through the Beppo-SAX and HETE-2 afterglow observation periods, mainly in the optical. Break observations in the Swift era are discussed in section 5.5.

2.3. Optical flashes

Prompt optical flashes (starting within tens of seconds after the gamma-ray trigger) have been reported from ground-based small robotic telescopes in a few bursts [4, 10]. These arise much earlier, are initially brighter and decay more steeply than more ubiquitous long-term, slow decaying optical afterglows generally detected since 1997. They are also rare: between 1999 and 2004 only a handful of prompt optical flashes were detected with robotic ground telescopes [10]. Since the Swift launch, more than twenty prompt UVOT (or ground-based robotic) optical flashes have been seen, mostly at times starting several hundreds of seconds after the trigger. None have been as bright as the first one detected in GRB 990123, except for the most notable distant GRB 050904, whose optical brightness is comparable to that of GRB 990123 [57]. This is futher discussed further in section 6.5.

2.4. Association with supernovae

At least some long GRBs are associated with supernova explosions. The first reported example was the GRB980425/SN1998bw association [156, 250, 485]. SN 1998bw was a peculiar and energetic Type Ib/c supernova. Using it as a template, other possible associations have been claimed through identifying a so-called red supernova bump on the optical afterglow light curves of GRB 980326 [51], GRB 970228 [157,412], GRB 000911 [263], GRB 991208 [66], GRB 990712 [442], GRB 011121 [52], GRB 020405 [391] and GRB 031203 [72, 289]. The first unambiguous supernova signature (SN 2003dh) was detected in the $z = 0.168$ GRB 030329, firmly establishing the GRB-SN associations [204, 467]. Another GRB/SN event, GRB060218/SN2006aj, is discussed in section 3, and the supernova connection is further discussed in section 8.2.

2.5. X-ray flashes

X-ray flashes (XRFs) are a class of bursts whose light curves and spectra resemble typical GRB, except for the fact that their spectra are much softer, their spectral peaks $E_{\rm pk}$ being typically tens of keV or less [202, 232]. XRFs were first identified with the Beppo-SAX satellite and have been studied in greater detail and numbers with the HETE-2 satellite [26, 259]. Their fluxes and isotropic equivalent luminosities tend to be smaller than for GRB, which makes the afterglow searches more difficult. Nonetheless, several afterglows have been detected, and redshifts have been measured in some of them ([458], also sections 3 and 6).

2.6. Empirical correlations and distance estimators

The collimation-corrected total burst energy clustering around 10^{51} ergs, while making a stellar origin quite plausible, is unfortunately not sufficiently well defined to use as standard luminosity candles, whose apparent brightness would provide a distance determination. There are other possible distance measures, based on empirical correlations between burst observables. One of these is an apparent gamma-ray light curve variability correlation with the isotropic equivalent luminosity [125, 410]. Another is the time lag (between higher energy versus lower energy) gamma-rays and the isotropic luminosity [22, 346, 347]. Attempts at modelling the spectral lags have relied on observer-angle dependences of the Doppler boost [331, 443]. In these correlations the isotropic equivalent luminosity was used, in the absence of jet signatures, and they must be considered tentative for now. However, if confirmed, they could be invaluable for independently estimating GRB redshifts. A third one is a correlation between the spectral properties and the isotropic luminosity [7, 16, 59, 284]. These measures can be effectively calibrated only for light curves or spectra obtained with the same instrument and when redshifts are available. For the above methods the calibration set typically consists of a dozen bursts, which is insufficient to be considered reliable. The data set is now rapidly increasing with new Swift redshift determinations, but the Swift spectra are less well constrained at energies above 150 keV than with Beppo-SAX.

In recent years, attention has been drawn to a correlation between the photon spectral peak energy $E_{\rm pk}$ and the apparent isotropic energy $E_{\rm iso}$ or the isotropic luminosity $L_{\rm iso}$ [8] of the form $E_{\rm pk} \propto E_{\rm iso}^{1/2}$. For GRB, this correlation has been calibrated on a sample consisting of around ten bursts. While strongly suggestive, the sample is relatively small and the dispersion is large, so its usefulness as a distance measure is precarious. Another suggestive result is that for some x-ray flashes whose redshift has been measured the correlation continues to hold [259], even though the peak energy is $\sim$1.5 and the $E_{\rm iso}$ is $\sim$3 orders of magnitude lower than for GRB.

An interesting development of the $E_{\rm pk}$–$E_{\rm iso}$ correlation is the proposal of a relationship between the collimation-corrected total energy ($E_{\rm j}$ and the photon spectral peak). Modelling the jet break under the assumption that the jet expands into a uniform density external medium, this has the form $E_{\rm pk} \propto E_{\rm j}^{0.7}$ for a jet assumed to propagate in a homogeneous medium [86,165–167], and the relation appears to be tighter than the previously discussed $E_{\rm pk} \propto E_{\rm iso}^{1/2}$ (Amati) relation. This requires both an observed redshift and a light curve break for calibration. If it holds up for a larger calibration sample than the current ($\sim$18 bursts so far), it could be of promise as a cosmological tool [168, 260]. There are however problems to resolve before this becomes competitive with SNIa as a cosmological tool [144]. The main ones are the presence of outliers [335], the lack of a large low redshift sample for calibration (since using a high redshift sample requires assumptions about the cosmology which it is supposed to test), an evaluation of observational biases and selection effects and the dependence of the

results on model assumptions about the external medium and jet properties. The latter may be circumvented by relying only on observables, e.g. $E_{\rm peak}$ fluence (or peak flux) and the break time $t_{\rm br}$ [276, 340]. The dispersion, however, remains so far about 1.5–2 times larger than for SNIa.

3. Recent results from Swift and follow-up observations

Compared with previous missions, the swift results represent a significant advance on two main accounts. First, the sensitivity of the burst alert detector (BAT, in the range 20–150 keV) is somewhat higher than that of the corresponding instruments in CGRO-BATSE, BeppoSAX and HETE-2 [21]. Second, Swift can slew in less then 100 s in the direction determined by the BAT instrument, positioning its much higher angular resolution x-ray (XRT) and UV-Optical (UVOT) detectors on the burst [162].

As of December 2005, at an average rate of 2 bursts detected per week, over 100 bursts had been detected by BAT in about a year (compared with 300/year by BATSE; note the BAT field of view is 2 sr versus 4π in BATSE). Of these ∼100 bursts, 90% were detected and followed with the XRT within 350 s from the trigger and about half within 100 s [61], while ∼30% were detected also with the UVOT [423]. Of the total, over 23 resulted in redshift determinations. Included in this total sum are nine short GRB, of which five had detected x-ray afterglows, three had optical and one had a radio afterglow, with five host galaxy detections and redshift determinations. These were the first ever short GRB afterglows detected and followed.

The new observations show increase in the total redshift determinations to over 50 since 1997, when BeppoSAX enabled the first one. The median redshift of the Swift bursts is $z \gtrsim 2$, which is a factor ∼2 higher than the median of the BeppoSAX and HETE-2 redshifts [42]. This is a statistically significant difference between the Beppo-SAX and Swift redshift samples [17, 221]. This may in part be ascribed to the better sensitivity of the BAT detector but mostly to the prompt and accurate positions from XRT and UVOT, making ground-based detection at a stage when the afterglow is much brighter possible by a larger number of robotic and other telescopes. As of January 2006 the highest Swift-enabled redshift is that of GRB 050904, obtained with the Subaru telescope, $z = 6.29$ [229], and the second highest is GRB 050814 at $z = 5.3$, whereas the previous Beppo-SAX era record was $z = 4.5$. The relative paucity of UVOT detections versus XRT detections may be ascribed in part to this higher median redshift and in part to the higher dust extinction at the implied shorter rest-frame wavelenghts for a given observed frequency [423], although additional effects may be at work too.

In some of the bursts, both of the 'long' ($t_\gamma \gtrsim 2$ s) and 'short' ($t_\gamma \leqslant 2$ s) categories as defined by BATSE, the Swift BAT results, show faint soft gamma-ray extensions or tails, which extend the duration by a substantial factor beyond what BATSE would have detected [162]. A rich trove of information on the burst and afterglow physics has come from detailed XRT light curves, starting on average 100 s after the trigger, together with the corresponding BAT light curves and spectra. This suggests a canonical x-ray afterglow picture [348] which includes one or more of the following: (1) an initial steep decay $F_X \propto t^{-\alpha_1}$ with a temporal index $3 \lesssim \alpha_1 \lesssim 5$ and an energy spectrum $F_\nu \propto \nu^{-\beta_1}$ with energy spectral index $1 \lesssim \beta_1 \lesssim 2$ (or photon number index $2 \lesssim \alpha + 1 \lesssim 3$), extending up to a time $300\,{\rm s} \lesssim t_1 \lesssim 500\,{\rm s}$, (2) a flatter decay portion $F_X \propto t^{-\alpha_2}$ with temporal index $0.2 \lesssim \alpha_2 \lesssim 0.8$ and energy index $0.7 \lesssim \beta_2 \lesssim 1.2$, at times $10^3\,{\rm s} \lesssim t_2 \lesssim 10^4\,{\rm s}$, (3) a 'normal' decay $F_X \propto t^{-\alpha_3}$ with $1.1 \lesssim \alpha_3 \lesssim 1.7$ and $0.7 \lesssim \beta_3 \lesssim 1.2$ (generally unchanged the previous stage), up to a time $t_3 \sim 10^5$ s or in some cases longer, (4) in some cases, a steeper decay $F_X \propto t^{-\alpha_4}$ with $2 \lesssim \alpha_4 \lesssim 3$, after $t_4 \sim 10^5$ s and (5) in about half the afterglows, one or more x-ray flares

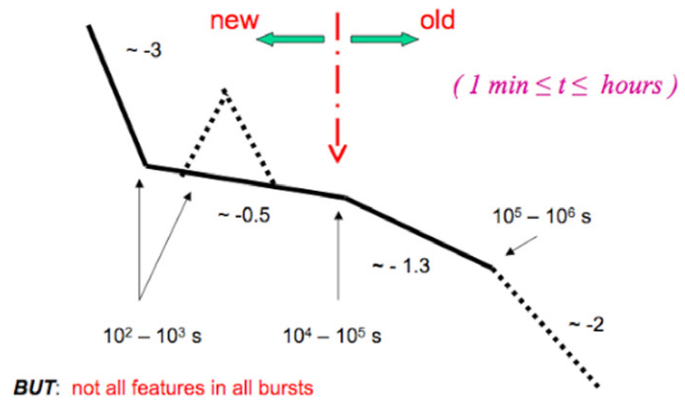

Figure 3. Schematic features seen in early x-ray afterglows detected with the Swift XRT instrument (e.g. [348, 544] (see text).

are observed, sometimes starting as early as 100 s after trigger and sometimes as late as 10^5 s. The energy in these flares ranges from a per cent up to a value comparable to the prompt emission (in GRB 050502b). The rise and decay times of these flares is unusually steep, depending on the reference time t_0, behaving as $(t - t_0)^{\pm\alpha_{\rm fl}}$ with $3 \lesssim \alpha_{\rm fl} \lesssim 6$, and energy indices which can be also steeper (e.g. $\beta_{\rm fl} \lesssim 1.5$) than during the smooth decay portions. The flux level after the flare usually decays to the value extrapolated from the value before the flare rise (see figure 3). The above characteristics are derived mainly from long bursts, but, interestingly, at least one of the short bursts shows similar features. However, the evidence for late time activity is more sketchy in short bursts, so the analogy must be considered with caution.

An exciting result from Swift was the detection of the long burst GRB 050904, which broke through the astrophysically and psychologically significant redshift barrier of $z \sim 6$, which is thought to mark the approximate end of the 'dark ages', when re-ionization of the intergalactic medium by the first generation of light sources approaches completion. This burst was very bright, both in its prompt γ-ray emission ($E_{\gamma,\rm iso} \sim 10^{54}$ erg) and in its x-ray afterglow. Prompt ground-based optical/IR upper limits and a J-band detection suggested a photometric redshift $z > 6$ [195], and spectroscopic confirmation soon followed with the 8.2 m Subaru telescope, giving $z = 6.29$ [229]. There are several striking features to this burst. One is the enormous x-ray brightness, exceeding for a full day the x-ray brightness of the most distant x-ray quasar known to date, SDSS J0130 + 0524, by up to a factor 10^5 in the first minute [505]. The implications as a tool for probing the intergalactic medium are thought provoking. Another feature is the extremely variable x-ray light curve, showing many large amplitude flares extending up to at least a day. A third exciting feature is the report of a brief, very bright, IR flash [57], comparable in brightness to the famous $m_V \sim 9$ optical flash in GRB 990123.

A third major advance from Swift was the discovery and localization of short GRB afterglows. As of December 2005 nine short bursts had been localized by Swift, while in the same period HETE-2 discovered two, and one was identified with the IPN network. In five of the short bursts, GRB 050509b, 050709, 050724 and 051221a an x-ray afterglow was measured and followed up, with GRB 050709, 050724 and 051221a also showing an optical afterglow and 050724 a radio afterglow, while 040924 had an optical afterglow but not an x-ray one [136]. These are the first afterglows detected for short bursts. Also, for the first time, host galaxies were identified for these short bursts, which in a number of cases are early

type (ellipticals) and in other cases are irregular galaxies (e.g. [392]. The redshifts of four of them are in the range $z \sim 0.15$–0.5, while another one was determined to be $z = 0.8$ (and less securely, it has been argued that this latter may instead be $z \simeq 1.8$ [41]). The median z is $\lesssim 1/3$–$1/2$ that of the long bursts. There is no evidence for significant star formation in these host environments (except for GRB 050709 [135, 392]), which is compatible with what one expects for an old population, such as neutron star mergers or neutron star-black hole mergers, the most often discussed progenitor candidates (although it would also be compatible with other progenitors involving old compact stars). While the evidence for a neutron star or black merger is suggestive, the evidence is not unequivocal. For example, the observations suggest a typical time delay of at least several Gyr between the start formation epoch and the explosion of short GRBs [338, 547]. There are a number of unresolved issues related to this (see section 7). The first short burst afterglow followed up by Swift, GRB 050509b, was a rather brief (∼30 ms), moderate luminosity ($L_{\rm iso} \sim 10^{50}\,{\rm erg\,s^{-1}}$) but low fluence ($E_{\rm iso} \sim 2 \times 10^{48}\,{\rm erg}$) burst with a simple power-law x-ray afterglow which could only be followed for several hundreds of seconds [161]. The third one, GRB 050724, was brighter, $E_{\rm iso} \sim 3 \times 10^{50}\,{\rm erg}$, and could be followed in x-rays with Swift for at least 10^5 s [28] and with Chandra up to 2×10^6 s [163]. The remarkable thing about this burst's x-ray afterglow is that it shows some similarities to the typical x-ray light curves described above for long GRB—except for the lack of a slow-decay phase and for the short prompt emission which places it in the category of short bursts, as well as the elliptical host galaxy candidate. It also has bumps in the x-ray light curve at 100 s and at 3×10^4 s, which resemble some of the long burst x-ray flares and whose origin is unclear. The first bump or flare has the same fluence as the prompt emission, while the later one has $\sim 10\%$ of that. The interpretation of these pose interesting challenges, as discussed below and in section 7,

A fourth exciting result from Swift was the detection of a long burst, GRB 060218, which was also seen with the XRT and UVOT instruments [64] and which is associated with SN 2006aj [71, 326, 327, 466]. The redshift is $z = 0.033$, and the contributions to the optical light curve as well as the spectrum are similar to those of the Ic type SN1998bw. The result is so exciting is that it is the first time that a GRB/SN has been observed minutes after the γ-ray trigger at x-ray and UV/optical wavelengths. This is discussed further in section 8.2.

4. Theoretical framework

4.1. The relativistic fireball model

As discussed in the introduction, the ultimate energy source of GRB is convincingly associated with a catastrophic energy release in stellar mass objects. For long bursts, this is almost certainly associated with the late stages of the evolution of a massive star, namely the collapse of its core [356, 529], which at least in some cases is associated with a detectable supernova. For short bursts, it has long been assumed [109, 353] that they were associated with compact binary mergers (NS–NS or NS–BH), a view which is gaining observational support [37, 135], although the issue cannot be considered settled yet. In both cases, the central compact object is likely to be a black hole of several solar masses (although it might, temporarily, be a fast rotating high-mass neutron star, which must eventually collapse to a black hole). In any case, the gravitational energy liberated in the collapse or merger involves the order of a few solar masses, which is converted into free energy on timescales of milliseconds inside a volume of the order of tens of kilometres cubed. This prompt energy is then augmented by a comparable amount of energy release in a similar or slightly larger volume over a longer timescale of seconds to hundreds of seconds, by the continued infall or accretion of gas onto the central

object, either from the central parts of the massive progenitor star or from the debris of the disrupted compact stars which was temporarily held up by its rotation.

The principal result of the sudden release of this large gravitational energy (of the order of a solar rest mass) in this compact volume is the conversion of a fraction of that energy into neutrinos, initially in thermal equilibrium, and gravitational waves (which are not in thermal equilibrium), while a significantly smaller fraction (10^{-2}–10^{-3}) goes into a high temperature fireball ($kT \gtrsim$ MeV) consisting of $e^{\pm}$, γ-rays and baryons. The fireball is transparent to the gravitational waves and, beyond several interaction lengths, also to the neutrinos. This leads to the prompt emission (on timescales of a few seconds) of roughly comparable energy amounts (several $\times 10^{53}$ ergs) of thermal $\nu_e\bar{\nu}_e$ with typical energies 10–30 MeV and of gravitational waves mainly near 10^2–10^3 Hz. These two, by far most dominant, energy forms are so far undetected and are further discussed in section 9. A smaller fraction of the liberated energy, or of order 10^{50}–10^{52} ergs, remains trapped in an $e^{\pm}$, γ-ray and baryon fireball, which can also contain a comparable (or in some scenarios a larger) amount of magnetic field energy. This amount of energy is observed, mainly as non-thermal gamma-rays. While being smaller than the predicted thermal neutrino and gravitational wave fluence, this is nonetheless a formidable electromagnetic energy output, much more intense than any other explosive event in the universe. While the total energy is comparable to the electromagnetic and kinetic energy of supernovae, the difference is that in supernovae the energy is doled out over months, mainly at optical wavelengths, while in GRB most of the electromagnetic energy is spilled out in a matter of seconds and mainly at γ-ray wavelengths.

The leading model for the electromagnetic radiation observed from GRBs is based on the relativistic fireball created in the core collapse or merger. The photon luminosity inferred from the energies and timescales discussed and from the observations is many orders of magnitude larger than the Eddington luminosity $L_{\rm E} = 4\pi GMm_{\rm p}c/\sigma_{\rm T} = 1.25 \times 10^{38}\,(M/M_{\odot})\,{\rm erg\,s^{-1}}$, above which radiation pressure exceeds self-gravity, so the fireball expands. The first (thermal) fireball models were assumed to reach relativistic expansion velocities [67, 173, 353, 457]. However, the ultimate expansion velocity depends on the baryon load of the fireball [354]. If the fireball energy involved all the baryons in the core (solar masses) the expansion would be sub-relativistic. However, near the black hole the density is reduced due to accretion and centrifugal forces, it is likely that baryons are much depleted in the region where the fireball forms, with a tendency to form high entropy (high energy/mass ratio) radiation bubbles. Dynamically dominant magnetic fields would also tend to involve fewer baryons. A phenomenological argument shows that the expansion must, indeed, be highly relativistic. This is based on the fact that most of the GRB spectral energy is observed above 0.5 MeV, so that the mean free path for the $\gamma\gamma \rightarrow e^{\pm}$ process in an isotropic plasma (an assumption appropriate for a sub-relativistically expanding fireball) would be very short. This leads to a contradiction, since many bursts show spectra extending above 1 GeV, so the flow must be able to avoid degrading these via photon–photon interactions to energies below the threshold $m_{\rm e}c^2 = 0.511$ MeV [199]. To avoid this, it seems inescapable that the flow must be expanding with a very high Lorentz factor Γ, since then the relative angle at which the photons collide is less than Γ^{-1} and the threshold for the pair production is then diminished. This condition is

$$\Gamma \gtrsim 10^2[(\epsilon_\gamma/10\,{\rm GeV})(\epsilon_{\rm t}/{\rm MeV})]^{1/2}\,, \tag{1}$$

in order for photons ϵ_γ to escape annihilation against target photons of energy $\epsilon_{\rm t} \sim 1$ Mev [199, 306]. That is, a relativistically expanding fireball is expected, with bulk Lorentz factors $\Gamma = 100\Gamma_2 \gtrsim 1$.

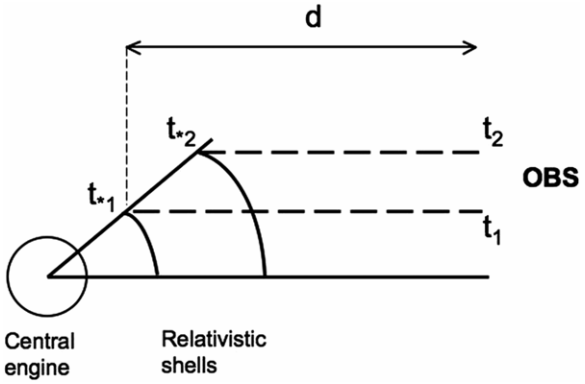

Figure 4. Illustration of the emission from spherical relativistic shells in the source frame and the relativistic time delay leading to the relation between source frame time and observer time.

4.2. Reference frames and timescales in relativistic flows

The emitting gas moves relativistically with velocity $\beta = v/c = (1 - 1/\Gamma^2)^{1/2}$ relative to a laboratory frame K_* which may be taken to be the origin of the explosion or stellar frame (which, aside from a cosmological Doppler or redshift factor, is the same as the Earth frame K of an observer). The lengths, times, thermodynamic and radiation quantities of the gas are best evaluated in the gas rest frame (the comoving frame) K' and are obtained in the stellar/lab frame through Lorentz transformations. Thus, a proper length $\mathrm{d}r'$ in the comoving frame has a stellar/lab frame length $\mathrm{d}r_* = \mathrm{d}r'/\Gamma$ (if both ends r_{*1} and r_{*2} of the length $\mathrm{d}r_* = r_{*1} - r_{*2}$ in K_* are measured at the same time so $\mathrm{d}t_* = 0$ in K_*, i.e. the usual Fitz-Gerald contraction). Similarly, a proper time interval $\mathrm{d}t'$ in the comoving frame has a duration $\mathrm{d}t_* = \mathrm{d}t'\Gamma$ in K_* (provided the times t_{*1} and t_{*2} of $\mathrm{d}t_* = t_{*1} - t_{*2}$ in K_* are measured at same positions x_{*1} and x_{*2} in K_* so $\mathrm{d}x_* = 0$, the usual time-dilation effect). The time needed in the stellar/lab frame K_* for the gas to move from x_{*1} to x_{*2} is the usual $\mathrm{d}t_* = t_{*1} - t_{*2} = \mathrm{d}r_*/\beta c \approx \mathrm{d}r_*/c$.

When it comes to observations at Earth of radiation emitted from the relativistically moving gas, even though the Earth frame K is essentially the same as the K_* stellar/lab frame, in addition to the above Lorentz transformations one has to also consider the classical light travel time delay (Doppler) effect, e.g. [435]. In the observer frame K one can use the same spatial coordinates $r \equiv r_*$ and $\mathrm{d}r \equiv \mathrm{d}r_*$ as in K_*, but the actual time of arrival of signals as measured by an observer, which is for brevity denoted just t, differs from t_* by the above Doppler effect, $t \neq t_*$. Since this observed time t is the actual observable, it is customary to describe GRB problems in terms of t (remembering it is $\neq t_*$) and r (which is $=r_*$). Considering a gas which expands radially in a direction at an angle $\cos\theta = \mu$ with respect to the observer line of sight, if a first photon is emitted when the gas is at the radius $r_{*1} = r_1$ (which is at a distance d from the observer) at t_{*1}, this photon arrives at the observer at an observer time $t_1 = t_{*1} - \mathrm{d}/c$. A second photon emitted from a radius $r_{*2} = r_2$ at time t_{*2} will arrive at an observer time $t_2 = t_{*2} + (\mathrm{d}/c - \beta\mu\mathrm{d}t_*)$, where $\mathrm{d}t_* = t_{*1} - t_{*2}$. This is illustrated in the source frame in figure 4. For an observer close to the line of sight the observed time difference between the arrival of the two photons is

$$\mathrm{d}t = \mathrm{d}t_*(1 - \beta\mu) \simeq \mathrm{d}t_*(1/2\Gamma^2 + \theta^2/2) \simeq \mathrm{d}r/(2\Gamma^2 c)(1 + \Gamma^2\theta^2) \simeq \mathrm{d}r/(2\Gamma^2 c)\ , \qquad (2)$$

where we assumed $\Gamma \gg 1$ for an approaching gas ($\mu = \cos\theta > 0$) along a radial direction well inside the light cone $\theta \ll \Gamma^{-1}$.

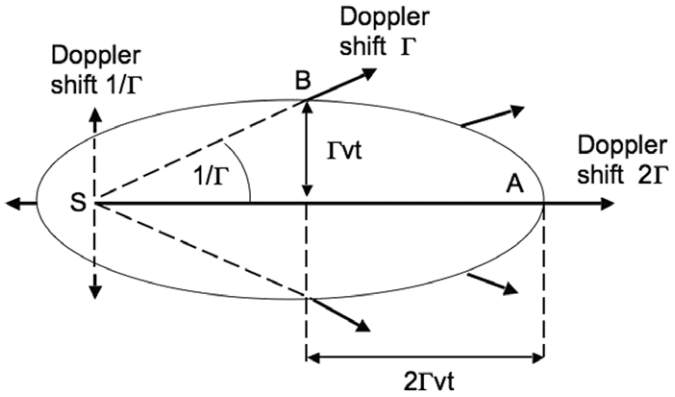

Figure 5. For a distant observer (located to the right) viewing a shell which expands spherically from S with $\Gamma = \sqrt{1-(v/c)^2} \gg 1$, the locus of the points from which radiation reaches it at a later time t appears as a spheroid (equal arrival time surface). Most of the radiation arrives from the forward (right) hemisphere, which is strongly Doppler-boosted inside the light cone $1/\Gamma$ (after [415]). The apparent transverse radius of the ellipsoid is $r_\perp \simeq \Gamma ct$ and its semi-major axis is $r_\parallel \simeq 2\Gamma ct$, where t is observer time.

While both $\mathrm{d}t$ and $\mathrm{d}t_*$ are in the same reference frame, $K = K_*$, the difference is that $\mathrm{d}t_*$ is the time difference between the emission of the two photons and $\mathrm{d}t$ is the time difference between the reception of the two photons. The general relation between the observer frame and comoving frame quantities is given through the Doppler factor $\mathcal{D}$,

$$\mathcal{D} = [\Gamma(1-\beta\mu)]^{-1}, \tag{3}$$

where $\mathcal{D} \sim 2\Gamma$ for an approaching gas with $\Gamma \gg 1$, $\mu \to 1$ and $\theta < \Gamma^{-1}$ (blueshift) or $\mathcal{D} \sim 1/2\Gamma$ for a receding gas with $\mu \to -1$ (redshift). Thus, the relation between the comoving frame $\mathrm{d}t'$ and the observer frame time $\mathrm{d}t$ is

$$\mathrm{d}t = \mathcal{D}^{-1}\mathrm{d}t' = \Gamma(1-\beta\mu)\mathrm{d}t' \simeq \mathrm{d}t'/2\Gamma, \tag{4}$$

where an approaching gas is assumed with $\theta < \Gamma^{-1}$ (while $\mathrm{d}t_* = \mathrm{d}t'\Gamma$). This is illustrated in terms of observer-frame quantities in figure 5. Note that in all the above transformations we have neglected cosmological effects, which would result in multiplying any reception or observer-frame times by an additional factor $(1+z)$ for signals emanating from a source at redshift z.

The relation between the source frame and observer frame frequency, solid angle, specific intensity, temperature, volume, specific emissivity, specific absorption coefficient and radial width are obtained in terms of the Doppler factor using relativistic invariants [435], $\nu = \mathcal{D}\nu'$, $\mathrm{d}\Omega = \mathcal{D}^{-2}\mathrm{d}\Omega'$, $I_\nu(\nu) = \mathcal{D}^3 I'_{\nu'}(\nu')$, $T(\nu) = \mathcal{D}T'(\nu')$, $\mathrm{d}V = \mathcal{D}\mathrm{d}V'$, $j_\nu(\nu) = \mathcal{D}^2 j'_{\nu'}(\nu')$, $\mu_\nu(\nu) = \mathcal{D}^{-1}\mu'_{\nu'}(\nu')$, $\delta r = \mathcal{D}\delta r'$. Here $\mu_\nu = n\sigma_\nu$ (in cm^{-1}, where n is density and σ_ν is absorption cross section), so both $\nu\mu_\nu$ and the optical depth $\mathrm{d}\tau = \mu_\nu.\mathrm{d}(\delta r)$ are invariants.

4.3. Relativistic dynamics

From general considerations, an outflow arising from an initial energy E_0 imparted to a mass $M_0 \ll E_0/c^2$ within a radius r_0 will lead to an expansion, which due to the initial high optical depth can be considered adiabatic. The pressure will be dominated by radiation, so the adiabatic index is $\gamma_a = 4/3$, and the comoving temperature T' (or comoving random Lorentz factor per particle γ') evolves with comoving volume V'as $T \propto V'^{1-\gamma_a}$. With a comoving volume

$V' \propto r^3$ (equation (8)) this means $T' \propto \gamma' \propto r^{-1}$. By conservation of energy, this decrease in internal energy per particle is balanced by an increase in its expansion-related energy, i.e. the bulk kinetic energy per particle or bulk Lorentz factor Γ, so that $\gamma\Gamma =$ constant, hence $\Gamma \propto r$. This expansion occurs at the expense of the comoving frame internal energy. Since the bulk Lorentz factor per particle cannot increase beyond the initial value of random internal energy per particle, $\gamma_0 = \eta = E_0/M_0c^2$, the bulk Lorentz factor only grows until it reaches $\Gamma_{\rm max} \sim \eta = E_0/M_0c^2$, which is achieved at a radius $r/r_0 \sim \eta$. Beyond this radius the flow begins to coast, with $\Gamma \sim \eta \sim$ constant [173, 353, 355, 457],

$$\Gamma(r) \sim \begin{cases} (r/r_0), & \text{for } r/r_0 \lesssim \eta,\ r \lesssim r_{\rm s} \\ \eta, & \text{for } r/r_0 \gtrsim \eta,\ r \gtrsim r_{\rm s}, \end{cases} \tag{5}$$

which defines a saturation radius $r_{\rm s} \sim r_0\eta$ beyond which the Lorentz factor is saturated. Another way to understand the initial acceleration [308] is that initially, at $r = r_0$, the gas particles have a bulk Lorentz factor $\Gamma \sim 1$ and have an isotropical distribution of velocities with random Lorentz factors $\gamma \sim \eta = E_0/M_0c^2$. As the particles expand outwards, when they have reached a radius r their velocity vectors will be confined inside an angle $(r/r_0)^{-1}$ of the radial direction. A transformation to a comoving frame moving radially with a bulk Lorentz factor $\Gamma(r) \sim r/r_0$ is needed for the velocity distribution to be isotropic in the comoving frame, as it should be.

As particles initially contained inside r_0 move outwards with velocity vectors which are increasingly radial, they form a radially expanding shell whose lab-frame width is initially $\delta r \sim \delta r_0 \sim r_0$. The radial velocity spread is $(c - v)/c = 1 - \beta \sim \Gamma^{-2}$, which causes a gradual spread of the lab-frame radial width $\delta r/r \sim \delta v/v \sim \Gamma^{-2}$. For typical values of $r_0 \sim 10^6$–10^7 cm and $\eta \lesssim 10^3$ this is negligible until well beyond the saturation radius, and a noticeable departure from the approximately constant width $\delta r \sim r_0$ starts to become appreciable only for radii in excess of a spreading radius r_δ where $\delta r \sim r\delta v/c \sim r_\delta\eta^{-2} \gtrsim r_0$. The laboratory frame width is therefore [308]

$$\delta r \sim \max[\delta r_0, r/\Gamma^2] \sim \begin{cases} \delta r_0 & \text{for } r \lesssim r_\delta, \\ r/\Gamma^2 & \text{for } r \gtrsim r_\delta, \end{cases} \tag{6}$$

where the spreading radius $r_\delta \sim \delta r_0\eta^2$ is a factor η larger than the saturation radius $r_{\rm s} \sim \delta r_0\eta$.

The comoving radial width $\delta r'$ is related to the lab width δr through $\delta r' = \delta r\mathcal{D} \sim \delta r\Gamma$. Hence

$$\delta r' \sim \begin{cases} \delta r_0\Gamma \sim r & \text{for } r \lesssim r_{\rm s}, \\ \delta r_0\eta & \text{for } r_{\rm s} \lesssim r \lesssim r_\delta, \\ r/\eta & \text{for } r \gtrsim r_\delta. \end{cases} \tag{7}$$

Since the dimensions transverse to the motion are invariant, the comoving volume is $V' \propto r^2\delta r'$, which behaves as [308]

$$V' \sim 4\pi r^2\delta r' \sim \begin{cases} 4\pi r^3 & \text{for } r \lesssim r_{\rm s}, \\ 4\pi\eta\delta r_0\, r^2 & \text{for } r_{\rm s} \lesssim r \lesssim r_\delta, \\ 4\pi\eta^{-1}r^3 & \text{for } r \gtrsim r_\delta, \end{cases} \tag{8}$$

and the comoving particle density $n' \propto V'^{-1}$. For an adiabatic expansion (valid for the high initial optical depths) and a relativistic gas polytropic index 4/3 (valid as long as the pressure is dominated by radiation), one has

$$\frac{E'}{E_0} = \frac{T'}{T_0} = \left(\frac{V_0}{V'}\right)^{1/3} \simeq \begin{cases} (\delta r_0/r) & \text{for } r < r_{\rm s}, \\ (\delta r_0/r_{\rm s})(r_{\rm s}/r)^{2/3} = \eta^{-1/3}(\delta r_0/r)^{2/3} & \text{for } r_{\rm s} < r < r_\delta, \\ (\delta r_0/r_{\rm s})(r_{\rm s}/r_\delta)^{2/3}(r_\delta/r) = \eta^{1/3}(\delta r_0/r) & \text{for } r > r_\delta, \end{cases} \tag{9}$$

where E', T', ρ', V' are comoving internal energy, temperature, density and volume.

The above equations refer to the release of an energy E_0 and mass M_0 corresponding to $\eta = E_0/M_0c^2$, originating inside a region of dimensions $\delta r_0 \sim r_0$. This mass and energy leaves the original region in a lab-frame (or observer frame) light-crossing time $\delta t_0 \sim \delta r_0/c$. For typical core collapse or compact merger stellar scenarios, the energy release volume is of the order of several Schwarzschild radii of the ensuing black hole (BH), few times $2GM_{\rm BH}/c^2$ with $M_{\rm BH} \gtrsim 2\,M_\odot$, say $r_0 \sim 10^7 m_1$ cm, where $m_1 = M_{\rm BH}/10M_\odot$, with a light-crossing timescale $t_0 \sim r_0/c \sim 3\times 10^{-4} m_1$ s. This is of the order of the dynamical (Kepler) timescale near the last stable circular orbit in a temporary accretion disc feeding the newly formed black hole (or near the light cylinder of an initial fast-rotating magnetar or neutron star, before it collapses to a black hole).

4.4. Optical depth and photosphere

As shown by [173, 353, 457] a relativistically expanding fireball initially has $e^\pm$ pairs in equilibrium which dominate the scattering optical depth, but the pairs fall out of equilibrium and recombine below a comoving temperature $T' \sim 17$ keV, and thereafter only a residual freeze-out density of pairs remains, which for η not too large (in practice $\eta \lesssim 10^5$, i.e. baryon loads not too small) is much less than the density of 'baryonic' electrons associated with the protons, $n_{\rm e} = n_{\rm p}$. For a typical burst conditions the initial black-body temperature T'_0 at $r_0 \sim 10^7$ cm is a few MeV, and pair recombination occurs at radii below the saturation radius. The scattering optical depth of a minishell (and of the whole outflow) is still large at this radius, due to the baryonic electrons. For a minishell of initial width δr_0 the optical depth varies as [308]

$$\tau_{\rm T} = (M_0\sigma_{\rm T}/4\pi r^2 m_{\rm p}) = \tau_0(\delta r_0/r)^2, \tag{10}$$

where $\tau_0 = (E_0\sigma_{\rm T}/4\pi r_0^2 m_{\rm p}c^2\eta)$, for $\delta r_0 \lesssim r/\Gamma^2$ or $r \lesssim r_\delta$. Assuming a burst with total energy $E_0 = 10^{52}E_{52}$ and total duration $t_{\rm grb}$ divided into minishells of duration $\delta t_0 = 3\times 10^{-4}$ s, each of energy $10^{47.5}E_{47.5}$ erg, these becomes optically thin at

$$r_{\rm t} = \tau_0^{1/2} r_0 = 3\times 10^{11} m_1^{-1}(E_{47.5}/\eta_2)^{1/2}\,{\rm cm}, \tag{11}$$

where henceforth the notation Q_x (where x is a number) indicates for the quantity Q in units of 10^x times its c.g.s. units.

For bursts of some substantial duration, e.g. an outflow duration $t_{\rm grb} = 10$ s as above, at any instant different parts of the flow have different densities and are above or below the saturation radius, so a continuous outflow picture is more appropriate [354]. In this 'wind' regime one defines the dimensionless entropy as $\eta = L/\dot M c^2$, and instead of integral conservation laws one uses the relativistic fluid differential equations. The Lorentz factor again grows linearly and saturates at the same radius $r_{\rm s} = r_0\eta$ (equation (5)), where $r_0 = \delta r_0$ is the minimum variability radius, and the adiabatic behaviour of equation (9) is the same for the temperature, and so on. The particle density follows from the mass conservation equation

$$n'_{\rm p} = (\dot M/4\pi r^2 m_{\rm p}c\Gamma) = (L/4\pi r^2 m_{\rm p}c^3\eta\Gamma) \tag{12}$$

and the optical depth is $\tau_{\rm T}(r) = \int_r^\infty n'_{\rm e}\sigma_{\rm T}[(1-\beta)/(1+\beta)]^{1/2}{\rm d}r' \sim n'_{\rm e}\sigma_{\rm T}(r/2\Gamma)$ which yields for the global photosphere [354]

$$r_{\rm ph} \simeq (\dot M\sigma_{\rm T}/8\pi m_{\rm p}c\Gamma^2) = (L\sigma_{\rm T}/8\pi m_{\rm p}c^3\eta\Gamma^2) \simeq 6\times 10^{11} L_{51}\eta_2^{-3}\,{\rm cm}. \tag{13}$$

The comoving temperature of the flow behaves as $T' \propto r^{-1}, r^{-2/3}$ and the observer-frame temperature $T = T'\Gamma$ is $T \sim T_0$, $T \sim T_0(r/r_{\rm s})^{-2/3}$ for $r < r_{\rm s}$, $r > r_{\rm s}$ (equation (9)).

The radiation escaping from a radius r (e.g. the photospheric radius $r_{\rm ph}$) which is released at the same stellar frame time t_* would arrive at the observer only from within the angles inside

the light cone, $\theta < \Gamma^{-1}$. The observer-frame time delay between light coming from central line of sight and the edges of the light cone (the so-called angular time [173]) is

$$t_{\rm ang} \simeq t \simeq (r/c)(1-\beta) \sim r/2c\Gamma^2 \,. \tag{14}$$

This is because the 'edge' of the light cone corresponds to an angle of $1/\Gamma$ from the line of sight and therefore $ct_{\rm ang} \sim r(1-\cos\theta) \sim r(1-\beta) \sim r/2\Gamma^2$, since at $\theta = 1/\Gamma$, $\cos\theta \approx \beta$. This time is the same as the observer-frame time of equation (2). Note that if the outflow duration $t_{\rm grb}$ is shorter than $t_{\rm ang}$ of equation (14), the latter is the observed duration of the photospheric radiation (due to the angular time delay). Otherwise, for $t_{\rm grb} > t_{\rm ang}$, the photospheric radiation is expected for a lab-frame duration $t_{\rm grb}$.

4.5. Thermal versus dissipative fireballs and shocks

The spectrum of the photosphere would be expected to be a black body [173,353,457], modified at most by comptonization at the higher energy part of the spectrum. However, the observed γ-ray spectrum observed is generally a broken power law, i.e. highly non-thermal. In addition, a greater problem is that the expansion would lead to a conversion of internal energy into kinetic energy of expansion, so even after the fireball becomes optically thin, it would be highly inefficient, most of the energy being in the kinetic energy of the associated protons, rather than in photons. For a photosphere occurring at $r < r_{\rm s}$, which requires high values of η, the radiative luminosity in the observer frame is undiminished, since $E'_{\rm rad} \propto r^{-1}$ but $\Gamma \propto r$ so $E_{\rm rad} \sim$ constant or $Lph \propto r^2\Gamma^2 T'^4 \propto$ constant, since $T' \propto r^{-1}$. However, for the more moderate values of η the photosphere occurs above the saturation radius, and whereas the kinetic energy of the baryons is constant, $E_{\rm kin} \sim E_0 \sim$ constant, the radiation energy drops as $E_{\rm rad} \propto (r/r_{\rm s})^{-2/3}$ or $L_{\rm ph} \sim L_0(r_{\rm ph}/r_{\rm s})^{-2/3}$ [309,318].

A natural way to achieve a non-thermal spectrum in an energetically efficient manner is by having the kinetic energy of the flow re-converted into random energy via shocks, after the flow has become optically thin [226,308,309,416,417,449]. Such shocks will be collisionless, i.e. mediated by chaotic electric and magnetic fields rather than by binary particle interactions, as known from interplanetary experiments and as inferred in supernova remnants and in active galactic nuclei (AGN) jets . As in these well-studied sources, these shocks can be expected to accelerate particles via the Fermi process to ultra-relativistic energies [2,45,112,273,462], and the relativistic electron component can produce non-thermal radiation via the synchrotron and inverse Compton (IC) processes. A shock is essentially unavoidable as the fireball runs into the external medium, producing a blast wave. The external medium may be the interstellar medium (ISM) or the pre-ejected stellar wind from the progenitor before the collapse. For an outflow of total energy E_0 and terminal coasting bulk Lorentz factor $\Gamma_0 = \eta$ expanding in an external medium of average particle density $n_{\rm ext}$, the external shock becomes important at a deceleration radius $r_{\rm dec}$ for which $E_0 = (4\pi/3)r_{\rm dec}^3 n_0 m_{\rm p} c^2 \eta^2$ [416],

$$r_{\rm dec} \sim (3E_0/4\pi n_{\rm ext} m_{\rm p} c^2 \eta^2)^{1/3} \sim 5.5 \times 10^{16} E_{53}^{1/3} n_0^{-1/3} \eta_{2.5}^{-2/3} \,{\rm cm}. \tag{15}$$

At this radius the initial bulk Lorentz factor decreases to approximately half its original value, as the fireball ejecta is decelerated by the swept-up external matter. The amount of external matter swept at this time is a fraction η^{-1} of the ejecta mass M_0, $M_{\rm ext} \sim M_0/\eta$ (in contrast to the sub-relativistic supernova expansion, where deceleration occurs when this fraction is $\sim$1).

The light travel time difference between a photon originating from $r = 0$ and a photon originating from matter which has moved to a radius r with a Lorentz factor Γ is $\Delta t \sim (r/c)(1-\beta) \sim r/2c\Gamma^2$ [415], and the emission from a photosphere or from a shock emission region at radius r moving at constant Γ is also received from within the causal light

cone angle Γ^{-1} on an observer angular timescale $t \sim r/2c\Gamma^2$ [416, 309]. For an explosion which is impulsive (i.e. essentially instantaneous as far as observed relativistic time delays) a similarity solution of the relativistic flow equations shows that the bulk of the ejected matter at a radius r is mainly concentrated inside a region of width $\Delta r \sim r/2\Gamma^2$ [46, 47]. The time delay between radiations along the central line of sight originating from the back and front edges of this shell also arrives with a similar time delay $t \sim r/2c\Gamma$. Thus, the timescale over which the deceleration is observed to occur is generally

$$t_{\rm dec} \sim r_{\rm dec}/(2c\Gamma^2) \sim 10(E_{53}/n_0)^{1/3}\eta_{2.5}^{-8/3}\,{\rm s}, \tag{16}$$

and this is the observer timescale over which the external shock radiation is detected. This is provided that the explosion can be taken to be impulsive, which can be defined as the outflow having a source-frame (and observer frame) duration $t_{\rm grb} < t_{\rm dec}$ (however, see section 4.6). Variability on timescales shorter than $t_{\rm dec}$ may occur on the cooling timescale or on the dynamic timescale for inhomogeneities in the external medium but is not ideal for reproducing highly variable profiles [450], and may therefore be applicable to the class of long, smooth bursts. However, it can reproduce bursts with several peaks [365], and if the external medium is extremely lumpy ($\Delta n_0/n_0 \gtrsim 10^5 - 10^6$) it might also describe spiky GRB light curves [103].

Before the ejecta runs into the external medium, 'internal shocks' can also occur as faster portions of the ejecta overtake slower ones, leading to pp collisions and π^0 decay gamma-rays [399] and to fast time-varying MeV gamma-rays [417]. The latter can be interpreted as the main burst itself. If the outflow is described by an energy outflow rate L_0 and a mass loss rate $\dot{M}_0 = {\rm d}M_0/{\rm d}t$ starting at a lower radius $r_{\rm l}$, maintained over a time T, then the dimensionless entropy is $\eta = L_0/\dot{M}_0c^2$, and the behaviour is similar to that in the impulsive case, $\Gamma \propto r$ and comoving temperature $T' \propto r^{-1}$, followed by saturation $\Gamma_{\rm max} \sim \eta$ at the radius $r/r_0 \sim \eta$ [354]. For variations of the output energy or mass loss of order unity, the ejected shells of different Lorentz factors $\Delta\eta \sim \eta$ are initially separated by ct_v (where $t_v \leqslant T$ are the typical variations in the energy at $r_{\rm l}$), and they catch up with each other at an internal shock (or dissipation) radius

$$r_{\rm dis} \sim ct_v\eta^2 \sim 3 \times 10^{14}t_{v,0}\eta_2^2\,{\rm cm}. \tag{17}$$

The time variability should reflect the variability of the central engine, which might be expected, e.g. from accretion disc intermittency and flares [341]. The radiation from the disc or flares, however, cannot be observed directly, since it occurs well below the scattering photosphere of the outflow and the variability of the photons below it is washed out [417]. The comoving Thomson optical depth is $\tau_{\rm T} = n'_{\rm e}\sigma_{\rm T}r/\Gamma$, and above the saturation radius $r_{\rm s} = r_0\eta$ where $\Gamma = \eta$, the radius of the photosphere ($\tau_{\rm T} = 1$), is given from equation (13) as

$$r_{\rm ph} \sim \begin{cases} 1.2 \times 10^{12}L_{51}\eta_2^{-3}\,{\rm cm} & \text{for } r > r_{\rm s}, \\ 1.2 \times 10^{10}L_{51}^{1/3}r_{07}^{2/3}\eta_2^{-1/3}\,{\rm cm} & \text{for } r < r_{\rm s}. \end{cases} \tag{18}$$

The location of this baryonic photosphere defines a critical dimensionless entropy $\eta_* = 562(L_{51}/r_{07})^{1/4}$ above (below) which the photosphere occurs below (above) the saturation radius [318]. For internal shocks to occur above the wind photosphere and above the saturation radius (so that most of the energy does not come out in the photospheric quasi-thermal radiation component) one needs to have $3.3 \times 10^1(L_{51}r_{0,7}/t_{v,0})^{1/5} \lesssim \eta \lesssim 5.62 \times 10^2(L_{51}/r_{0,7})^{1/4}$. The radial variation of the bulk Lorentz factor and the location of the various characteristic radii discussed above is shown in figure 6.

Such internal shock models have the advantage [417] that they allow an arbitrarily complicated light curve, the shortest variation timescale $t_{v,\rm min} \gtrsim 10^{-4}\,{\rm s}$ being limited only by the dynamic timescale at $r_0 \sim ct_{v,\rm min} \sim 10^7 r_{0,7}\,{\rm cm}$, where the energy input may be

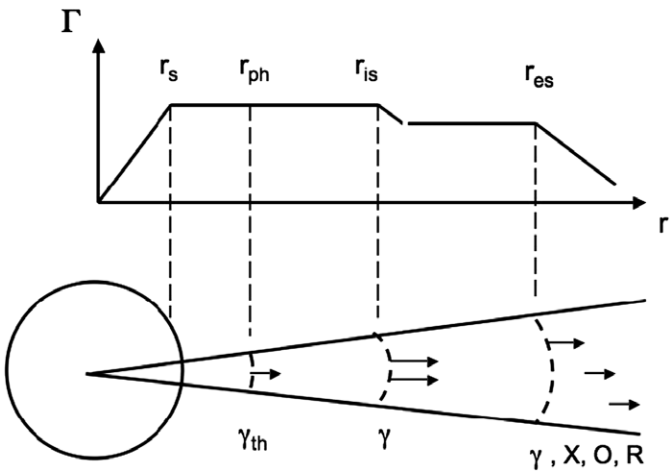

Figure 6. Jet Lorentz factor schematic behaviour and examples of nominal locations of the saturation radius r_s, photospheric radius r_{ph}, internal shock (or magnetic dissipation) radius r_{is} and external shock r_{es}. The photosphere produces thermal γ-rays, the internal shock/dissipation region produces the non-thermal γ-rays and the external shock region produces the afterglow.

expected to vary chaotically, while the total duration is $t_{grb} \gg t_v$. Such internal shocks have been shown to explicitly reproduce (and be required by) some of the more complicated light curves [236, 368, 450] (however, see [103, 438]). The gamma-ray emission of GRB from internal shocks radiating via a synchrotron and/or inverse Compton mechanism reproduces the general features of the gamma-ray observations [143, 463]. However, questions remain concerning the low energy (20–50 keV) spectral slopes for some bursts (see section spectrum). Alternatively, the main γ-ray bursts could be (at least in part) due to the early part of the external shock [103, 416]. Issues arise with the radiation efficiency, which for internal shocks is estimated to be moderate in the bolometric sense (5–20%), higher values ($\lesssim$30–50%) being obtained if the shells have widely differing Lorentz factors [33, 242, 463], although in this case one might expect large variations in the spectral peak energy E_{peak} between spikes in the same burst, which is problematic. The total efficiency is substantially affected by inverse Compton losses [372, 382]. The efficiency for emitting in the BATSE range is typically low $\sim$1–5%, both when the MeV break is due to synchrotron [192, 254, 463] and when it is due to inverse Compton [364].

4.6. Duration, reverse shocks, thin and thick shells

In the following discussion we assume for simplicity a uniform external medium. For a baryonic outflow such as we have been considering, the timescale $t_0 \sim r_0/c \sim$ ms represents a minimum variability timescale in the energy-mass outflow. (Note, however, if the gamma-ray emission arises from local dissipation events, such as magnetic reconnection in a Poynting flux dominated outflow, the minimum timescales could be smaller than the timescales of the central source variations). On the other hand, the total duration t_{grb} of the outflow, during which the central engine keeps pouring out energy and matter, is likely to be substantially longer than the minimum variability timescale t_0. The temporary accretion disc must have an outer radius larger than r_0 and a total accretion (or jet energization) time $t_{grb} \gg t_0$ (or the magnetar has a spin-down time $t_{grb} \gg t_0$). Thus, in general the total lab-frame width of the outflow ejecta will be $\Delta \approx ct_{grb}$, which may be viewed as composed of many radial minishells whose individual

widths are $\delta r \sim c\delta t_0$ or larger. While the saturation radius is still $r_s \sim \delta r_0 \eta$ where $\delta r_0 \sim r_0$ corresponds to the shortest variability time (and the smallest minishells coast after this r_s), the entirety of the ejecta reaches coasting speed only after its leading edge has moved to a larger radius $r_{s'} \sim \Delta\eta$ and the ejecta as a whole starts to spread at a larger radius $r_\Delta \sim \Delta\eta^2$ (even though individual minishells of initial width $\delta r \ll \Delta$ start to spread individually at the smaller radius $r_\delta \sim \delta r\ \eta^2$).

In general, whatever the duration $t_{\rm grb}$ of the outflow, one expects the external shock to have both a forward shock (blast wave) component propagating into the external medium and a reverse shock propagating back into the ejecta [309]. The forward shock and the reverse shock start forming as soon as the outflow starts, although their radiation is initially weak and increases progressively. The forward shock is highly relativistic, $\Gamma \sim \eta$ from the very beginning, but the reverse shock starts initially as a sub-relativistic sound wave (relative to the contact discontinuity or shock frame) and becomes progressively stronger as more external matter is swept up. (This describes the more frequently encountered 'thin shell' case, see below; the reverse shock becomes stronger with time only if the external density profile is shallower than r^{-2}, whereas the reverse shock strength is constant for an r^{-2} profile at $r < r_\delta$).

For an impulsive regime outflow, where $t_{\rm grb} < t_{\rm dec}$, i.e. when the outflow time is shorter than the time-delayed duration of the external shock when it starts to decelerate, equation (16), this deceleration time can be taken to be the observable duration of the peak emission from the external shock. Thereafter the expansion goes into a self-similar expansion with $\Gamma \propto r^{-3/2}$ [46, 416]. In this case, $t_{\rm dec}$ is also the observer time at which the reverse shock finishes crossing the ejecta, and at that time the reverse shock Lorentz factor $\bar\Gamma_r$ relative to the contact discontinuity frame has become marginally relativistic, $\bar\Gamma_r \sim 1$, while relative to the external gas or the observer, the reverse shocked gas is still moving at almost the same speed as the forward shocked gas [309, 312]. One consequence of this is that while the forward-shocked protons have highly relativistic random Lorentz factors, those in the reverse shock are marginally relativistic, and consequently the electrons in the forward shock are much more relativistic than those in the reverse shock, leading to a much softer (optical) spectrum of the reverse shocks [310, 313] (see section 5.2)

However, when the outflow time $t_{\rm grb}$ exceeds the deceleration time $t_{\rm dec}$ of equation (16), the eternal shock dynamics is different [449]. In this case there is an initial intermediate regime $\Gamma \propto r^{-1/2}$ (obtained for a constant external density ρ and a constant kinetic luminosity L at $t < t_{\rm grb}$ from the momentum balance in the shock frame $L/(r^2\Gamma^2 \propto \rho\Gamma^2)$, and the transition to a self-similar expansion $\Gamma \propto r^{-3/2}$ [46, 444] occurs at the observer time $t_{\rm grb}$, instead of at $t_{\rm dec}$. Thus, the observer time for the transition to the self-similar expansion is

$$T = \max[t_{\rm grb}, 10(E_{53}/n_0)^{1/3}\eta_{2.5}^{-8/3}\ {\rm s}]. \tag{19}$$

This defines a critical initial Lorentz factor $\Gamma_0 \sim \eta$ of the burst by setting $T = t_{\rm grb}$ in place of $t_{\rm dec}$ in equation (16),

$$\Gamma_{\rm BM} \simeq 300(E_{53}/n_0)^{1/8}(T/10\ {\rm s})^{-3/8}. \tag{20}$$

For $\eta < \Gamma_{\rm BM}$, $T = t_{\rm dec}$ we have the usual 'thin shell' case, where deceleration and transition to the self-similar expansion occur at the usual $r_{\rm dec}$, $t_{\rm dec}$, and at this time the reverse shock crosses the ejecta and is marginally relativistic. For $\eta > \Gamma_{\rm BM}$ we have a 'thick shell' case, where deceleration and transition to the self-similar regime occur at $T = t_{\rm grb}$ and $r_{\rm BM} \sim 2cT\Gamma_{\rm BM}^2$, when $\Gamma \sim \Gamma_{\rm BM}$. In this $\eta > \Gamma_{\rm BM}$ case, the reverse shock becomes relativistic, and by the time it has crossed the ejecta (at time $T = t_{\rm grb}$) the reverse shock Lorentz factor in the contact discontinuity frame is $\bar\Gamma_r \sim \eta/2\Gamma_{\rm BM} \gg 1$ and the forward shock Lorentz factor at this time is $\Gamma \simeq \Gamma_{\rm BM}$.

4.7. Spectrum of the prompt GRB emission

The prompt emission observed from classical GRB (as opposed to XRFs or SGRs) has most of its energy concentrated in the gamma-ray energy range 0.1–2 MeV. The generic phenomenological photon spectrum is a broken power law [20] with a break energy in the above range, and power law extensions down into the x-ray, and up into the 100 MeV to GeV ranges (although a substantial fraction of GRB have soft x-ray excesses above this, and some are classified as x-ray rich (XRR) [390], a classification intermediate between XRF and GRB). For classical GRB the photon energy flux $F_{\rm E} \propto E^{-\beta}$ has typical indices below and above the typical observed break energy $E_{\rm br} \sim 0.2\,{\rm MeV}$ of $\beta_1 \sim 0$ and $\beta_2 \sim 1$ [20]. (Pre-BATSE analyses sometimes approximated this as a bremsstrahlung-like spectrum with an exponential cutoff at $E_{\rm br}$, but BATSE showed that generally the extension above the break is a power law.) A synchrotron interpretation is thus natural, as has been argued, e.g. since the earliest external shock synchrotron models were formulated.

The simplest synchrotron shock model starts from the conditions behind the relativistic forward shock or blast wave [416, 309]. The post-shock particle and internal energy density follow from the relativistic strong shock transition relations [46],

$$\begin{aligned} n_2 &= (4\Gamma_{21}+3)n_1 \simeq 4\Gamma_{21}n_1, \\ e_2 &= (\Gamma_{21}-1)n_2 m_{\rm p}c^2 \simeq \Gamma_{21}n_2 m_{\rm p}c^2 \simeq 4\Gamma_{21}^2 n_1 m_{\rm p}c^2, \end{aligned} \tag{21}$$

where it is assumed that the upstream material is cold. Here n is number density and e is internal energy density, both measured in the comoving frames of the fluids, $\Gamma_{21} \simeq \Gamma$ is the relative Lorentz factor between the fluids 2 (shocked, downstream) and 1 (unshocked, upstream) and the Lorentz factor of the shock front itself is $\Gamma_{\rm sh} = \sqrt{2}\Gamma_{21}$, valid for $\Gamma_{21} \gg 1$. For internal shocks the jump conditions can be taken to be approximately the same but replacing Γ_{21} by a lower relative Lorentz factor $\Gamma_r \sim 1$.

The typical proton crossing a strong shock front with a relative bulk Lorentz factor Γ_{21} acquires (in the comoving frame) an internal energy characterized by a random (comoving) Lorentz factor $\gamma_{p,m} \sim \Gamma$ [309]. The comoving magnetic field behind the shock can build up due to turbulent dynamo effects behind the shocks [309, 310] (as also inferred in supernova remnant shocks). More recently, the Weibel instability has been studied in this context [300, 303, 345, 464]. While the efficiency of this process remains under debate, one can parametrize the resulting magnetic field as having an energy density behind the shock which is a fraction ϵ_B of the equipartition value relative to the proton random energy density behind the shock, $B' \sim [32\pi\epsilon_B n_{\rm ex}(\gamma'_{\rm p}-1)m_{\rm p}c^2]^{1/2}\Gamma$, where the post-shock proton comoving internal energy is $(\gamma'_{\rm p}-1)m_{\rm p}c^2 \sim 1$ (or $\sim \Gamma$) for internal (external) shocks [309, 417]. Scattering of electrons (and protons) by magnetic irregularities upstream and downstream can lead to a Fermi acceleration process resulting in a relativistic power law distribution of energies $N(\gamma) \propto \gamma^{-p}$ with $p \geqslant 2$. It should be stressed that although the essential features of this process are thought to be largely correct, and it is widely used for explaining supernova remnant, AGN and other non-thermal source radiation spectra, the details are only sketchily understood, [2, 45, 112, 230, 273, 462]. (Possible difficulties with the simplest version of Fermi acceleration and alternative possibilities were discussed, e.g. in [24, 200, 422].) The starting minimum (comoving) Lorentz factor of the thermal electrons injected into the acceleration process, $\gamma_{e,m}$, would in principle be the same as for the protons, Γ, (they experience the same velocity difference); hence, both before and after acceleration they would have $\sim (m_{\rm e}/m_{\rm p})$ less energy than the protons. However, the shocks being collisionless, i.e. mediated by chaotic electric and magnetic fields, they can redistribute the proton energy between the electrons and protons, up to some fraction ϵ_e of the thermal energy equipartition value with the protons, so

$\gamma_{e,m} \sim \epsilon_e(m_{\rm p}/m_{\rm e})\Gamma$ [310,312]. If only a fraction $\zeta_e \leqslant 1$ of all the shocked thermal electrons is able to achieve this ϵ_e initial equipartition value to be injected into the acceleration process then the initial minimum electron random comoving Lorentz factor is $\gamma_m \sim (\epsilon_e/\zeta_e)(m_{\rm p}/m_{\rm e})\Gamma$ [63], where henceforth we ignore the subscript e in $\gamma_{e,m}$. More accurately, integrating over the power law distribution, one has $\gamma_m = g(p)(m_{\rm p}/m_{\rm e})(\epsilon_e/\zeta_e)\Gamma \sim 310[g(p)/(1/6)](\epsilon_e/\zeta_e)\Gamma$, where $g(p) = (p-2)/(p-1)$. The observer frame synchrotron spectral peak is

$$\nu_{\rm m} \sim \Gamma(3/8\pi)(eB'/m_{\rm e}c)\gamma_m^2 \sim 2\times 10^6 B'\gamma_m^2\Gamma\ {\rm Hz}, \tag{22}$$

and the optically thin synchrotron spectrum is [435]

$$F_\nu \propto \begin{cases} \nu^{1/3} & \text{for } \nu < \nu_{\rm m}, \\ \nu^{-(p-1)/2} & \text{for } \nu > \nu_{\rm m}, \end{cases} \tag{23}$$

assuming that the radiative losses are small (adiabatic regime). For the forward external shock at deceleration, typical values are, e.g. $B' \sim 30(\epsilon_{B,-1}n_{\rm ex})^{1/2}\eta_{2.5}$ G, $\Gamma \sim \eta \sim 3\times 10^2$, $\gamma_m \sim 10^5(\epsilon_{e,-1}/\zeta_{e,-1})\eta_{2.5}$ and $\nu_{\rm m} \sim 2\times 10^{20}(\epsilon_{e,-1}/\zeta_{e,-1})^2(\epsilon_{B,-1}n_{\rm ex})^{1/2}\eta_{2.5}^4$ Hz, while for internal shocks typical values are, e.g. $B' \sim 3\times 10^5(\epsilon_{B,-1}n'_{13})^{1/2}\Gamma_{\rm rel,0}$ G, $\Gamma_{\rm rel} \sim 1\Gamma_{\rm rel,0}$, $\gamma_m \sim 3\times 10^3(\epsilon_{e,-1}/\zeta_{e,-1})\Gamma_{\rm rel,0}$ and $\nu_{\rm m} \sim 2\times 10^{19}(\epsilon_{e,-1}/{\rm zeta}_{e,-1})^2(\epsilon_{B,-1}n'13)^{1/2}\Gamma_{r,0}^3\eta_{2.5}$ Hz. For the prompt emission, the high energy slope $\beta_2 = (p-1)/2$ is close to the mean high energy slope of the band fit, while the low energy slope can easily approach $\beta_1 \sim 0$ considering observations from, for example, a range of B' values (a similar explanation as for the flattening of the low energy synchrotron slope in flat spectrum radio-quasars). The basic synchrotron spectrum is modified at low energies by synchrotron self-absorption [184, 226, 310, 312], where it makes the spectrum steeper ($F_\nu \sim \nu^2$ for an absorption frequency $\nu_{\rm a} < \nu_{\rm m}$). It is also modified at high energies, due to inverse Compton effects [99, 310, 312, 417, 447, 539], extending into the GeV range.

The synchrotron interpretation of the GRB radiation is the most straightforward. However, a number of effects can modify the simple synchrotron spectrum. One is that the cooling could be rapid, i.e. when the comoving synchrotron cooling time $t'_{\rm sy} = 9m_{\rm e}^3c^5/4e^4B'^2\gamma_e) \sim 7\times 10^8/B'^2\gamma_e$ s is less than the comoving dynamic time $t'_{\rm dyn} \sim r/2c\Gamma$, the electrons cool down to $\gamma_c = 6\pi m_{\rm e}c/\sigma_{\rm T}B'^2t'_{\rm dyn}$ and the spectrum above $\nu_{\rm c} \sim \Gamma(3/8\pi)(eB'/m_{\rm e}c)\gamma_c^2$ is $F_\nu \propto \nu^{-1/2}$ [170, 451]. Also, the distribution of observed low energy spectral indices β_1 (where $F_\nu \propto \nu^{\beta_1}$ below the spectral peak) has a mean value $\beta_1 \sim 0$, but for a fraction of bursts this slope reaches positive values $\beta_1 > 1/3$ which are incompatible with a simple synchrotron interpretation [390]. Possible explanations include synchrotron self-absorption in the x-ray [185] or in the optical range up-scattered to x-rays [364], low-pitch angle scattering or jitter radiation [301, 302], observational selection biases [282] and/or time-dependent acceleration and radiation [283], where low-pitch angle diffusion can also explain high energy indices steeper than predicted by isotropic scattering. Other models invoke a photospheric component and pair formation [318], see below.

There has been extensive work indicating that the apparent clustering of the break energy of prompt GRB spectra in the 50–500 keV range may be real [390], rather than due to observational selection effects [383]. That is, if this is a real clustering, what is the physical reason for it. (Note, however, that if x-ray flashes or XRF, discussed below, form a continuum with GRB then this clustering stretches out to much lower energies; at the moment, however, the number of XRFs with known break energies is small.) Since the synchrotron peak frequency seen by the observer is directly dependent on the bulk Lorentz factor, which may be random, the question arises whether this peak is indeed due to synchrotron or due to some other effect. An alternative is to attribute a preferred peak to a black body at the comoving pair recombination temperature in the fireball photosphere [110]. In this case a steep low energy spectral slope

is due to the Rayleigh–Jeans part of the photosphere, and the high energy power law spectra and GeV emission require a separate explanation. For such photospheres to occur at the pair recombination temperature in the accelerating regime requires an extremely low baryon load. For very large baryon loads, a related explanation has been invoked [477], considering scattering of photospheric photons off MHD turbulence in the coasting portion of the outflow, which up-scatters the adiabatically cooled photons up to the observed break energy.

Pair formation can become important [372, 382, 417] in internal shocks or dissipation regions occurring at small radii, since a high comoving luminosity implies a large comoving compactness parameter

$$\ell' = n'_\gamma \sigma_{\rm T} r_{\rm dis}/\Gamma \sim (\alpha L \sigma_{\rm T}/4\pi r_{\rm dis} m_{\rm e} c^3 \Gamma^3) \gtrsim 1 \,, \tag{24}$$

where $\alpha \lesssim 1$ is the luminosity fraction above the electron rest mass. Pair-breakdown may cause a continuous rather then an abrupt heating and lead to a self-regulating moderate optical thickness pair plasma at sub-relativistic temperature, suggesting a comptonized spectrum [170]. Copious pair formation in internal shocks may in fact extend the photosphere beyond the baryonic photosphere value (18). A generic model has been proposed [318, 322, 436, 404, 437, 402] which includes the emission of a thermal photosphere as well as a non-thermal component from internal shocks outside of it, subject to pair breakdown, which can produce both steep low energy spectra, preferred breaks and a power law at high energies. A moderate to high scattering depth can lead to a Compton equilibrium which gives spectral peaks in the right energy range [397, 398]. An important aspect is that Compton equilibrium of internal shock electrons or pairs with photospheric photons lead to a high radiative efficiency, as well as to spectra with a break at the right preferred energy and steep low energy slopes [374, 375, 419]. It also leads to possible physical explanations for the Amati [8] or Ghirlanda [166] relations between spectral peak energy and burst fluence [419, 476].

4.8. Alternative prompt emission models

There are several alternative models for the prompt GRB emission, which so far have not found wide use for explaining the observations. The most plausible of these, despite the technical difficulties which impair its applicability, considers the main γ-ray burst emission to arise from magnetic reconnection or dissipation processes, if the ejecta is highly magnetized or Poynting-dominated [106, 287, 312, 314, 476, 477, 480]. The central engine could also in principle be a temporary highly magnetized neutron star or magnetar [523]. These scenarios would lead to alternative dissipation radii, instead of equation (17), where reconnection leads to particle acceleration, and a high radiative efficiency is in principle conceivable due to the very high magnetic field. An external shock would follow after this, whose radius in the 'thin shell' limit would be again given by equation (15), with a standard forward blast wave but no (or a weaker) reverse shock [312, 313], due to the very high Alfvén speed in the ejecta. For a long duration outflow, however, the dynamics and the deceleration radius would be similar to the 'thick shell' case of section 4.6, i.e. the case with a relativistic reverse shock [287]. Following the claim of an observed high gamma-ray polarization in the burst GRB 021206 [74], there was increased attention on such models for some time (e.g. [287]) and on whether the usual baryonic (i.e. sub-dominant magnetization) jets might be also able to produce such high polarization [91, 111, 176, 178, 264, 288, 332, 513]. The issue may remain unresolved, as the observational analysis appears to be inconclusive [73, 434, 526].

Other alternative models include different central energy sources such as strange stars ([35, 68, 105, 358]) and charged black hole electric discharges [432], while retaining essentially similar fireball-shock scenarios. A model unifying SGR, XRF and GRB [120, 121] postulates a

very thin (10^{-4} rad) precessing, long-lived magnetized jet. This requires a separate explanation for the light curve ('jet') breaks, and the interaction during precession with the massive progenitor is unclear. Another speculative radiation scenario considers non-fluid ejecta in the form of discrete 'bullets' [201] or 'cannon-balls' ejected at relativistic velocities, which assume no collective interactions (i.e. no collisionless shocks) and instead rely on particle–particle interactions and produce prompt emission by blue-shifted bremsstrahlung and also produce afterglows by IC scattering progenitor or ambient photons [79, 91]. The predictions are similar to those of the standard fluid jet with shocks or dissipation. However, the basic ansatz of coherent bullet formation, acceleration to relativistic velocities and their survival against plasma instabilities is an unanswered issue in this model. It is also farther from astrophysical experience, whereas other well-observed systems such as AGN jets, which are known to be fluid (as is almost everything else in astrophysics at high energy per particle values), involve dynamical and radiation physics concepts which are quite plausibly extended to the GRB context. Fluid or plasma GRB outflow and jet models are supported better by theoretical work and simulations and are so far not only compatible with observations but have produced predictions borne out by observations. Nonetheless, even in this standard scenario, the models remain largely phenomenological. The detailed nature of the underlying central engine and progenitor are poorly known, and the micro-physics of particle acceleration, magnetic field amplification in shocks and/or reconnection or dissipation is not well understood, and the radiation mechanisms are, at least for the prompt emission, the subject of discussion.

5. Afterglow radiation models

5.1. The standard model

The external shock starts to develop as soon as the ejecta expands into the external medium. As the ejecta plows ahead, it sweeps up an increasing amount of external matter, and the bolometric luminosity of the shock increases as $L \propto t^2$ (equating in the contact discontinuity frame the kinetic flux $L/4\pi r^2\Gamma^2$ to the external ram pressure $\rho_{\rm ext}\Gamma^2$ while $\Gamma \sim \Gamma_0 = \eta \sim$ constant, $r \propto 2\Gamma^2 ct \propto t$ [416]). The luminosity peaks after Γ has dropped to about half its initial value, at a radius $r_{\rm dec}$ at an observer time $t_{\rm dec}$ given by equations (15) and (16). Thereafter, as more matter is swept up, the bulk Lorentz factor and the radius vary as [416, 366]

$$\begin{aligned} &\Gamma \propto r^{-3/2} \propto t^{-3/8}, \quad r \propto t^{1/4}\ \text{(adiabatic)},\\ &\Gamma \propto r^{-3} \propto t^{-3/7}, \quad r \propto t^{1/7}\ \text{(radiative)}, \end{aligned} \tag{25}$$

or in general $\Gamma \propto r^{-g} \propto t^{-g/(1+2g)}$, $r \propto t^{1/(1+2g)}$ with $g = (3, 3/2)$ for the radiative (adiabatic) regime. In the adiabatic case the radiative cooling time, e.g. synchrotron, is longer than the observer-frame dynamical time $t \sim r/2c\Gamma^2$, so the energy is approximately conserved $E = (4\pi/3)r^3 n_0 m_{\rm p} c^2 \Gamma^2 \sim$ constant (cf equation (15)), while in the radiative case the cooling time is shorter than the dynamic time and momentum is conserved (as in the snow-plow phase of supernova remnants), $n_0 r^3 \Gamma \sim$ constant. Thus, after the external shock luminosity peaks, one expects the bolometric luminosity to decay as $L \propto t^{-1}$ in the adiabatic regime [416] or steeper in the radiative regime, in a gradual fading. The observed time-radius relation is more generally $t \sim r/Kc\Gamma^2$, where $K = 2$ in the constant Γ regime and $K = 4$ in the self-similar (BM) regime [444, 511].

The spectrum of radiation is likely to be due to synchrotron radiation, whose peak frequency in the observer frame is $\nu_{\rm m} \propto \gamma B' \gamma_e^2$, and both the comoving field B' and electron Lorentz factor γ_e are likely to be proportional to γ [309]. This implies that as γ decreases, so will $\nu_{\rm m}$, and the radiation will move to longer wavelengths. Consequences of this are the

expectations that the burst would leave a radio remnant [357] after some weeks and before that an optical [227] transient. The observation of linear polarization at the few per cent level observed in a number of optical or IR afterglows (e.g. [483]) supports the paradigm of synchrotron emission as the dominant emission mechanism in the afterglow.

The first self-consistent afterglow calculations [313] took into account both the dynamical evolution and its interplay with the relativistic particle acceleration and a specific relativistically beamed radiation mechanism resulted in quantitative predictions for the entire spectral evolution, going through the x-ray, optical and radio range. For a spherical fireball advancing into an approximately smooth external environment, the bulk Lorentz factor decreases as in inverse power of the time (asymptotically $t^{-3/8}$ in the adiabatic limit), and the accelerated electron minimum random Lorentz factor and the turbulent magnetic field also decreases as inverse power laws in time. The synchrotron peak energy corresponding to the time-dependent minimum Lorentz factor and magnetic field then moves to softer energies as $t^{-3/2}$. These can be generalized in a straightforward manner when in the radiative regime or in the presence of density gradients, and so on. The radio spectrum is initially expected to be self-absorbed and becomes optically thin after $\sim$ hours. For times beyond $\sim$10 min, the dominant radiation is from the forward shock, for which the flux at a given frequency and the synchrotron peak frequency decay as [313]

$$F_\nu \propto t^{-(3/2)\beta}, \qquad \nu_{\rm m} \propto t^{-3/2}, \tag{26}$$

as long as the expansion is relativistic. This is referred to as the 'standard' (adiabatic) model, where $g = 3/2$ in $\Gamma \propto r^{-g}$ and $\beta = {\rm d}\log F_\nu/{\rm d}\log\nu$ is the photon spectral energy flux slope. More generally [315] the relativistic forward shock flux and frequency peak are given by

$$F_\nu \propto t^{[3-2g(1-2\beta)]/(1+2g)} \qquad \text{and} \qquad \nu_{\rm m} \propto t^{-4g/(1+2g)}, \tag{27}$$

where $g = (3/2, 3)$ for the adiabatic (radiative) regime. The transition to the non-relativistic expansion regime has been discussed, e.g. by [83, 281, 530]. A reverse shock component is also expected [310, 313, 315, 452], with high initial optical brightness (but much faster decay rate than the forward shock, see section 5.2). Remarkably, the simple 'standard' model where reverse shock effects are ignored is a good approximation for modelling observations starting a few hours after the trigger, as during 1997–1998.

The afterglow spectrum at a given instant of time depends on the flux observed at different frequencies from electrons with (comoving) energy $\gamma_e m_{\rm e}c^2$ and bulk Lorentz factor Γ, whose observed peak frequency is $\nu = \Gamma\gamma_e^2(eB'/2\pi m_{\rm ec})$. Three critical frequencies are defined by the three characteristic electron energies. These are $\nu_{\rm m}$ (the 'peak' or injection frequency corresponding to γ_m), $\nu_{\rm c}$ (the cooling frequency) and $\nu_{\rm M}$ (the maximum synchrotron frequency). There is one more frequency, $\nu_{\rm a}$, corresponding to the synchrotron self-absorption at lower frequencies. For a given behaviour of Γ with r or t (e.g. adiabatic, $\Gamma \propto r^{-3/2}$) and values of the isotropic equivalent kinetic energy of the explosion, of the electron index (e.g. $p = 2.2$) and the efficiency factors $\epsilon_e, \zeta_e, \epsilon_B$, one can obtain the time dependence of the characteristic observer-frame frequencies, also including a cosmological redshift factor z [541]

$$\nu_{\rm m} = (6\times10^{15}\,{\rm Hz})\,(1+z)^{1/2} g(p)^2 (\epsilon_e/\zeta_e)^2 \epsilon_B^{1/2} E_{52}^{1/2} t_d^{-3/2}, \tag{28}$$

$$\nu_{\rm c} = (9\times10^{12}\,{\rm Hz})(1+z)^{-1/2}\epsilon_B^{-3/2} n^{-1} E_{52}^{-1/2} t_d^{-1/2}, \tag{29}$$

$$\nu_{\rm a} = (2\times10^{9}\,{\rm Hz})(1+z)^{-1}(\epsilon_e/\zeta_e)^{-1}\epsilon_B^{1/5} n^{3/5} E_{52}^{1/5}, \tag{30}$$

$$F_{\nu,\rm max} = (20\,{\rm mJy})(1+z)\epsilon_B^{1/2} n^{1/2} E_{52} d_{L,28}^{-2}, \tag{31}$$

where $t_d = (t/{\rm day})$ and $g(p) = (p-2)/(p-1)$. The final GRB afterglow synchrotron spectrum is a four-segment broken power law [187, 316, 451, 541] separated by the typical

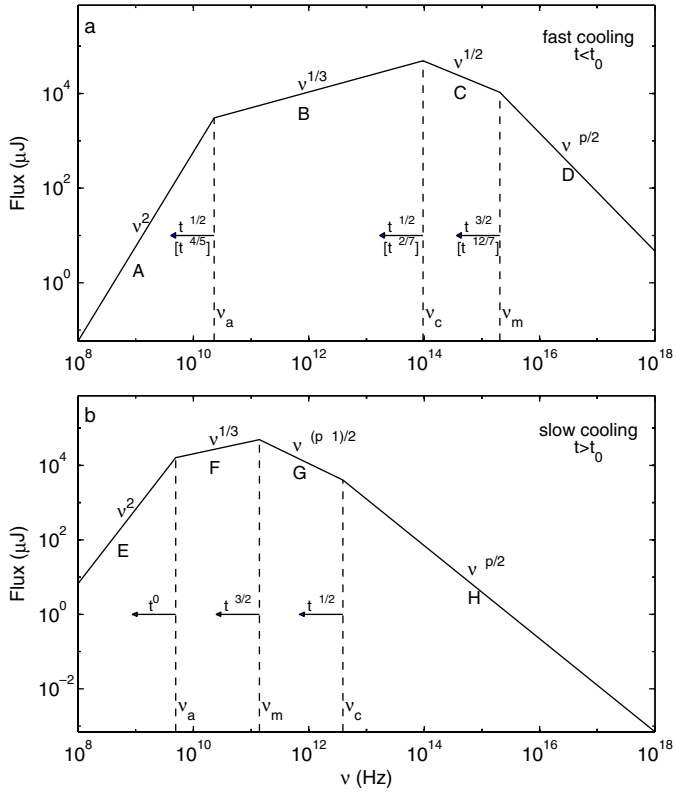

Figure 7. Fast cooling and slow cooling synchrotron spectra [451].

frequencies ν_a, ν_m and ν_c (figure 7). Depending on the order between ν_m and ν_c, there are two types of spectra [451]. For $\nu_m < \nu_c$, called the 'slow cooling case', the spectrum is

$$F_\nu = F_{\nu,\max}\begin{cases}(\nu_a/\nu_m)^{1/3}(\nu/\nu_a)^2 & \nu < \nu_a,\\ (\nu/\nu_m)^{1/3} & \nu_a \leqslant \nu < \nu_m,\\ (\nu/\nu_m)^{-(p-1)/2} & \nu_m \leqslant \nu < \nu_c,\\ (\nu_c/\nu_m)^{-(p-1)/2}(\nu/\nu_c)^{-p/2} & \nu_c \leqslant \nu \leqslant \nu_M.\end{cases} \tag{32}$$

For $\nu_m > \nu_c$, called the 'fast cooling case', the spectrum is

$$F_\nu = F_{\nu,\max}\begin{cases}(\nu_a/\nu_c)^{1/3}(\nu/\nu_a)^2 & \nu < \nu_a,\\ (\nu/\nu_c)^{1/3} & \nu_a \leqslant \nu < \nu_c,\\ (\nu/\nu_c)^{-1/2} & \nu_c \leqslant \nu < \nu_m,\\ (\nu_m/\nu_c)^{-1/2}(\nu/\nu_m)^{-p/2} & \nu_m \leqslant \nu \leqslant \nu_M.\end{cases} \tag{33}$$

A useful tabulation of the temporal indices α and spectral indices β is given in table 1 of [541], corresponding to the various forward shock spectral regimes of equations (32) and (33), for a homogeneous or a wind external medium. In the above, the normalization $F_{\nu,\max}$ is obtained by multiplying the total number of radiating electrons $4\pi r^3 n_1/3$ by the peak flux from a single electron [451], which is only a function of B and is independent of the energy (γ_e) of the electron [451, 525]. There are more complicated regimes for various cases of self-absorption [185], e.g. there can also be an intermediate fast cooling optically thick power law segment of the synchrotron spectrum where $F_\nu \propto \nu^{11/8}$.

Table 1. Temporal exponents of the peak frequency $\nu_{\rm m}$, the maximum flux $F_{\nu_{\rm m}}$, the cooling frequency $\nu_{\rm c}$ and the flux in a given bandwidth F_ν, for the forward (f) and reverse (r) shocks, calculated both in the adiabatic regime $\nu_{\rm m} < \nu < \nu_{\rm c}$ ($F_\nu \propto F_{\nu_{\rm m}}(\nu_{\rm m}/\nu)^\beta \propto t^{-\alpha}\nu^{-\beta}$, where $\beta = (p-1)/2$) and in the cooling regime $\nu_{\rm c} < \nu_{\rm m} < \nu$ ($F_\nu \propto (\nu_{\rm c}/\nu_{\rm m})^{1/2}(\nu_{\rm m}/\nu)^\beta \propto t^{-\alpha}\nu^{-\beta}$, where $\beta = p/2$). For $s = 1$ this gives the usual (i.e. without 'refreshment') forward and reverse shock behaviour [418, 448].

	$\nu_{\rm m}$	$F_{\nu_{\rm m}}$	$\nu_{\rm c}$	F_ν: $\nu_{\rm m} < \nu < \nu_{\rm c}$	F_ν: $\nu > \max(\nu_{\rm c}, \nu_{\rm m})$
f	$-\dfrac{24-7k+sk}{2(7+s-2k)}$	$\dfrac{6s-6+k-3sk}{2(7+s-2k)}$	$-\dfrac{4+4s-3k-3sk}{2(7+s-2k)}$	$-\dfrac{6-6s-k+3sk+\beta(24-7k+sk)}{2(7+s-2k)}$	$-\dfrac{-4-4s+k+sk+\beta(24-7k+sk)}{2(7+s-2k)}$
r	$-\dfrac{12-3k+sk}{2(7+s-2k)}$	$\dfrac{6s-12+3k-3sk}{2(7+s-2k)}$	$-\dfrac{4+4s-3k-3sk}{2(7+s-2k)}$	$-\dfrac{12-6s-3k+3sk+\beta(12-3k+sk)}{2(7+s-2k)}$	$-\dfrac{8-4s-3k+sk+\beta(12-3k+sk)}{2(7+s-2k)}$

The predictions of the fireball shock afterglow model [313] were made in advance of the first x-ray detections by Beppo-SAX [76] allowing subsequent follow-ups [138, 304, 484] over different wavelengths, which showed a good agreement with the standard model, e.g. [411, 475, 496, 509, 510, 530]. The comparison of increasingly sophisticated versions of this theoretical model (e.g. [98, 99, 187, 384, 451, 525]) against an increasingly detailed array of observations (e.g. as summarized in [483]) has provided confirmation of this generic fireball shock model of GRB afterglows.

A snapshot spectrum of the standard model at any given time consists generally of a three or four segment power law with two or three breaks, such as those shown in figure 7. (More rarely, a five segment power law spectrum may also be expected [185]). The observations (e.g. [483]) are compatible with an electron spectral index $p \sim 2.2$–2.5, which is typical of shock acceleration, e.g. [451, 509, 525], etc. As the remnant expands the photon spectrum moves to lower frequencies, and the flux in a given band decays as a power law in time, whose index can change as the characteristic frequencies move through it. Snapshot spectra have been deduced by extrapolating measurements at different wavelengths and times, and assuming spherical symmetry and using the model time dependences [510, 525], fits were obtained for the different physical parameters of the burst and environment, e.g. the total energy E, the magnetic and electron–proton coupling parameters ϵ_B and ϵ_e and the external density n_0. These lead to typical values $n_0 \sim 10^{-2}$–$10\,\mathrm{cm}^{-3}$, $\epsilon_B \sim 10^{-2}$, $\epsilon_e \sim 0.1$–0.5 and $E \sim 10^{52}$–10^{54} ergs (if spherical; but see section 5.5).

5.2. *Prompt flashes and reverse shocks*

An interesting development was the observation [4] of a prompt and extremely bright ($m_v \sim 9$) optical flash in the burst GRB 990123, the first data point for which was at 15 s after the GRB started (while the gamma-rays were still going on). This observation was followed by a small number of other prompt optical flashes, generally not as bright. A prompt multi-wavelength flash, contemporaneous with the γ-ray emission and reaching such optical magnitude levels is an expected consequence of the reverse component of external shocks [310, 313, 315, 452]. Generally the reverse shock can be expected to be mildly relativistic (thin shell case; see, however, below). In this case the thermal Lorentz factor of the reverse electrons is roughly $\gamma_e^r \sim \epsilon_e m_\mathrm{p}/m_\mathrm{e}$ whereas in the forward shock, the thermal Lorentz factor of the electrons is $\gamma_e^f \sim \epsilon_e \Gamma m_\mathrm{p}/m_\mathrm{e}$. In this case the reverse electrons radiate a much softer radiation than the forward shock electrons. This follows also from the fact that the reverse shock has a similar total energy as the forward shock but consists of Γ times more electrons, hence the energy per electron is $1/\Gamma$ times smaller [313]. In general, since the pressure (and hence the magnetic energy density) is the same in the forward and reverse shocked regions, one has the following relations between forward and reverse shock radiation properties [448]: (1) The peak flux of the reverse shock, at any time, is larger by a factor of Γ than that of the forward shock, $F^r_{\nu,\mathrm{max}} = \Gamma F^f_{\nu,\mathrm{max}}$; (2) The typical frequency of the minimal electron in the reverse shock is smaller by a factor of Γ^2, $\nu^r_\mathrm{m} = \nu^f_\mathrm{m}/\Gamma^2$; (3) The cooling frequency of the reverse and forward shock are equal, $\nu^r_\mathrm{c} = \nu^f_\mathrm{c} = \nu_\mathrm{c}$ (under the assumption that ϵ_B is the same in the forward and reverse shocked gas; this might not be true if the ejecta carries a significant magnetic field from the source); (4) Generally (also in refreshed shocks) $\nu^{r,f}_\mathrm{a} < \nu^{r,f}_\mathrm{m}$ and $\nu^{r,f}_\mathrm{a} < \nu_c$. The self-absorption frequency of the reverse shock is larger than that of the forward shock. The characteristic frequencies and flux temporal slopes for a standard afterglow are given by the case (r) with $s = 0$ in table 1 below.

The prompt optical flashes, starting with GRB 990123, have been generally interpreted [315, 337, 452] as the radiation from a reverse (external) shock, although a prompt optical flash

could be expected from either an internal shock or the reverse part of the external shock or both [313]. The decay rate of the optical flux from reverse shocks is much faster (and that of internal shocks is faster still) than that of forward shocks, so the emission of the latter dominates after tens of minutes [175]. Such bright prompt flashes, however, appear to be relatively rare. Other early optical flashes, e.g. in GRB 021004, GRB 021211, GRB 041219a, GRB 050904 are also consistent with the reverse shock interpretation [116, 133, 134, 243, 521, 522, 542]. After the launch of Swift, new prompt optical observations with robotic telescopes have greatly added to the phenomenology of prompt flashes (see section 3).

5.3. Dependence on external density, injection variability and anisotropy

If the external medium is inhomogeneous, e.g. $n_{\rm ext} \propto r^{-k}$, the energy conservation condition is $\Gamma^2 r^{3-k} \sim$ constant, so $\Gamma \propto t^{1/(4-k)}$, $r \propto t^{-(3-k)/(8-2k)}$, which changes the temporal decay rates [316]. This might occur if the external medium is a stellar wind from the evolved progenitor star of a long burst, e.g. $n_{\rm ext} \propto r^{-2}$, such light curves fitting some bursts better with this hypothesis [69, 275].

Another departure from a simple injection approximation is one where E_0 (or L_0) and Γ_0 are not a simple delta function or top hat functions. An example is if the mass and energy injected during the burst duration $t_{\rm grb}$ (say tens of seconds) obeys $M(>\gamma) \propto \gamma^{-s}$, $E(>\gamma) \propto \gamma^{1-s}$, i.e. more energy emitted with lower Lorentz factors at later times but still shorter than the gamma-ray pulse duration [418, 448]. The ejecta dynamics becomes

$$\Gamma(r) \propto r^{-(3-k)/(1+s)} \propto t^{-(3-k)/(7+s-2k)}, \qquad r \propto t^{(1+s)/(7+s-2k)}. \tag{34}$$

This can drastically change the temporal decay rate, extending the afterglow lifetime in the relativistic regime. It can provide an explanation for shallower decay rates, if the progressively slower ejecta arrives continuously, re-energizing the external shocks ('refreshed' shocks) on timescales comparable to the afterglow timescale [84, 256, 418, 448]. While observational motivations for this were already present in the Beppo-SAX era, as discussed in the above references, this mechanism has been invoked more recently in order to explain the Swift prompt x-ray afterglow shallow decays (see section 6.2). When the distribution of Γ is discontinuous, it can also explain a sudden increase in the flux, leading to bumps in the light curve. After the onset, the non-standard decay rates for the forward and reverse shock are tabulated for different cases [448] in table 1.

Other types of non-standard decay can occur if the outflow has a transverse θ dependent gradient in the energy or Lorentz factor, e.g. as some power law $E \propto \theta^{-a}$, $\Gamma \propto \theta^{-b}$ [316]. Expressions for the temporal decay index $\alpha(\beta, s, d, a, b, ..)$ in $F_\nu \propto t^\alpha$ are given by [316,448], which now depend also on s, d, a, b, etc (and not just on β as in the standard relation of equation (26). The result is that the decay can be flatter (or steeper, depending on s, d, etc)) than the simple standard $\alpha = (3/2)\beta$. Such non-uniform outflows have been considered more recently in the context of jet breaks based on structured jets (section 5.5).

Evidence for departures from the simple standard model was present even before the new Swift observations, e.g. by sharp rises or humps in the light curves followed by a renewed decay, as in GRB 970508 [373, 386] or shallower than usual light curve decays. Time-dependent model fits [369] to the x-ray, optical and radio light curves of GRB 970228 and GRB 970508 indicated that in order to explain the humps, a non-uniform injection or an anisotropic outflow is required. Another example is the well-studied wiggly optical light curve of GRB 030329, for which refreshed shocks provide the likeliest explanation [182]. Other ways to get light curve bumps which are not too steep after $\sim$ hours to days is with micro-lensing [159, 186], late injection [218, 538] or inverse Compton effects [198, 447, 539]. The changes in the shock

physics and dynamics in highly magnetized or Poynting dominated outflows were discussed, e.g. in [177, 182, 287, 314, 477, 480, 543]. More examples and references to departures from the standard model are discussed, e.g. in [483, 541]. Departures from spherical symmetry and jet effects are discussed in the next two subsections.

5.4. Equal arrival time surface and limb brightening effect

As illustrated in figure 5, for a distant observer the photons from a spherically expanding shell are received from an equal-arrival time surface which is an ellipsoid (if Γ = constant). The photons arriving from the line of sight originated at larger radii than photons arriving from the light-cone at $\theta \sim \Gamma$. At smaller radii the outflow had a higher magnetic field and higher density, so the radiation from the $1/\Gamma$ edge is harder and more intense. Thus an interesting effect, which arises even in spherical outflows, is that the effective emitting region seen by the observer resembles a ring [174, 183, 367, 445, 510]. This limb brightening effect is different in the different power law segments of the spectrum. When one considers the change in Γ due to deceleration, the ellipsoid is changed into an egg shape, which is similarly limb-brightened. This effect is thought to be implicated in giving rise to the radio diffractive scintillation pattern seen in several afterglows, since this requires the emitting source to be of small dimensions (the ring width), e.g. in GRB 970508 [512]. This provided an important observational check, giving a direct confirmation of the relativistic source expansion and a direct determination of the (expected) source size [228, 512]. The above treatments were based on the simple asymptotic scaling behaviour for the Lorentz factor $\Gamma \sim$ constant at $r \leqslant r_{\rm dec}$ and $\Gamma \propto r^{-3/2}$ ($\Gamma \propto r^{-3}$) at $r \gtrsim r_{\rm dec}$ for the adiabatic (fully radiative) cases (section 4.5). More exact treatments are possible [43, 44] based on following analytically and numerically the detailed dynamical evolution equations for the Lorentz factor through and beyond the transition between pre-deceleration and post-deceleration. The shape of the equi-temporal surfaces is modified, and the expected light curves will be correspondingly changed. The exact afterglow behaviour will depend on the unknown external medium density and on whether and what kind of continued energy injection into the shock occurs, which introduces an additional layer of parameters to be fitted.

5.5. Jets

The spherical assumption is valid even when considering a relativistic outflow collimated within some jet of solid angle $\Omega_j < 4\pi$, provided the observer line of sight is inside this angle and $\Gamma \gtrsim \Omega_j^{-1/2}$ [308], so the light-cone is inside the jet boundary (causally disconnected) and the observer is unaware of what is outside the light cone. However, as the ejecta is decelerated, the Lorentz factor eventually drops below this value, and a change is expected in the dynamics and the light curves [413, 414]. It is thought that this is what gives rise to the achromatic optical light curve breaks seen in many afterglows [140, 252].

The jet opening angle can be obtained form the observer time $t_{\rm j}$ at which the flux F_ν decay rate achromatically changes to a steeper value, assuming that this corresponds to the causal (light-cone) angle $\Gamma(t)^{-1}$ having become comparable to (and later larger than) the jet half-angle θ_j [413]. Assuming a standard adiabatic dynamics and a uniform external medium, the jet opening half-angle is

$$\theta_j \sim 5{\rm deg}\, t_{\rm j,d}^{3/8} E_{53}^{-1/8} n_{\rm ex}^{1/8} (\eta_\gamma/0.2)^{1/8} ([1+z]/2)^{-3/8}, \tag{35}$$

where E_{53} is the isotropic equivalent gamma-ray energy in ergs, $t_{\rm j,d} = t_{\rm j}/{\rm day}$ and η_γ is radiative efficiency [140]. The degree of steepening of the observed flux light curve can be estimated

by considering that while the causal angle is smaller than the jet opening angle, the effective transverse area from which radiation is received is $A \sim r_\perp^2 \sim (r/\Gamma)^2 \propto t^2\Gamma^2$, whereas after the causal angle becomes larger than the jet angle, the area is $A \sim r^2\theta_j^2$. Thus the flux after the break, for an adiabatic behaviour $\Gamma \propto t^{-3/8}$ (valid if there is no sideways expansion) is steeper by a factor $\propto \Gamma^2 \propto t^{-3/4}$ [315], a value in broad agreement with observed breaks. After this time, if the jet collimation is simply ballistic (i.e. not due to magnetic or other dynamical effects) the jet can start expanding sideways at the comoving (relativistic) speed of sound, leading to a different decay $\Gamma \propto t^{-1/2}$ and $F_\nu \propto t^{-p} \propto t^{-2}$ [414].

A collimated outflow greatly alleviates the energy requirements of GRB. If the burst energy were emitted isotropically, the energy required spreads over many orders of magnitude, $E_{\gamma,\mathrm{iso}} \sim 10^{51}$–$10^{54}$ erg [252]. However, taking into account the jet interpretation of light curve breaks in optical afterglows [140,362,363] the spread in the total γ-ray energy is reduced to one order of magnitude, around a less demanding mean value of $E_{\gamma,\mathrm{tot}} \sim 1.3 \times 10^{51}$ erg [53]. This is not significantly larger than the kinetic energies in core-collapse supernovae, but the photons are concentrated in the gamma-ray range, and the outflow is substantially more collimated than in the SN case. Radiative inefficiencies and the additional energy which must be associated with the proton and magnetic field components increase this value (e.g. the η_γ factor in equation (35)), but this energy is still well within the theoretical energetics $\lesssim 10^{53.5}$–10^{54} erg achievable in *either* NS–NS, NS–BH mergers [314] or in collapsar models [356, 389, 529] using MHD extraction of the spin energy of a disrupted torus and/or a central fast spinning BH. It is worth noting that jets do not invalidate the usefulness of spherical snapshot spectral fits, since the latter constrain only the *energy per solid angle* [317].

Equation (35) assumes a uniform external medium, which fits most afterglows, but in some cases a wind-like external medium ($n_{\mathrm{ext}} \propto r^{-2}$) is preferred [69, 275, 361]. For an external medium varying as $n_{\mathrm{ext}} = Ar^{-k}$ one can show that the the Lorentz factor initially evolves as $\Gamma \propto (E/A)^{1/2} r^{-(3-k)/2} \propto (E/A)^{1/(8-2k)} t^{-(3-k)/(8-2k)}$, and the causality (or jet break) condition $\Gamma \sim \theta_j^{-1}$ leads to a relation between the observed light curve break time t_j and the inferred collimation angle θ_j which is different from equation (35), namely $\theta_j \propto (E/A)^{-1/(8-2k)} (t_\mathrm{j}/[1+z])^{(3-k)/(8-2k)} \propto (E/A)^{-1/4} (t_\mathrm{j}/[1+z])^{1/4}$, where the last part is for $k = 2$. Another argument indicating that the medium in the vicinity of at least some long-GRB afterglows is not stratified, e.g. as r^{-2}, is the observation of a sharp jet-break in the optical afterglow light curves (as, e.g. in GRB 990510, 000301c, 990123). As pointed out by [257], relativistic jets propagating in a wind-like external medium are expected to give rise to a very gradual and shallow break in the afterglow light curve.

The discussion above also makes the simplifying assumption of a uniform jet (uniform energy and Lorentz factor inside the jet opening angle or top-hat jet model). In this case the correlation between the inverse beaming factor $f_b^{-1} = (\theta_j^2/2)^{-1}$ (or observationally, the jet break time from which θ_j is derived) and the isotropic equivalent energy or fluence $E_{\gamma,\mathrm{iso}}$ is interpreted as being due to a distribution of jet angles, larger angles leading to lower $E_{\gamma,\mathrm{iso}}$, according to $E_{\gamma,\mathrm{iso}} \propto \theta_j^{-2}$. There is, however, an equally plausible interpretation for this correlation, namely that one could have a universal jet profile such that the energy per unit solid angle is $\mathrm{d}E_\gamma/\mathrm{d}\Omega \propto \theta^{-2}$, where θ is the angle measured from the axis of symmetry [424,540]. (To avoid a singularity, one can assume this law to be valid outside some small core solid angle.) This model also explains the [140,362] correlation; the different E_{iso} would be due to the observer being at different angles relative to the jet axis. This hypothesis has been tested in a variety of ways [188, 193, 258, 334]. Attempts to extend the universal θ^{-2} jet structure to include x-ray flashes (section 2.5), together with the use of the Amati relation between the spectral peak energy E_{peak} and $E_{\gamma,\mathrm{iso}}$ (section 2.6), leads to the conclusion that a top-hat model is preferred over a universal θ^{-2} jet model [259]. Uniform jets seen off-axis have also been

considered as models for XRF in a unified scheme, e.g. [533, 180]. On the other hand, another type of universal jet profile with a Gaussian shape [87, 537] appears to satisfy both the jet break-$E_{\gamma,\rm iso}$ and $E_{\rm peak}$–$E_{\gamma,\rm iso}$ correlations for both GRB and XRFs. More extensive discussion of this is given in [541].

The uniform and structured jets are expected to produce achromatic breaks in the light curves, at least for wavebands not too widely separated. However, in some bursts there have been indications of different light curve break times for widely separated wavebands, e.g. GRB 030329, suggesting different beam opening angles for the optical/x-ray and the radio components [39]. Such two-component jets could arise naturally in the collapsar model, e.g. with a narrow, high Lorentz factor central jet producing γ, x-ray and optical radiation and a wider slower outflow, e.g. involving more baryon-rich portions of the envelope producing radio radiation [403]. A wider component may also be connected to a neutron-rich part of the outflow [378]. More recent discussions of possible chromatic breaks are given in [118, 371].

6. Current theoretical issues in afterglow models

The afterglow is generally assumed to become important after the time when the self-similar $\Gamma \propto r^{-3/2}$ behaviour starts. From equation (19) for the deceleration time $t_{\rm dec} \sim (r_{\rm dec}/2c\Gamma^2)$ and taking into account the gradual transition to the self-similar regime [244], this is approximately

$$t_{\rm ag} \sim T \sim {\rm Max}[t_{\rm grb}(1+z), \qquad 15(E_{53}/n_0)^{1/3}\eta_{2.5}^{-8/3}[(1+z)/2]\,{\rm s}], \tag{36}$$

where $t_{\rm grb}$ is the duration of the outflow, i.e. an upper limit for the duration of the prompt γ-ray emission and a cosmological time dilation factor is included. (Note that in some bursts the γ-rays could continue in the self-similar phase). The afterglow emission from the forward and the reverse shock emission starts immediately after the ejecta starts to sweep up matter, but it does not peak (and become dominant over the prompt emission or its decaying tail) until the time $\sim t_{\rm ag}$, marking the beginning of the self-similar blast wave regime.

Denoting the frequency and time dependence of the afterglow spectral energy flux as $F_\nu(t) \propto \nu^{-\beta}t^{-\alpha}$, the late x-ray afterglow phases (3) and (4) of section 3 seen by Swift are similar to those known previously from Beppo-SAX (the theoretical understanding of which is discussed in section 5 and in [541]). The 'normal' decay phase (3), with temporal decay indices $\alpha \sim 1.1$–1.5 and spectral energy indices $\beta \sim 0.7$–1.0, is what is generally expected from the evolution of the forward shock in the Blandford–McKee self-similar late time regime, under the assumption of synchrotron emission.

6.1. Early steep decay

Among the new afterglow features detected by Swift (see figure 3), the steep initial decay phase $F_\nu \propto t^{-3} - t^{-5}$ in x-rays of the long GRB afterglows is one of the most striking. There are several possible mechanisms which could cause this. The most obvious first guess would be to attribute it to the cooling following cessation of the prompt emission (internal shocks or dissipation). If the comoving magnetic field in the emission region is random [or transverse], the flux per unit frequency along the line of sight in a given energy band, as a function of the electron energy index p, decays as $F_\nu \propto t^{-\alpha}$ with $\alpha = -2p$ $[(1-3p)/2]$ in the slow cooling regime, where $\beta = (p-1)/2$, and it decays as $\alpha = -2(1+p)$, $[-(2-3p)/2]$ in the fast cooling regime, where $\beta = p/2$, i.e. for the standard $p = 2.5$ this would be $\alpha = -5$, $[-3.25]$ in the slow cooling or $\alpha = -7$, $[-2.75]$ in the fast cooling regime, for random [transverse] fields [315]. In some bursts this may be the explanation, but in others the time and spectral

indices do not correspond well. In addition, if the flux along the line of sight decays as steeply as above, the observed flux would be dominated by the so-called high latitude emission, which is discussed next.

At present, the most widely considered explanation for the fast decay, both of the initial phase (1) and of the steep flares, attributes it to the off-axis emission from regions at $\theta > \Gamma^{-1}$ (the curvature effect or high latitude emission [235]. In this case, after the line of sight gamma-rays have ceased, the off-axis emission observed from $\theta > \Gamma^{-1}$ is $(\Gamma\theta)^{-6}$ smaller than that from the line of sight. Integrating over the equal arrival time region, this flux ratio becomes $\propto(\Gamma\theta)^{-4}$. Since the emission from θ arrives $(\Gamma\theta)^2$ later than that from $\theta = 0$, the observer sees the flux falling as $F_\nu \propto t^{-2}$, if the flux were frequency independent. For a source-frame flux $\propto \nu'^{-\beta}$, the observed flux per unit frequency varies then as

$$F_\nu \propto (t - t_0)^{-2-\beta}, \tag{37}$$

i.e. $\alpha = 2 + \beta$. This 'high latitude' radiation, which for observers outside the line cone at $\theta > \Gamma^{-1}$ would appear as prompt γ-ray emission from dissipation at radius r, appears to observers along the line of sight (inside the light cone) to arrive delayed by $t \sim (r\theta^2/2c)$ relative to the trigger time, and its spectrum is softened by the Doppler factor $\propto t^{-1}$ into the x-ray observer band. For the initial prompt decay, the onset of the afterglow (e.g. phases 2 or 3), which also comes from the line of sight, may overlap in time with the delayed high latitude emission. In equation (37) t_0 can be taken as the trigger time or some value comparable or less than equation (36). This can be used to constrain the prompt emission radius [266]. When $t_{\rm dec} < T$, the emission can have an admixture of high latitude and afterglow, and this can lead to decay rates intermediate between the two [350]. Values of t_0 closer to the onset of the decay also lead to steeper slopes. It is possible to identify for various bursts values of t_0 near the rising part of the last spike in the prompt emission which satisfy the subsequent steep decay slope [278]. Structured jets, when viewed on-beam produce essentially the same slopes as homogeneous jets, while off-beam observing can lead to shallower slopes [107]. For the flares, if their origin is assumed to be internal (e.g. some form of late internal shock or dissipation) the value of t_0 is just before the flare, e.g the observer time at which the internal dissipation starts to be observable [536]. This interpretation appears, so far, compatible with most of the Swift afterglows [348, 370, 544].

Alternatively, the initial fast decay may be due to the emission of a cocoon of exhaust gas [376], where the temporal and spectral index are explained through an approximately power-law behaviour of escape times and spectral modification of multiply scattered photons. The fast decay may also be due to the reverse shock emission, if inverse Compton up-scatters primarily synchrotron optical photons into the x-ray range. The decay starts after the reverse shock has crossed the ejecta and electrons are no longer accelerated, and may have both a line of sight and an off-axis component [241]. This poses strong constraints on the Compton-y parameter and cannot explain decays much steeper than $\alpha = -2$ or $-2-\beta$ if the off-axis contribution dominates. Models involving bullets, whose origin, acceleration and survivability is unexplained, could give a prompt decay index $\alpha \sim -3$ to -5 [81], with a bremsstrahlung energy index $\beta \sim 0$ which is not observed in the fast decay; switching to a synchrotron or IC mechanisms requires additional parameters. Finally, a patchy shell model, where the Lorentz factor is highly variable in angle, would produce emission with $\alpha \sim -2.5$. Thus, such mechanisms may explain the more gradual decays but not the more extreme $\alpha = -5, -7$ values encountered in some cases. It should be noted, however, that the Swift x-ray observations suggest that the steep decay is a direct continuation of the prompt emission [350], which in turn suggests that the prompt and the fast decaying emission both arise from the same physical region, posing a problem for the models in this paragraph (but not for the high latitude emission model).

6.2. Shallow decay

The slow decay portion of the x-ray light curves ($\alpha \sim -0.3 - 0.7$), ubiquitously detected by Swift, is not entirely new, having been detected in a few cases by BeppoSAX. This, as well as the appearance of wiggles and flares in the x-ray light curves after several hours, was the motivation for the 'refreshed shock' scenario [418, 448] (section 5.3). Refreshed shocks can flatten the afterglow light curve for hours or days, even if the ejecta is all emitted promptly at $t = T \lesssim t_\gamma$ but with a range of Lorentz factors, say $M(\Gamma) \propto \Gamma^{-s}$, where the lower Γ shells arrive much later to the foremost fast shells which have already been decelerated. Thus, for an external medium of density $\rho \propto r^{-k}$ and a prompt injection where the Lorentz factor spread relative to ejecta mass and energy is $M(\Gamma) \propto \Gamma^{-s}$, $E(\Gamma) \propto \Gamma^{-s+1}$, the forward shock flux temporal decay is given by [448]

$$\alpha = [(k-4)(1+s) + \beta(24 - 7k + sk)]/[2(7+s-2k)]\,, \tag{38}$$

(for more details, see table 1). It needs to be emphasized that in this model all the ejection can be prompt (e.g. over the duration $\sim T$ of the gamma-ray emission) but the low Γ portions arrive at (and refresh) the forward shock at late times, which can range from hours to days, i.e. it is not the central engine which is active late, but its effects are seen late. Fits of such refreshed shocks to observed shallow decay phases in Swift bursts [181] lead to a Γ distribution which is a broken power law, extending above and below a peak around $\sim$45.

There is a different version of refreshed shocks, which does envisage central engine activity extending for long periods of time, e.g. $\lesssim$ day (in contrast to the $\lesssim$ minutes engine activity in the model above). Such long-lived activity may be due to continued fall-back into the central black hole [528] or a magnetar wind [85, 348, 538]. One characteristic of both types of refreshed models is that after the refreshed shocks stop and the usual decay resumes, the flux level shows a step-up relative to the previous level, since new energy has been injected.

From current analyses, the refreshed shock model is generally able to explain the flatter temporal x-ray slopes seen by Swift, both when it is seen to join smoothly on the prompt emission (i.e. without an initial steep decay phase) or when seen after an initial steep decay. Questions remain concerning the interpretation of the fluence ratio in the shallow x-ray afterglow and the prompt gamma-ray emission, which can reach $\lesssim$1 [350]. This requires a higher radiative efficiency in the prompt gamma-ray emission than in the x-ray afterglow. One might speculate that this might be achieved if the prompt outflow is Poynting-dominated or if a more efficient afterglow hides more of its energy in other bands, e.g. in GeV or IR. Alternatively [179, 219], a previous mass ejection might have emptied a cavity into which the ejecta moves, leading to greater efficiency at later times (although this would not work above the cooling frequency, which from the spectrum appears to be required in about half the cases) or otherwise the energy fraction going into the electrons increases $\propto t^{1/2}$. Other possible ways of addressing this include the afterglow coming from off-axis directions [108] and exploring plausible reasons for having underestimated in previous studies the energy of the ejecta [179].

6.3. X-ray flares

Refreshed shocks can also explain some of the x-ray flares whose rise and decay slopes are not too steep. However, this model encounters difficulties with the very steep flares with rise or decay indices $\alpha \sim \pm 5, \pm 7$, such as inferred from the giant flare of GRB 0500502b [60] around 300 s after the trigger. Also, the flux level increase in this flare is a factor $\sim$ 500 above the smooth afterglow before and after it, implying a comparable energy excess in the low versus high Γ material. An explanation based on inverse Compton scattering in the reverse shock [241] can explain a single flare at the beginning of the afterglow, with not too steep

decay. For multiple flares, models invoking encountering a lumpy external medium have generic difficulties explaining steep rises and decays [333, 544], although extremely dense, sharp-edged lumps, if they exist, might satisfy the steepness [102].

Currently the more widely considered model for the flares ascribes them to late central engine activity [348, 370, 544]. The strongest argument in favour of this is that the energy budget is more easily satisfied, and the fast rise/decay is straightforward to explain. In such a model the flare energy can be comparable to the prompt emission; the fast rise comes naturally from the short time variability leading to internal shocks (or to rapid reconnection), while the rapid decay may be due to the high latitude emission following the flare, with t_0 reset to the beginning of each flare (see further discussion in [536]). However, some flares are well modelled by refreshed forward shocks, while in others this is clearly ruled out and a central engine origin is better suited [531]. Aside from the phenomenological desirability based on energetics and timescales, a central engine origin is conceivable, within certain time ranges, based on numerical models of the burst origin in long bursts. These are interpreted as being due to core collapse of a massive stellar progenitor, where continued infall into fast rotating cores can continue for a long time [528]. However, large flares with a fluence which is a sizable fraction of the prompt emission occurring hours later remain difficult to understand. It has been argued that gravitational instabilities in the infalling debris torus can lead to lumpy accretion [379]. Alternatively, if the accreting debris torus is dominated by MHD effects, magnetic instabilities can lead to extended, highly time variable accretion [393], which may give rise to GRB x-ray flares [395].

6.4. Late steep decay and jet breaks

The late steep decay phase (4) of section 3 is seen in a modest fraction of the Swift bursts, mainly in x-rays and mainly but not exclusively in long bursts. The natural interpretation is that these are caused by the fact that the outflow is collimated into a jet break: when the decrease of the ejecta Lorentz factor leads to the light-cone angle becoming larger than the jet angular extent, $\Gamma_j(t) \gtrsim 1/\theta_j$ (e.g. section 5.5), the light curve steepens achromatically. For the Swift bursts, it is noteworthy that this final steepening has been seen in less than $\sim 10\%$ of the afterglows followed and then with reasonable confidence mainly in x-rays. The corresponding optical light curve breaks have been few and not well constrained. The UVOT finds afterglows in only $\sim 30\%$ of the bursts, and ground-based optical/IR telescopes have yielded few continued late time light curves monitored. This is unlike the case with the ~ 20 Beppo-SAX bursts, for which an achromatic break was reported in the optical [140], while in rarer cases there was an x-ray or radio break reported, which in a few cases appeared to occur at a different time than the optical break (e.g. [38]).

The relative paucity of optical breaks in Swift afterglows may be an observational selection effect due to the larger median redshift, and hence fainter and redder optical afterglow at the same observer epoch. At higher redshifts the break occurs later in the observer frame, which compounds a possible reluctance to commit large telescope time on more frequently reported bursts (roughly 2/week from Swift versus an earlier 2/month with Beppo-SAX). One can speculate that the apparent scarcity of detected light curve breaks might indicate that at higher redshifts the opening angle is intrinsically larger. However, continued monitoring of the x-ray light curves with both Swift and Chandra is resulting in a growing number of bursts with high quality late x-ray light curves showing in some cases a clear break and in others the absence of a break up to weeks (also in short bursts, e.g. [62, 190]). This is an evolving topic, with some indications that light curve breaks may not (or not always) appear achromatic [118, 371].

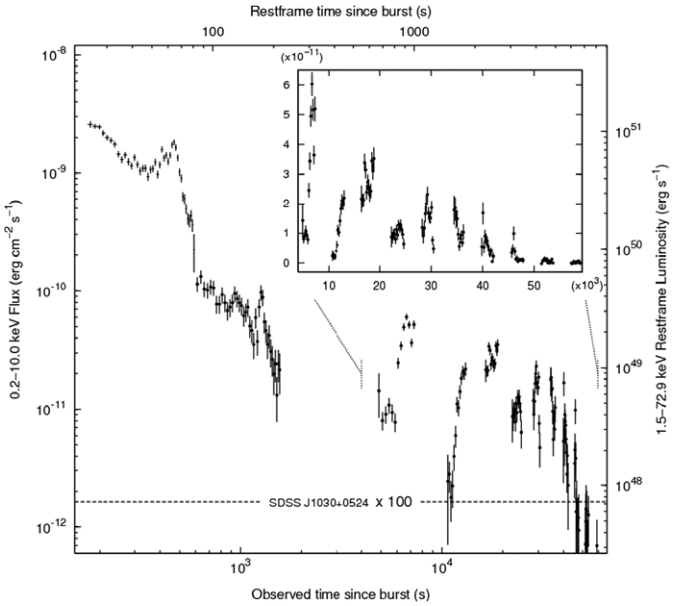

Figure 8. The x-ray afterglow of the GRB 050094 at $z = 6.29$ [505], showing for comparison the flux level of one of the most luminous x-ray quasars at a comparable redshift, SDSS J1030 + 524 (multiplied by 100). The inset shows the GRB variability in the 10–70 ks timeframe.

6.5. Prompt optical flashes and high redshift afterglows

Optical/UV afterglows have been detected with the Swift UVOT telescope in roughly half the bursts for which an x-ray afterglow was seen. For a more detailed discussion of the UVOT afterglow observations see [423]. Of particular interest is the ongoing discussion on whether 'dark GRB' are really optically deficient or the result of observational bias [42]. Another puzzle is the report of a bimodal intrinsic brightness distribution in the rest-frame R-band [277, 343]. This suggests possibly the existence of two different classes of long bursts or at least two different types of environments.

Compared with a few years ago, a much larger role is being played by ground-based robotic optical follow-ups, due to the increased rate of several arc-second x-ray alerts from XRT and the larger number of robotic telescopes brought on-line in the last years. For the most part, these detections have yielded optical decays in the $\gtrsim$ few 100 s range, initial brightness $m_V \sim 14$–17 and temporal decay slopes $\alpha \sim 1.1$–1.7 previously associated with the evolution of a forward shock [41, 136]. In a few cases, a prompt optical detection was achieved in the first 12–25 s [439, 440, 492].

The most exciting prompt robotic IR detection (and optical non-detection) is that of GRB 050904 [57, 195]. This object, at the unprecedented high redshift of $z = 6.29$ [229], has an x-ray brightness exceeding for a day that of the brightest x-ray quasars (see figure 8) [505]. Its O/IR brightness in the first 500 s (observer time) was comparable to that of the extremely bright ($m_V \sim 9$) optical flash in GRB 990123, with a similarly steep time-decay slope $\alpha \sim 3$ [57]. Such prompt, bright and steeply decaying optical emission is expected from the reverse shock as it crosses the ejecta, marking the start of the afterglow [313, 315, 452].

However, aside from the two glaring examples of 990123 and 050904, in the last six years there have been less than a score of other prompt optical flashes, typically with more modest initial brightnesses $m_v \gtrsim 13$. There are a number of possible reasons for this paucity of

optically bright flashes, if ascribed to reverse shock emission. One is the absence or weakness of a reverse shock, e.g. if the ejecta is highly magnetized [313]. A moderately magnetized ejecta is in fact favoured for some prompt flashes [542]. Alternatively, the deceleration might occur in the thick-shell regime ($T \gg t_{\rm dec}$, see equation (36), which can result in the reverse shock being relativistic, boosting the optical reverse shock spectrum into the UV [240] (in this case a detection by UVOT might be expected, unless the decay is faster than the typical 100–200 s for UVOT slewing and integration). Another possibility, for a high comoving luminosity, is a copious pair formation in the ejecta, causing the reverse shock spectrum to peak in the IR [322]. Since both GRB 990123 and GRB 050904 had $E_{\rm iso} \sim 10^{54}$ erg, among the top few per cent of all bursts, the latter is a distinct possibility, compatible with the fact that the prompt flash in GRB 050904 was bright in the IR I-band but not in the optical. On the other hand, the redshift $z = 6.29$ of this burst and a Ly-α cutoff at ∼800 nm would also ensure this (and GRB 990123, at $z = 1.6$, was detected in the V-band). However, the observations of optical flashes in these two objects but not in lower $E_{\rm iso}$ objects appears compatible with having a relativistic (thick shell) reverse shock with pair formation. Even in the absence of pairs, more accurate calculations of the reverse shock [299, 336] find the emission to be significantly weaker than was estimated earlier. Another possibility is that the cooling frequency in reverse shock is typically not much larger than the optical band frequency. In this case the optical emission from the reverse shock drops to zero very rapidly soon after the reverse shock has crossed the ejecta and the cooling frequency drops below the optical and there are no electrons left to radiate in the optical band [299].

7. Short GRB in the Swift era

7.1. Short GRB observations

Swift, and in smaller numbers HETE-2, have provided the first bona fide short burst x-ray afterglows followed up starting ∼100 s after the trigger, leading to localizations and redshifts. In the first of these, GRB 050509b [161], the extrapolation of the prompt BAT emission into the x-ray range and the XRT light curve from 100 s to about 1000 s (after which only upper limits exist, even with Chandra, due to the faintness of the burst) can be fitted with a single power law of $\alpha \sim 1.2$ (1.12 to 1.29 90% conf) or separately as $\alpha_{\rm BAT} = 1.34$ (0.27 to 2.87 90% conf) and $\alpha_{\rm XRT} = 1.1$(0.57 to 2.36 90% conf). The x-ray coverage was sparse due to orbital constraints, the number of x-ray photons being small, and no optical transient was identified, probably due to the faintness of the source. An optical host was however identified, an elliptical galaxy [55]. The next one, discovered by HETE-2, was GRB 050709 [499]. Its host [135] is an irregular galaxy at $z = 0.16$ (and the observations ruled out any supernova association). Even earlier, HETE-2 reported the short GRB 040924 [481], with a soft gamma-ray prompt emission and a faint broken power law optical afterglow [210]. A proposed host galaxy at $z = 0.86$ shows star formation and evidence for an associated 1998bw-like SN contribution to the light curve [460], which suggests this is perhaps the short end of the long burst or XRF distribution. The next Swift short burst, GRB 050724, was relatively bright, and besides x-rays, it also yielded both a decaying optical and a radio afterglow [37]. This burst, together with a significant part of other short bursts, is associated with an elliptical host galaxy. It also had a low-luminosity soft gamma-ray extension of the short hard gamma-ray component (which would have been missed by BATSE), and it had an interesting x-ray afterglow extending beyond 10^5 s [28] (figure 9). The soft gamma-ray extension, lasting up to 200 s, when extrapolated to the x-ray range overlaps well with the beginning of the XRT afterglow, which between 100 and 300 s has $\alpha \sim -2$, followed by a much steeper drop $\alpha \sim -5 - 7$ out to ∼600 s, then a more

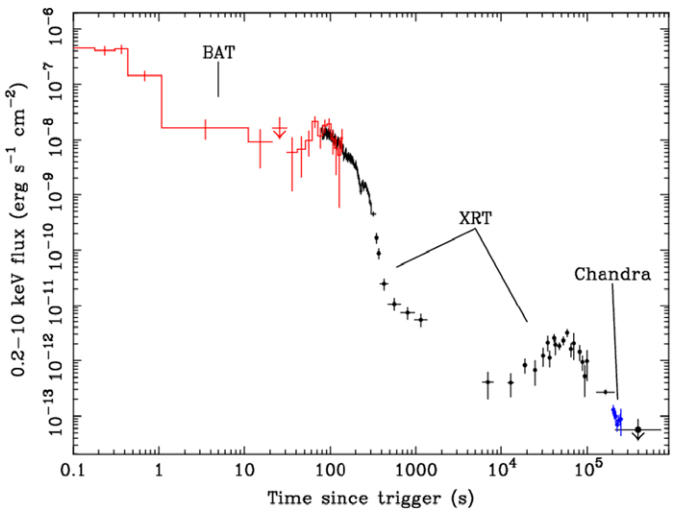

Figure 9. The afterglow of GRB 050724 [28], showing the Swift results on the prompt BAT emission extrapolated to the x-ray range and the subsequent XRT emission, as well as the late Chandra follow-up.

moderate decay $\alpha \sim -1$. An unexpected feature is a strong flare peaking at 5×10^4 s, whose energy is 10% of the prompt emission, while its amplitude is a 10 times increase over the preceding slow decay. Among more recent Swift short bursts, GRB 050813 [421, 454] had an x-ray afterglow, a possible elliptical host, and was reported to be near a galaxy cluster at $z = 1.7$–1.9 [41]. GRB 051210 [262] had an x-ray power law afterglow, with bumps or flares, and optical identifications are still under consideration. GRB 051221a had x-ray and optical afterglows, and the host is a star forming galaxy at $z = 0.55$ [461].

7.2. Short GRB prompt and afterglow emission

The main challenges for an understanding of the mechanism of short bursts are the relatively long, soft tail of the prompt emission and the strength and late occurrence of the x-ray bumps or flares. A possible explanation for the extended long soft tails ($\sim$100 s) may be that the compact binary progenitor is a black hole—neutron star system [28], for which analytical and numerical arguments ([93], and references therein) suggest that the disruption and swallowing by the black hole may lead to a complex and more extended accretion rate than for double neutron stars (cf [325, 113]). The flares, for which the simplest interpretation might be to ascribe them to refreshed shocks (compatible with a short engine duration $T \lesssim t_\gamma \sim 2$ s and a distribution of Lorentz factors), require the energy in the slow material to be at least ten times as energetic as the fast material responsible for the prompt emission, for the GRB 050724 flare at 10^4 s. The rise and decay times are moderate enough for this interpretation within the errors. On the other hand, if the decay slope is -2.8, this is steeper than expected for refreshed shocks but consistent with the high-latitude $-2-\beta$ model; a time origin t_0 can be determined at the beginning of the flare, and late Chandra observations indicate that the decay after that resumes where it had left off before the flare, which is more consistent with a late engine activity interpretation [278], requiring a factor 10 less energy budget than the refreshed shock interpretation. Another interpretation for such flares might be an accretion-induced collapse of a white dwarf in a binary, leading to a flare when the fireball created by the collapse hits the

companion [290], which might explain moderate energy one-time flares of duration $\lesssim 10^2$ s. However, for repeated, energetic flares, as also in the long bursts, the total energetics are easier to satisfy if one postulates late central engine activity (lasting at least half a day), containing $\sim$10% of the prompt fluence [28]. A possible way to produce this might be temporary choking up of an MHD outflow [393] (cf [490]), which might also imply a linear polarization of the x-ray flare [115]. Such MHD effects could plausibly also explain the initial $\sim$100 s soft tail. Another magnetic mechanism proposed for late x-ray flares in short bursts invokes a temporary post-merger massive neutron star [88]. However, a justification for substantial $\gtrsim 10^5$ s features remains so far on rather tentative grounds.

The similarity of the x-ray afterglow light curve with those of long bursts is, in itself, an argument in favour of the prevalent view that the afterglows of both long and short bursts can be described by the same paradigm, independently of any difference in the progenitors. This impression is reinforced by the fact that the x-ray light curve temporal slope is, on average, that expected from the usual forward shock afterglow model and that in GRB 050724 the x-ray afterglow shows what appears like an initial steep decay, a normal decay and a significant bump or flare. The identification of jet breaks in short bursts is still preliminary and the subject of debate. In two short bursts (so far) evidence has been reported for a jet break [37, 62, 360]. (However, in GRB 050724 a late Chandra observation indicates no x-ray break [190].) Taking these breaks as jet breaks, the average isotropic energy of these SHBs is a factor $\sim$100 smaller, while the average jet opening angle (based on the two breaks) is a factor $\sim$2 larger than those of typical long GRBs [136, 360]. Using standard afterglow theory, the bulk Lorentz factor decay can be expressed through $\Gamma(t_d) = 6.5(n_0/E_{50})^{1/8} t_d^{-3/8}$, where $t_d = (t/\mathrm{day})$, n_0 is the external density in units of cm^{-3} and E_{50} is the isotropic equivalent energy in units of 10^{50} ergs. If the jet break occurs at $\Gamma(t_j) = \theta_j^{-1}$, for a single-sided jet, the jet opening angle and the total jet energy E_j are

$$\theta_j = 9^\circ (n_0/E_{50})^{1/8} t_{j,d}^{3/8}, \qquad E_\mathrm{j} = \pi \theta_j^2 E \sim 10^{49} n_0^{1/4} (E_{50} t_{j,d})^{3/4}\,\mathrm{erg}. \tag{39}$$

For the afterglows of GRB 050709 and GRB 050724, the standard afterglow expressions for the flux level as a function of time before and after the break lead to fits [360] which are not completely determined, allowing for GRB050709 either a very low or a moderately low external density and for GRB050724 a moderately low to large external density. The main uncertainty is in the jet break time, which is poorly sampled, and so far mainly in x-rays. A better determined case of an x-ray light curve break is that of GRB 051221a, where combined Swift XRT and Chandra observations indicate a late break at $t_j \sim 5$ days, leading to an estimated $\theta_j \sim 15^\circ$ [62]. This is similar to jet angles calculated numerically for compact merger scenarios by [6, 222]. It is worth noting, however, that there are some indications that light curve breaks may not (or not always) be achromatic [118, 371]. We note that chromatic breaks have been argued for in some long bursts, e.g. GRB 030329, suggesting different beam opening angles for the optical/x-ray and the radio components ([39]; see also [378]), and independently of whether this is the explanation, a similar phenomenon may be present in short bursts.

7.3. Short burst hosts and progenitors

The most dramatic impact of Swift concerning short GRB, after the discovery and characterization of the afterglows, has been in providing the first significant identifications of host galaxies, with the implications and constraints that this puts on the progenitor issue. Out of ten short bursts detected until the end of 2005, four of the hosts (GRB 040924, 050509b, 050724 and 050813; [28, 37, 161]) are elliptical galaxies, one (GRB 050709, [135]) is a nearby irregular galaxy and one (GRB 050906, [220]) is a star-forming galaxy. The number of elliptical hosts is

of significant interest for the most frequently discussed progenitor of short GRB, the merger of neutron star binaries [28, 109, 269, 353], which would be relatively much more plentiful in old stellar population galaxies such as ellipticals. The argument partly depends on the expected long binary merger times, which in early population synthesis and merger simulations [51] was taken to be in excess of 10^8 years. More recent populations' synthesis calculations [32] have reduced this to the point where compact mergers could be expected in substantial numbers also in young, e.g. star-forming galaxies, although statistically most mergers would be expected in old galaxies. The preponderance of claimed elliptical hosts, where star formation is absent, argues against alternative short burst origins such as short-lived outflows from massive stellar collapses [489]. The lack of any observed supernova emission weeks after the burst [135, 205] also argues against a massive stellar collapse (where an Ib/c supernova could be expected) and also against a gravitational collapse of C/O white dwarfs to neutron stars leading to a supernova Ia [80].

An alternative interpretation of short bursts is that they may be the initial brief, hard spike seen in giant flares of soft gamma repeaters or SGR [214, 359]. SGRs must be young objects, due to the fast field decay rate, and the total energy in giant SGR flares detected so far is at least two orders of magnitude too small to explain the short burst fluxes detected at $z \gtrsim 0.2$. The lack of recent star formation activity in the four mentioned elliptical hosts also indicates that at least some short bursts cannot be ascribed to SGRs. A statistical analysis indicates that the fraction of short bursts which could be due to SGRs is less than 15% (or less than 40% at 95% confidence level) [339]. It is interesting that a correlation analysis of short bursts with x-ray selected galaxy clusters [169] gives a better than 2σ angular cross-correlation with clusters up to $z = 0.1$, which compared with model predictions would indicate that most short bursts originate within ∼270 Mpc. Any connection between alternative candidates and a possible third category of bursts, intermediate between short and long [207, 208, 305, 330], remains so far unexplored.

7.4. Short burst redshifts and progenitor lifetimes

With over a half dozen reasonably well-studied short bursts (as of end of 2005), their distribution in redshift space and among host galaxy types, including both ellipticals and spiral/irregulars [392], is similar to that of other old population objects and thus is compatible with neutron star binaries or black hole-neutron star binaries [338]. This progenitor identification, however, cannot be considered secure, so far. Nonetheless, the most striking thing about short hard burst (or SHBs) hosts is that it includes a number of ellipticals, with low star formation rate (SFR), e.g. 050909b, 050724; and even for those SHBs with star forming hosts, e.g. 050709, 051221a, the SFR is lower than the median SFR for the long GRB hosts [41]. This confirms that they are a distinct population, as indicated also by their intrinsic spectral-temporal properties versus those of long bursts [19, 246, 346]. Using the BATSE flux distribution and the observed redshifts, the SHB local rates are inferred to be at least $\sim 10\,\mathrm{Gpc}^{-3}\,\mathrm{yr}^{-1}$ [194, 338] without beaming corrections and larger including beaming. The progenitor lifetimes lead to interesting constraints, e.g. the simple time delay distribution $P(t) \propto t^{-1}$ expected from galactic double neutron star systems appears in conflict with the low average redshift of SHBs [158, 338], although it is not ruled out [194]. This has led to inferring a typical lifetime for the progenitors of ∼6 Gyr and the suggestion that they might be neutron star-black hole binaries, rather than double neutron stars. However if the redshift $z \approx 1.8$ for GRB 050813 is correct, the lifetime of the progenitor would be constrained to $\lesssim 10^3$ Gyr [41]. On the other hand, consideration of the star formation history of both early and late type galaxies suggests that at least half of the SHB progenitors have lifetimes in excess of ∼10 Gyr [547]. Population synthesis models of

double compact binaries [31] indicate two populations, with short (10^{-2}–0.2 Myr) and long (10^2–10^4 Myr) merger times, with NS–NS and BH–NS binaries distributed roughly 1 : 1 and 4 : 1 between these two merger time ranges, in apparent agreement with current SHB redshift and host distributions between ellipticals and SFR galaxies. The origin of a fraction of double neutron stars in globular clusters [189] would help to explain short bursts which are offset from their host galaxy.

8. Long GRB progenitors in light of Swift

8.1. Long GRB hosts and progenitors

Out of the ∼90 long bursts ($t_\gamma \gtrsim 2$ s) detected by Swift up to the end of 2005, in all the cases where a host galaxy was identified this was of an early type, usually a blue star-forming galaxy [54, 455, 468]. This was also the case for the some thirty cases measured by Beppo-SAX (e.g. [483] in the previous seven years. More recent observational studies have also indicated that the long GRB host galaxy metallicity is generally lower than that of the average massive star forming galaxies [270, 271, 468]. This has implications for the expected redshift distribution of GRB [344] (cf [49, 524, 22]), indicating that ∼40% of long GRB may originate from $z \gtrsim 4$. Long GRB may, in principle, be detectable up to $z \lesssim 25$–30 [70, 261, 175].

The preponderance of short-lived massive star formation in such young galaxies, as well as the identification of an SN Ib/c light curve peaking weeks after the burst in a few cases, has provided strong support for a massive stellar collapse origin of long GRBs, as argued by [356, 528, 529]. The relatively long duration of the gamma-ray emission stage in these bursts ($2\ \mathrm{s} \lesssim t_\gamma \lesssim 10^3$ s) is generally ascribed to a correspondingly long duration for the accretion of the debris [292, 389] falling into the central black hole which must form as the core of massive star collapses. (For initial stellar masses in excess of about 28–30 $M_\odot$, the core is expected to collapse to a BH, e.g. [147], while for smaller initial masses $10\,M_\odot \lesssim M_* \lesssim 28\,M_\odot$ the collapsing core mass is below the Chandrasekhar mass and is expected to lead to a neutron star.) This accretion onto the black hole feeds a relativistic jet, which breaks through the infalling core and the stellar envelope along the direction of the rotation axis.

A related massive core collapse mechanism has been considered by [488, 489] taking into account MHD effects in the disc and BH, in which the basic accretion time is short enough to be identified with short bursts, but magnetic tension can result in suspended accretion leading to long bursts. A mechanism based on the shorting of a charge separation built up around newly formed black holes has been discussed by [432, 433]. Other mechanism invoked include collapse of a neutron star to a strange star (e.g. [35, 68, 105]. The most widely adopted scenario, from this list, is the first one, in which the long GRB derive their energy from either the gravitational energy liberated by the torus of debris accreting onto the central BH formed by the massive core collapse or by the extraction of the rotational energy of the BH, mediated by the presence of the debris torus, whose accretion lifetime in both the cases is identified with the duration of the 'prompt' gamma-ray emitting phase of the burst.

8.2. Supernova connection

In the year following the launch of Swift no supernovae were identified in association with GRB. In fact, there are some upper limits on possible supernovae, the most notable ones being on the short bursts GRB 050509b [205] and GRB 050709 [135]. However, from the previous eight-year period there are two well-documented cases of supernovae associated with long bursts and several more weaker cases, where the evidence suggests a long GRB–SN

connection. The first evidence for a long GRB-supernova association was discovered in GRB 980425, which appeared associated with SN 1998bw [156, 250]. This was a peculiar, more energetic than usual Type Ib/c supernova, where the apparently associated GRBs properties seemed the same as usual, except for the redshift being extremely small ($z \sim 0.0085$). This implied the lowest ever long GRB isotropic equivalent energy $E_\gamma \sim 10^{48}$ erg, which resulted in the association being treated cautiously. However, using SN 1998bw as a template, other possible associations were soon claimed through detection of reddened bumps in the optical afterglow light-curves after a time delay compatible with a supernova brightness rise-time, e.g. in GRB 980326 [51], GRB 970228 [157, 412], GRB 000911 [263], GRB 991208 [66], GRB 990712 [442], GRB 011121 [52] and GRB 020405 [391].

The first unambiguous GRB–SN association was identified in GRB 030329, at a redshift $z = 0.169$, through both a supernova light-curve reddened bump and, more convincingly, by measuring in it a supernova spectrum of type Ib/c (i.e. the same type as in 1998bw) [204,467]. As a corollary, this observation rules out the 'supra-nova' model [498], in which a core collapse to neutron star and a supernova was assumed to occur months before a second collapse of the NS into a BH and a GRB; the delay between GRB 030329 and SN 2003dh is less than two days and is compatible with both events being simultaneous [204]. For pre-Swift GRB–SN associations, see, e.g. [534, 535].

More recently, Swift observed with all three instruments, BAT, XRT and UVOT, an unusually long (∼2000 s), soft burst, GRB 060218 [64], which was found to be associated with SN2006aj, a very nearby ($z = 0.033$) type Ic supernova [71, 326, 327, 466, 296, 381]. This supernova light curve peaked earlier than most known supernovae, and its time origin can also be constrained to be within less than a day from the GRB trigger. This is the first time that a connected GRB and supernova event has been observed starting in the first ∼100 s in x-rays and UV/Optical light, and the results are of great interest. The early x-ray light curve shows a slow rise and plateau followed by a drop after $\sim 10^3$ s, with a power law spectrum and an increasing black-body like component which dominates at the end. The most interesting interpretation involves shock breakout of a semi-relativistic component in a WR progenitor wind [64] (cf [119, 474]). After this a more conventional x-ray power law decay follows, and a UV component peak at a later time can be interpreted as being due to the slower supernova envelope shock. Another GRB/SN detection based on Swift afterglow observations is that associated with GRB 050525A [95].

8.3. Jet dynamics, cocoons and progenitors

For both long and short bursts, the most widely discussed central engine invokes a central black hole and a surrounding torus, either produced by a massive stellar core collapse (long bursts) or the merger of NS–NS or NS–BH binaries (short bursts). The latter mechanism is observationally on a less firm footing than the first, and in both collapse and merger cases the black hole could be preceded by a temporary massive, highly magnetized neutron star. There are two ultimate energy sources: the gravitational binding energy of the torus and the spin energy of the black hole. A possible third is the magnetic energy stored during the collapse, which derives its energy from the other two. Two main ways have been discussed for extracting the accretion energy and black hole spin energy, namely a neutrino-drive wind [109, 150, 292, 430, 431], and the Blandford–Znajek [48] mechanism. Both mechanisms lead to an optically thick $e^{\pm}$ jet or fireball, but the second is dynamically Poynting-dominated, i.e. dominated by strong magnetic fields threading the black hole [274, 286, 314, 486]. Needless to say, identification of the content of the fireball and the mechanism of GRB prompt emission would shed light on the mechanism that powers the central engine. Hence the excitement

following claims of a very large gamma-ray polarization in GRB 021206 [74] suggesting a strongly magnetized central engine. This observation has been challenged [434, 526]. A strong gamma-ray polarization could in principle be expected from a pure Poynting-flux dominated jet [288] or in a baryonic hydrodynamic jet with a globally organized magnetic field configuration [176, 178, 513]. A strong but less extreme magnetization of the jet is inferred from a combined reverse–forward shock emission analysis of GRB 990123 [114, 542].

In all models, an $e^{\pm}, \gamma$ fireball is expected as a result of the dissipation associated with the transient core collapse or merger event. The initial chaotic motions and shears are also expected to lead to a build-up of significant magnetic stresses [477]. A combination of the relativistic lepton ($e^{\pm}$) and MHD fields up to $\sim 10^{15}$ Gauss can provide the driving stresses leading to a highly relativistic expansion with $\Gamma_j \gg 1$. The fireball is very likely also to involve some fraction of baryons, and uncertainties in this 'baryon pollution' [354] remain difficult to quantify until 3D MHD calculations capable of addressing baryon entrainment become available. If the progenitor is a massive star, the expectation is that the fireball will likely be substantially collimated, due to the transverse containing pressure of the stellar envelope, which, if fast-rotating, provides a natural fireball escape route along the centrifugally lightened rotation axis.

The development of a jet and its Lorentz factor in a collapsar has been discussed analytically in [265, 297, 319, 519]. The essence of the dynamics of the jet in a burst from a massive star is that as long as the central BH accretes, it injects along the rotation axis a relativistic jet, whose dimensionless entropy must be comparable to or larger than the final bulk Lorentz factor of the jet once it has emerged from the star, $\eta = (L/\dot{M}c^2) \gtrsim \Gamma_j \gtrsim 100$. Even though such a jet is highly relativistic as it is injected, the overburden of the stellar core and envelope slow the progress of the jet head down to a sub-relativistic speed of advance, which gradually increases as the jet moves down the density gradient of the star. The difference between the injection and advance speed causes gas and energy spill-over into a transrelativistic cocoon of waste heat [265, 297, 319] surrounding the jet, which may be detectable [376, 403]. By the time it reaches the boundary of the He core ($R_{\rm He} \sim 10^{11}$ cm) the jet head has reached a speed $v_j \sim c$. This takes, in the star's frame, $\sim$10 s, hence the central engine must continue injecting energy and momentum into the jet for at least this long. A very sharp drop in density is predicted by stellar models at this radius, beyond which a tenuous hydrogen envelope extends as a power law. In going down this sharp gradient, the jet head Lorentz factor shoots up to a value comparable to its final value, $\Gamma_j \gtrsim 100$ ([319, 519]).Once the jet head is relativistic, it becomes ballistic, and it is no longer affected by whether the central engine energy injection continues or not. A constraint on the mass of the envelope is that the mass overburden within the jet solid angle must be less than the jet total energy divided by $\Gamma_j c^2$ ([297]). If the star has lost its H envelope, this condition is guaranteed, e.g. as in Wolf–Rayet type stars, where a stellar wind phase leads to envelope loss previous to the core collapse phase. WR stars are, in fact, thought to be the progenitors of type Ib/c supernovae, which is the only type so far seen in a few cases associated with GRB. A modest envelope, however, should still be compatible with a high Lorentz factor, which could be tested through detection of weak H lines in a GRB associated supernova (and may also be tested through tera-electron-volt neutrino observations, [407]).

The 2D development of a relativistic jet making its way out through a star have been calculated numerically by e.g. [5, 546], while magnetically dominated jets are discussed by [106, 394, 523]. Jets in compact mergers have been calculated numerically by [6, 222]. The relativistic numerical calculations of GRB jets are, so far, mainly hydrodynamic and involve approximations about the energy and momentum injection at the lower boundary, the numerical difficulties in covering the entire dynamical range being extreme. The results [546] show that a jet of $\Gamma_j \sim 100$ can escape a star of radius comparable to a WR ($R_* \sim 10^{11}$ cm).

The angular structure of the jet is, as expected, one where the Lorentz factor and energy per solid angle tapers off towards the edges, where instabilities cause mixing with and drag by the stellar envelope walls. An analytical argument [265] shows that this tapering off can result in an energy profile $E_{\rm j}(\theta) \propto \theta^{-2}$. Such a jet profile is a possible interpretation [424, 540] of the observational correlation between the isotropic equivalent jet energy and the jet break time derived from a sample of burst afterglows [140, 362].

9. Very high energy photons and non-electromagnetic emission

The highly relativistic nature of the outflows is inferred from and constrained by the observations of giga-electron volt photons, which indicate the need for bulk Lorentz factors of $\Gamma \gtrsim 10^2$ [25,123,199]. Such Lorentz factors result in synchrotron spectra which in the observer frame extend beyond 100 MeV, and inverse Compton (IC) scattering of such synchrotron photons leads to the expectation of GeV and TeV spectral components [312]. While $\lesssim$18 GeV photons have been observed (e.g. [213]), TeV photons are likely to be degraded to lower energies by $\gamma\gamma$ pair production, either in the source itself or (unless the GRB is at very low redshifts) in the intervening intergalactic medium [75, 94].

Besides emitting in the currently studied sub-GeV electromagnetic channels, GRBs are likely to be even more luminous in other channels, such as neutrinos, gravitational waves and cosmic rays. For instance, nucleons entrained in the fireball will have $\gtrsim$100 GeV bulk kinetic energies in the observer frame, which can lead to inelastic collisions resulting in pions, muons, neutrinos and electrons as well as their anti-particles. The main targets for the relativistic baryons are other particles in the relativistic outflow and particles in the external, slower moving environment. The expected flux and spectrum of 1–30 GeV neutrinos and γ-rays resulting from pion decay due to interactions within the expanding plasma depends, for example, on the neutron/proton ratio and on fireball inhomogeneities, while that due to interactions with the surrounding medium depends on the external gas density and its distribution; and both depend on the Lorentz factor. Massive progenitors offer denser targets for nuclear collisions and a larger photon density for $p\gamma$ and $\gamma\gamma$ interactions, leading to modification of the photon spectra. On the other hand GRB from NS–NS mergers would be characterized by neutron-rich outflows, leading to stronger 5–10 GeV neutrinos and photons from np collisions [18,34,426]. Photo-pion signatures of $\gtrsim$100 GeV photons and 10^{14}–10^{18} eV neutrinos may be expected to be relatively stronger in massive (high soft photon density) progenitors. Knowing what fraction of GRB, if any, arises from NS mergers is vital for facilitating interferometric gravitational wave detections, e.g. with LIGO. And, conversely, detection with LIGO would provide important clues as to whether short bursts are NS–NS (or NS–BH) mergers or whether massive stellar collapses are asymmetric enough to produce substantial gravitational wave emission and serve as a test of the relationship between long GRB and supernovae.

The Fermi mechanism in shocks developing in the GRB outflow can also accelerate protons to observer-frame energies of up to $\sim 10^{20}$ eV [506,508]. Internal shocks leading to the observed γ-rays have a high comoving photon density and lead to $p\gamma$ photopion production and to $\gtrsim$100 TeV neutrinos [515]. In external shocks due to deceleration by the external medium, the reverse shock moving into the ejecta can produce optical photons (section 5.2) which result in photopion production and $\gtrsim 10^{19}$ eV neutrinos [516]. Neutrinos in the TeV to EeV range may be easier to detect than those at $\sim$10 GeV energies, due to their higher interaction cross section, with instruments currently under construction. Such neutrinos would serve as diagnostics of the presence of relativistic shocks and as probes of the acceleration mechanism and the magnetic field strength. The flux and spectrum of $\gtrsim 10^{19}$ eV neutrinos depends on the density of the surrounding gas, while the $\gtrsim 10^{14}$ eV neutrinos depend on the fireball Lorentz

factor. Hence, the detection of very high energy neutrinos would provide crucial constraints on the fireball parameters and GRB environment.

9.1. UHE photons from GRB

Ultra-high energy emission, in the range of GeV and harder, is expected from electron inverse Compton in external shocks [312] as well as from internal shocks [372] in the prompt phase. The combination of prompt MeV radiation from internal shocks and a more prolonged GeV IC component for external shocks [311] is a likely explanation for the delayed GeV emission seen in some GRB [213]. (The alternative invoking photomeson processes from ejecta protons impacting a nearby binary stellar companion are given in [227].) The GeV photon emission from the long-term IC component in external afterglow shocks has been considered by [99, 100, 539, 501, 502]. The IC GeV photon component is likely to be significantly more important [539] than a possible proton synchrotron or electron synchrotron component at these energies. Another possible contributor at these energies may be π^0 decay from $p\gamma$ interactions between shock-accelerated protons and MeV or other photons in the GRAB shock region [58, 142, 479]. However, under the conservative assumption that the relativistic proton energy does not exceed the energy in relativistic electrons or in γ-rays and that the proton spectral index is -2.2 instead of -2, both the proton synchrotron and the $p\gamma$ components can be shown to be substantially less important at GeV–TeV than the IC component [539]. Another GeV photon component is expected from the fact that in a baryonic GRB outflow neutrons are likely to be present, and when these decouple from the protons, before any shocks occur, pn inelastic collisions will lead to pions, including π^0, resulting in UHE photons which cascade down to the GeV range [18, 101, 426]. The final GeV spectrum results from a complex cascade, but a rough estimate indicates that 1–10 GeV flux should be detectable [18] with GLAST [172] for bursts at $z \lesssim 0.1$.

In these models, due to the high photon densities implied by GRB models, $\gamma\gamma$ absorption within the GRB emission region must be taken into account [23, 280, 397, 398, 409]. One interesting result is that the observation of photons up to a certain energy, say 10–20 GeV with EGRET, puts a lower limit on the bulk Lorentz factor of the outflow, from the fact that the compactness parameter (optical depth to $\gamma\gamma$) is directly proportional to the comoving photon density, and both these as well as the energy of the photons depend on the bulk Lorentz factor. This has been used by [280] to estimate lower limits on $\Gamma \lesssim 300$–600 for a number of specific bursts observed with EGRET. On the other hand, for GRB with $\Gamma \gtrsim 850$, TeV photons can escape the source [409].

Long GRBs have recently been shown to be associated with supernovae (section 8.2). If GRBs also accelerate cosmic rays, as suspected, then these could leave long-lasting UHE photon signatures in supernova remnants which were associated with GRBs at the time of their explosion. One example may be the SN remnant W49B, which may be a GRB remnant. A signature of a neutron admixture in the relativistic cosmic ray outflow would be a TeV gamma-ray signature due to inverse Compton interactions following neutron decay [217] (see also [13]). Continued magnetic outflows upscattering companion photons may also reveal GRB remnants [401]. The imaging of the surrounding emission could provide new constraints on the jet structure of the GRB.

The recent detection of delayed x-ray flares during the afterglow phase of gamma-ray bursts (GRBs) with the Swift satellite (e.g. [348, 370, 544]) suggests an inner-engine origin of these flares, at radii inside the deceleration radius characterizing the beginning of the forward shock afterglow emission. Given the observed temporal overlapping between the flares and afterglows, one expects an inverse Compton (IC) emission arising from such flare photons

scattered by forward shock afterglow electrons [504]. The jet may also IC upscatter shock break-out x-ray photons [405]. This IC emission would produce GeV–TeV flares, which may be detected by GLAST and ground-based TeV telescopes. The detection of GeV–TeV flares combined with low energy observations may help to constrain the poorly known magnetic field in afterglow shocks.

At higher energies, a tentative $\gtrsim$0.1 TeV detection at the 3σ level of GRB970417a has been reported with the water Cherenkov detector Milagrito [12]. Another possible TeV detection [388] of GRB971110 has been reported with the GRAND array, at the 2.7σ level. Stacking of data from the TIBET array for a large number of GRB time windows has led to an estimate of a $\sim 7\sigma$ composite detection significance [9]. Better sensitivity is expected from the upgraded larger version of MILAGRO, as well as from atmospheric Cherenkov telescopes under construction such as VERITAS, HESS, MAGIC and CANGAROO-III [128, 206, 209, 231, 470, 520, 352]. However, GRB detections in the TeV range are expected only for rare nearby events, since at this energy the mean free path against $\gamma\gamma$ absorption on the diffuse IR photon background is $\sim$ few hundred Mpc [75, 94]. The mean free path is much larger at GeV energies, and based on the handful of GRBs reported in this range with EGRET, several hundred should be detectable with large area space-based detectors such as GLAST [298, 539].

9.2. Cosmic rays from GRB

In the standard fireball shock model of the prompt γ-ray emission, say from internal shocks or magnetic dissipation, and also in the external afterglow shocks, the same acceleration mechanisms which lead to the non-thermal electron power laws implied by the observed photon spectra must also lead to proton acceleration. Using the shock parameters inferred from broad-band photon spectral fits, one infers that protons can be accelerated to Lorentz factors up to $\lesssim 10^{11}$ in the observer frame [495, 508], i.e. to so-called GZK energy of $E_p \sim 10^{20}$ eV. This is interesting mainly for 'baryonic' jets, where the bulk of the energy is carried by baryons, whereas in Poynting-dominated jets there would be much fewer protons to accelerate. Well below the GZK energy, protons interacting with the MeV photons present in GRB or with thermal nucleons are above the pion production threshold and can produce ultra-high energy neutrinos, as discussed below.

Discussions of GRB as cosmic ray sources are mainly oriented at exploring their contribution to the energy range above EeV (10^{18} eV; e.g. [506]), referred to as ultra-high energy cosmic rays or UHECRs. (A model where GRBs are responsible for CRs ranging from PeV to GZK is given in [527].) At EeV and higher energies the observed UHECR isotropy and the small expected magnetic deflection suggests an extra-galactic origin. The requirement that they are not attenuated by the cosmic microwave background through photomeson interactions constrains that they are originated within a volume inside a radius of 50–100 Mpc, the so-called 'GZK' volume [77]. Two broad classes of models suggested are the 'top–down' scenarios, which attribute UHECR to decay of fossil grand unification defects, and the 'bottom–up' scenarios, which assume UHECRs are accelerated in astrophysical sources. One of the most prominent candidate sources for bottom–up scenarios is GRBs [324, 495, 508] (two others are AGNs, e.g. [36] and cluster shocks, e.g. [216]). The most commonly discussed version of this scenario considers the UHECR to be protons accelerated in GRB internal shocks [506, 507, 508], while another version attributes them to acceleration in external shocks [102, 493, 495]. (For UHECR acceleration in alternative GRB models, see, e.g. [90, 122].)

The persuasiveness of this scenario is largely based on two coincidences, namely the required condition to accelerate protons to GZK energies is similar to the requirement for

generating the prompt observed gamma-rays in GRB and the observed UHECR energy injection rate into the universe ($\sim 3 \times 10^{44}\,\mathrm{erg\,Mpc^{-3}\,yr^{-1}}$) is similar to the local GRB γ-ray energy injection rate [495,508]. These coincidences have been questioned, e.g. [456,471], but these objections have been resolved using new data and further considerations [493,506], and GRBs remain a promising candidate for UHECRs. However, there are some caveats of principle. The internal shock scenario relies on the assumption that GRB prompted gamma-ray emission is due to internal shocks. Although this is the leading scenario, there is no strong proof so far, as is the case for the external shock (e.g. there are efficiency and spectrum issues, etc). On the other hand, a Poynting flux dominated GRB model would have to rely on magnetic dissipation and reconnection, accelerating electrons and hence also accelerating protons—but details remain to be investigated. The external shock model would have to rely on a magnetized medium [493] to reach the desired cosmic ray energy (as expected in pulsar wind bubbles [245] in the supranova scenario [498], which however has become less likely since the almost simultaneous GRB 030329/SN 2003dh and the more recent GRB 060218/SN2006aj association).

Direct confirmation of a GRB origin of UHECRs will be difficult. The next generation cosmic ray detectors such as the *Pierre Auger Observatory* [15] will have a substantially enhanced effective target area, which will greatly improve the cosmic ray count statistics. This will help to disentangle the two scenarios (top–down or bottom–up) and will reveal whether a GZK feature indeed exists. Within the bottom–up scenario, the directional information may either prove or significantly constrain the alternative AGN scenario and may eventually shed light on whether GRBs are indeed the sources of UHECRs.

9.3. UHE neutrinos contemporary with gamma-rays

Internal shocks in the GRB jet take place at a radius $r_i \sim 2\Gamma_i^2 c\delta t \sim 5 \times 10^{12}\delta t_{-3}\Gamma_{300}^2$ cm. Here $\Gamma_i = 300\,\Gamma_{300}$ is the bulk Lorentz factor of the GRB fireball ejecta and $\delta t = 10^{-3}\delta t_{-3}$ s is the variability time scale. Observed γ-rays are emitted from the GRB fireball when it becomes optically thin at a radius $\gtrsim r_i$. Shock accelerated protons interact dominantly with observed synchrotron photons with ∼MeV peak energy in the fireball to produce a Delta resonance, $p\gamma \rightarrow \Delta^+$ [515]. The threshold condition to produce a Δ^+ is $E_p E_\gamma = 0.2\Gamma_i^2\,\mathrm{GeV}^2$ in the observer frame, which corresponds to a proton energy of $E_p = 1.8 \times 10^7 E_{\gamma,\mathrm{MeV}}^{-1}\Gamma_{300}^2$ GeV. The subsequent decays $\Delta^+ \rightarrow n\pi^+ \rightarrow n\mu^+\nu_\mu \rightarrow ne^+\nu_e\bar{\nu}_\mu\nu_\mu$ produce high energy neutrinos in the GRB fireball contemporaneous with γ-rays [400,515]. Assuming that the secondary pions receive 20% of the proton energy per interaction and each secondary lepton shares 1/4 of the pion energy, each flavour of neutrino is emitted with 5% of the proton energy, dominantly in the PeV range.

The diffuse muon neutrino flux from GRB internal shocks due to proton acceleration and subsequent photopion losses is shown as the short dashed line in figure 10. The flux is compared with the Waxman–Bahcall limit of cosmic neutrinos, which is derived from the observed cosmic ray flux [516]. The fluxes of all neutrino flavours are expected to be equal after oscillation in vacuum over astrophysical distances.

The GRB afterglow arises as the jet fireball ejecta runs into the ambient inter-stellar medium (ISM), driving a blast wave ahead into it and a reverse shock back into the GRB jet ejecta. This (external) reverse shock takes place well beyond the internal shocks, at a radius $r_e \sim 4\Gamma_e^2 c\Delta t \sim 2 \times 10^{17}\Gamma_{250}^2\Delta t_{30}$ cm [516]. Here $\Gamma_e \approx 250\Gamma_{250}$ is the bulk Lorentz factor of the ejecta after the partial energy loss incurred in the internal shocks and $\Delta t = 30\Delta t_{30}$ s is the duration of the GRB jet. Neutrinos are produced in the external reverse shock due to $p\gamma$ interactions of internal shock accelerated protons predominantly with synchrotron soft x-ray

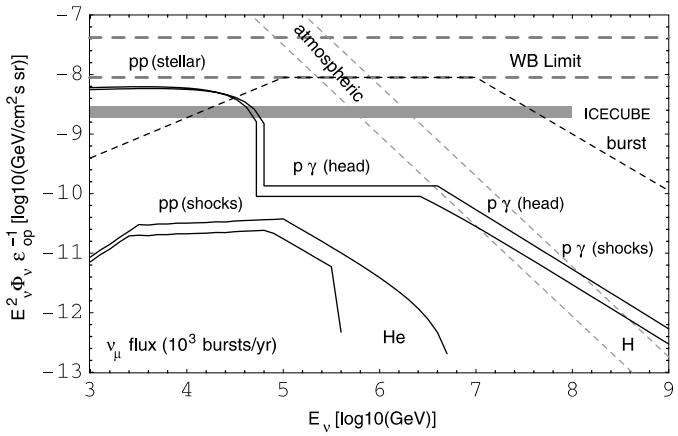

Figure 10. Diffuse muon neutrino flux arriving simultaneously with the γ-rays from shocks outside the stellar surface in observed GRB (dark short-dashed curve), compared to the Waxman–Bahcall (WB) diffuse cosmic ray bound (light long-dashed curves) and the atmospheric neutrino flux (light short-dashed curves). Also shown is the diffuse muon neutrino precursor flux (solid lines) from sub-stellar jet shocks in two GRB progenitor models, with stellar radii $r_{12.5}$ (H) and r_{11} (He). These neutrinos arrive 10–100 s before the γ-rays from electromagnetically detected bursts (with similar curves for ν_μ, ν_e and ν_τ) [407].

photons produced by the reverse shock. The efficiency of pion conversion from $p\gamma$ interactions in this afterglow scenario is much smaller than in the internal shocks [516].

In the case of a massive star progenitor the jet may be expanding into a wind, emitted by the progenitor prior to its collapse. In this case, the density of the surrounding medium, at the external shock radius, may be much higher than that of the typical ISM density of $n \simeq 1\,\mathrm{cm}^{-3}$. For a wind with mass loss rate of $10^{-5}\,M_\odot\,\mathrm{yr}^{-1}$ and velocity of $v_w = 10^3\,\mathrm{km\,s}^{-1}$, the wind density at the typical external shock radius would be $\simeq 10^4\,\mathrm{cm}^{-3}$. The higher density implies a lower Lorenz factor of the expanding plasma during the reverse shocks stage, and hence a larger fraction of proton energy lost to pion production. Protons of energy $E_p \gtrsim 10^{18}$ eV lose all their energy to pion production in this scenario [82, 497, 516] producing EeV neutrinos.

9.4. Precursor neutrinos

As discussed before, the core collapse of massive stars are the most likely candidates for long duration GRBs, which should lead to the formation of a relativistic jet initially buried inside the star. The jet burrows through the stellar material and may or may not break through the stellar envelope [323]. Internal shocks in the jet, while it is burrowing through the stellar interior, may produce high energy neutrinos through proton–proton (pp) and photomeson ($p\gamma$) interactions [407]. High energy neutrinos are produced through pion decays which are created both in pp and $p\gamma$ interactions. The jets which successfully penetrate through the stellar envelope result in GRBs (γ-ray bright bursts) and the jets which choke inside the stars do not produce GRBs (γ-ray dark bursts). However, in both the cases high energy neutrinos produced in the internal shocks are emitted through the stellar envelope since they interact very weakly with matter.

High energy neutrinos from the relativistic buried jets are emitted as precursors ($\sim$10–100 s prior) to the neutrinos emitted from the GRB fireball in the case of an electromagnetically observed burst. In the the case of a choked burst (electromagnetically undetectable) no direct detection of neutrinos from individual sources is possible. However the diffuse neutrino signal

is boosted up in both scenarios. The diffuse neutrino flux from two progenitor star models are shown in figure 10, one for a blue super-giant (labelled H) of radius $R_* = 3 \times 10^{12}$ cm and the other a Wof–Rayet type (labelled He) of radius $R_* = 10^{11}$ cm. The Waxman–Bahcall diffuse cosmic ray bound [518], the atmospheric flux and the IceCube sensitivity to diffuse flux are also plotted for comparison. The neutrino component which is contemporaneous with the gamma-ray emission (i.e. which arrives after the precursor) is shown as the dark dashed curve and is plotted assuming that protons lose all their energy to pions in $p\gamma$ interactions in internal shocks.

Most GRBs are located at cosmological distances (with redshift $z \sim 1$) and individual detection of them by kilometre scale neutrino telescopes may not be possible. The diffuse ν flux is then dominated by a few nearby bursts. The likeliest prospect for UHE ν detection is from these nearby GRBs in correlation with electromagnetic detection. Detection of ultrahigh energy neutrinos which point back to their sources may establish GRBs as the sources of GZK cosmic rays.

The detection of ultrahigh energy neutrinos by future experiments such as ICECUBE [215], ANITA [11], KM3NeT [234] and Auger [15] can provide useful information, such as particle acceleration, radiation mechanism and magnetic field, about the sources and their progenitors. High energy neutrino astrophysics is an imminent prospect, with Amanda already providing useful limits on the diffuse flux from GRB [29, 469] and with ICECUBE [3, 212] on its way. The detection of TeV and higher energy neutrinos from GRB would be of great importance for understanding these sources, as well as the acceleration mechanisms involved. It could provide evidence for the hadronic versus the MHD composition of the jets, and if observed, could serve as an unabsorbed probe of the highest redshift generation of star formation in the Universe.

9.5. Gravitational waves

The gamma-rays and the afterglows of GRB are thought to be produced at distances from the central engine where the plasma has become optically thin, $r \geqslant 10^{13}$ cm, which is much larger than the Schwarzschild radius of a stellar mass black hole (or of a neutron star). Hence we have only very indirect information about the inner parts of the central engine where the energy is generated. However, in any stellar progenitor model of GRB one expects that gravitational waves should be emitted from the immediate neighbourhood of the central engine, and their observation should give valuable information about its identity. Therefore, it is of interest to study the gravitational wave emission from GRB associated with specific progenitors. Another reason for doing this is that the present and foreseeable sensitivity of gravitational wave detectors is such that for likely sources, including GRB, the detections would be difficult, and for this reason, much effort has been devoted to the development of data analysis techniques that can reach deep into the detector noise. A coincidence between a gravitational wave signal and a gamma-ray signal would greatly enhance the statistical significance of the detection of the gravitational wave signal [130,248]. It is therefore of interest to examine the gravitational wave signals expected from various specific GRB progenitors that have been recently discussed, and based on current astrophysical models, to consider the range of rates and strains expected in each case, for comparison with the LIGO sensitivity. A general reference is [491], which also discusses GRB-related sources of gravitational waves.

Regardless of whether they are associated with GRBs, binary compact object mergers (NS–NS, NS–BH, BH–BH, BH–WD, BH–Helium star, etc) [78,154,223,238,248,380,430,478] and stellar core-collapses [92, 149, 238,420 487–489] have been studied as potential gravitational wave (GW) sources. These events are also leading candidates for being GRB progenitors, and a coincidence between a GW signal and a gamma-ray signal would greatly enhance the statistical significance of the former [130]. A binary coalescence process can be divided into three phases: in-spiral, merger and ring-down [129, 238]. For collapsars, a rapidly rotating

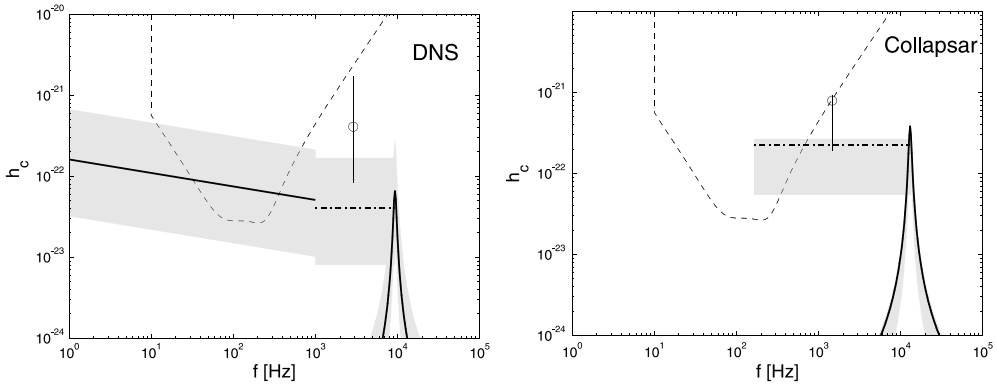

Figure 11. Gravitational wave strain from a double neutron merger (left) and a collapsar (right) compared with advanced LIGO sensitivity [238].

core could lead to development of a bar and to fragmentation instabilities which would produce similar GW signals as in the binary merger scenarios, although a larger uncertainty is involved. The GW frequencies of various phases cover the 10–10^3 Hz band which is relevant for the Laser Interferometer Gravitational-wave Observatory (LIGO) [279] and other related detectors such as VIRGO [500], GEO600 [164] and TAMA300 [473]. Because of the faint nature of the typical GW strain, only nearby sources (e.g. within ∼200 Mpc for NS–NS and NS–BH mergers and within ∼30 Mpc for collapsars) [238] have strong enough signals to be detectable by LIGO-II. When event rates are taken into account [30, 153], order of magnitude estimates indicate that after one-year operation of the advanced LIGO, one event for the in-spiral chirp signal of the NS–NS or NS–BH merger and probably one collapsar event (subject to uncertainties) would be detected [238]. Other binary merger scenarios such as BH–WD and BH–Helium star mergers are unlikely to be detectable [238], and they are also unfavoured as sources of GRBs according to other arguments [349].

A time-integrated GW luminosity of the order of a solar rest mass ($\lesssim 10^{54}$ erg) is predicted from merging NS–NS and NS–BH models [248,331,431], while the luminosity from collapsar models is more model-dependent but expected to be lower ([148, 328]; cf [487]). Specific estimates have been made of the GW strains from some of the most widely discussed current GRB progenitor stellar systems [238]. The expected detection rates of gravitational wave events with LIGO from compact binary mergers, in coincidence with GRBs, have been estimated by [130, 131]. If some fraction of GRBs is produced by DNS or NS–BH mergers, the gravitational wave chirp signal of the in-spiral phase should be detectable by the advanced LIGO within one year, associated with the GRB electromagnetic signal. One also expects signals from the black hole ring-down phase, as well as the possible contribution of a bar configuration from gravitational instability in the accretion disc following tidal disruption or infall in GRB scenarios.

The most promising GW–GRB candidates in terms of detections per year are the DNS and BH–NS mergers [238] (figure 11), based on assumed mean distances from the formation rates estimated by [153]. More recent rate estimates are given in [491], and rates incorporating new information relating to Swift short GRB detections are given in [31, 338]. Other binary progenitor scenarios, such as black hole–helium star and black hole–white dwarf merger GRB progenitors, are unlikely to be detectable, due to the low estimates obtained for the maximum non-axisymmetrical perturbations.

For the massive rotating stellar collapse (collapsar) scenario of GRB, the non-axisymmetrical perturbations are very uncertain, but may be strong [92, 149, 488], and the

estimated formation rates are much higher than for other progenitors [32, 149], with typically lower mean distances to the Earth. For such long GRB the rate estimates must incorporate the beaming correction [491]. This type of scenario is of special interest, since it has the most observational support from GRB afterglow observations. For collapsars, in the absence of detailed numerical 3D calculations specifically aimed at GRB progenitors, estimates were made [238] of the strongest signals that might be expected in the case of bar instabilities occurring in the accretion disc around the resulting black hole and in the maximal version of the recently proposed fragmentation scenario of the infalling cores. Although the waveforms of the gravitational waves produced in the break-up, merger and/or bar instability phase of collapsars are not known, a cross-correlation technique can be used making use of two co-aligned detectors. Under these assumptions, collapsar GRB models would be expected to be marginally detectable as gravitational wave sources by the advanced LIGO within one year of observations. Figure 11 depicts the characteristic GW strains for the double neutrons star merger and the collapsar model.

Other calculations of massive stellar collapse GRB [488, 489] take into account MHD effects in the disc and BH. More general studies of massive stellar core collapse event gravitational wave emission are presented in [151], considering both the core collapse SN and the progenitors of long GRB.

In the case of binaries the matched filtering technique can be used, while for sources such as collapsars, where the wave forms are uncertain, the simultaneous detection by two elements of a gravitational wave interferometer, coupled with electromagnetic simultaneous detection, provides a possible detection technique. Specific detection estimates have been made [238, 491] for both the compact binary scenarios and the collapsar scenarios,

Both the compact merger and the collapsar models have in common a high angular rotation rate, and observations provide evidence for jet collimation of the photon emission, with properties depending on the polar angle, which may also be of relevance for x-ray flashes. Calculations have been made [239] of the gravitational wave emission and its polarization as a function of angle expected from such sources. The GRB progenitors emit $l = m = 2$ gravitational waves, which are circularly polarized on the polar axis, while the + polarization dominates on the equatorial plane. Recent GRB studies suggest that the wide variation in the apparent luminosity of GRBs is caused by differences in the viewing angle or possibly also in the jet opening angle. Since GRB jets are launched along the polar axis of GRB progenitors, correlations among the apparent luminosity of GRBs ($L_\gamma(\theta) \propto \theta^{-2}$ and the amplitude as well as the degree of linear polarization P degree of the gravitational waves are expected, $P \propto \theta^4 \propto L_\gamma^{-2}$. At a viewing angle larger than the jet opening angle θ_j the GRB γ-ray emission may not be detected. However, in such cases an 'orphan' (see, e.g. [211, 406, 548]) long-wavelength afterglow could be observed, which would be preceded by a pulse of gravitational waves with a significant linearly polarized component. As the jet slows down and reaches $\gamma \sim \theta_j^{-1}$, the jet begins to expand laterally, and its electromagnetic radiation begins to be observable over increasingly wider viewing angles. Since the opening angle increases as $\sim \gamma^{-1} \propto t^{1/2}$, at a viewing angle $\theta > \theta_j$, the orphan afterglow begins to be observed (or peaks) at a time $t_p \propto \theta^2$ after the detection of the gravitational wave burst. The polarization degree and the peak time should be correlated as $P \propto t_p^2$.

Gravitational wave burst searches are underway with LIGO. The results from the third science run [1] searched for sub-second bursts in the frequency range 100–1100 Hz for which no waveform model is assumed, with a sensitivity in terms of the root-sum-square (rss) strain amplitude of $h_{rss} \sim 10^{-20}\,\mathrm{Hz}^{-1/2}$. No gravitational-wave signals were detected in the eight days of analysed data for this run. The search continues, as LIGO continues to be upgraded towards it ultimate target sensitivity.

Acknowledgments

Research partially supported through NSF AST 0307376 and NASA NAG5-13286. I am grateful for useful comments from two referees, as well as from P Kumar, N Gehrels, L Gou, E Ramirez-Ruiz, S Razzaque, M J Rees, X Y Wang and B Zhang.

References

[1] Abbot B *et al* 2006 *Class. Quantum. Grav.* **23** 29
[2] Achterberg A *et al* 2001 *Mon. Not. R. Astron. Soc.* **328** 393
[3] Ahrens J *et al* 2004 *New AR* **48** 519
[4] Akerlof K *et al* 1999 *Nature* **398** 400
[5] Aloy M *et al* 2000 *Astrophys. J.* **531** L119
[6] Aloy M, Janka H and Mueller E 2005 *Astron. Astrophys.* **436** 273
[7] Amati L *et al* 2001 *AIP Conf. Proc.* **599** 493
[8] Amati L *et al* 2002 *Astron. Astrophys.* **390** 81
[9] Amenomori M *et al* 2001 *AIP Conf. Proc.* **558** 844
[10] Andersen M I and Pedersen H 2004 *Astron. Nachrichten* **325** 490
[11] ANITA http://www.ps.uci.edu/ anita/
[12] Atkins R *et al* 2000 *Astrophys. J.* **533** L119
[13] Atoyan A, Buckley J and Krawczynski H 2006 *Astrophys. J.* **642** L153
[14] Pierre Auger experiment http://www.auger.org/
[15] AUGER http://www.auger.org/
[16] Bagoly Z *et al* 2002 *Astron. Astrophys.* **398** 919
[17] Bagoly Z *et al* 2006 *Astron. Astrophys.* (*Preprint*) astro-ph/0604326 at press
[18] Bahcall J N and Mészáros P 2000 *Phys. Rev. Lett.* **85** 1362
[19] Balázs L, Bagoly Z, Horváth I, Mészáros A and Mészáros P 2003 *Astron. Astrophys.* **401** 129–40
[20] Band D *et al* 1993 *Astrophys. J.* **413** 281
[21] Band D 2006 *Astrophys. J.* (*Preprint*) astro-ph/0602267 at press
[22] Band D, Norris J and Bonnell J 2004 *Astrophys. J.* **613** 484
[23] Baring M 2000 *AIP Conf. Proc.* **515** 238
[24] Baring M and Braby M 2004 *Astrophys. J.* **613** 460
[25] Baring M and Harding A 1997 *Astrophys. J.* **491** 663
[26] Barraud C *et al* 2004 *AIP Conf. Proc.* **727** 81
[27] Barthelmy S *et al* 2005 *Nature* **438** 994
[28] Barthelmy S *et al* 2005 *Nature* **438** 994
[29] Becker J *et al* 2006 *Astropart. Phys.* **25** 118–28
[30] Belczynski K, Bulik T and Rudak B 2002 *Astrophys. J.* **571** 394
[31] Belczynski K *et al* 2006 *Astrophys. J.* (*Preprint*) astro-ph/0601458 submitted
[32] Belczynski K, Bulik T and Rudak B 2002 *Astrophys. J.* **571** 394
[33] Beloborodov A 2000 *Astrophys. J.* **539** L29
[34] Beloborodov A M 2003 *Astrophys. J.* **588** 931
[35] Berezhiani Z *et al* 2003 *Astrophys. J.* **586** 1250
[36] Berezinsky V S, Gazizov A Z and Grigorieva S I 2005 *Phys. Lett.* B **612** 147
[37] Berger E *et al* 2005 *Astrophys. J.* **634** 501
[38] Berger E, Kulkarni S R and Frail D 2003 *Astrophys. J.* **590** 379
[39] Berger E *et al* 2003 *Nature* **426** 154
[40] Berger E 2004 *Astron. Soc. Pacific Conf. Series* **312** 163
[41] Berger E 2005 *Proc. Gamma Ray Bursts in the Swift Era (Washington, DC)* ed S Holt *et al AIP Conf. Proc.* (*Preprint*) astro-ph/0602004 at press
[42] Berger E *et al* 2005b *Astrophys. J.* **634** 501
[43] Bianco C L and Ruffini R 2005a *Astrophys. J. Lett.* **620** L23
[44] Bianco C L and Ruffini R 2005b *Astrophys. J. Lett.* **633** L13
[45] Blandford R and Eichler D 1987 *Phys. Rep.* **154** 1
[46] Blandford R and McKee C 1976 *Phys. Fluids* **19** 1130
[47] Blandford R and McKee C 1976b *Mon. Not. R. Astron. Soc.* **180** 343
[48] Blandford R and Znajek R 1977 *Mon. Not. R. Astron. Soc.* **179** 433

[49] Blain A. and Natarajan P 2000 *Mon. Not. R. Astron. Soc.* **312** L35
[50] Bloom J *et al* 1998 *Astrophys. J.* **507** L25
[51] Bloom J 1999 *Nature* **401** 453
[52] Bloom J *et al* 2002 *Astrophys. J.* **572** L45
[53] Bloom J, Frail D and Kulkarni S 2003 *Astrophys. J.* **594** 674
[54] Bloom J and Prochaska J 2005 *Proc. Gamma Ray Bursts in the Swift Era (Washington, DC)* ed S Holt *et al AIP Conf. Proc.* (*Preprint*) astro-ph/0602058 at press
[55] Bloom J *et al* 2006 *Astrophys. J.* **638** 354
[56] Boër M *et al* 2006 *Astrophys. J.* **638** 671
[57] Boër M *et al* 2006 *Astrophys. J.* **638** L71 (*Preprint*) astro-ph/0510381
[58] Böttcher M and Dermer C 1998 *Astrophys. J.* **499** L131
[59] Borgonovo L and Ryde F 2001 *Astrophys. J.* **548** 770
[60] Burrows D *et al* 2005a *Science* **309** 1833
[61] Burrows D 2005 *Proc. Gamma Ray Bursts in the Swift Era (Washington, DC)* ed S Holt *et al AIP Conf. Proc.* (*Preprint*) astro-ph/0511039 at press
[62] Burrows D *et al* 2006 *Astrophys. J.* (*Preprint*) astro-ph/0604320 submitted
[63] Bykov A M and Mészáros P 1996 *Astrophys. J.* **461** L37
[64] Campana S *et al* 2006 *Nature* (*Preprint*) astro-ph/0603279 at press
[65] Castro-Tirado A J *et al* 1999 *Science* **283** 2069
[66] Castro-Tirado A J *et al* 2001 *Astron. Astrophys.* **370** 398
[67] Cavallo G and Rees M J 1978 *Mon. Not. R. Astron. Soc.* **183** 359
[68] Cheng K S and Dai Z G 1986 *Phys. Rev. Lett.* **77** 1210
[69] Chevalier R and Li L-Zk 2000 *Astrophys. J.* **536** 195
[70] Ciardi B and Loeb A 2000 *Astrophys. J.* **540** 687
[71] Cobb B *et al* 2006 *Astrophys. J. Lett.* (*Preprint*) astro-ph/0603832 submitted
[72] Cobb *et al* 2004 *Astrophys. J.* **608** L93
[73] Coburn W and Boggs S 2003b *Preprint* astrop-ph/0310515
[74] Coburn W and Boggs S 2003 *Nature* **423** 415
[75] Coppi P and Aharonian F 1997 *Astrophys. J.* **487** L9
[76] Costa E *et al* 1997 *Nature* **387** 783
[77] Cronin J 2005 *Nucl. Phys. Proc. Suppl.* **138** 465–91 (*Preprint*) astro-ph/0402487
[78] Cutler C T *et al* 1993 *Phys. Rev. Lett.* **70** 2984
[79] Dado S, Dar A and de Rújula A 2002 *Astron. Astrophys.* **388** 1079
[80] Dado S, Dar A and de Rújula A 2005 *GCN* p 3424
[81] Dado S *et al Preprint* astro-ph/0512196
[82] Dai Z G and Lu T 2001 *Astrophys. J.* **551** 249
[83] Dai Z and Lu T 1999 *Astrophys. J.* **519** L155
[84] Dai Z and Lu T 2000 *Astrophys. J.* **537** 803
[85] Dai Z G 2004 *Astrophys. J.* **606** 1000
[86] Dai Z G, Liang E W and Xu D 2004 *Astrophys. J.* **612** L101
[87] Dai X and Zhang B 2005 *Astrophys. J.* **621** 875
[88] Dai Z G, Wang X Y, Wu X F and Zhang B 2006 *Science* **311** 1127
[89] Daigne F and Mochkovitch R 1998 *Mon. Not. R. Astron. Soc.* **296** 275
[90] Dar A and de Rújula A 2001 CERN-TH-2001-121 (*Preprint*) astro-ph/0105094
[91] Dar A and De Rújula A 2004 *Phys. Rep.* **405** 203
[92] Davies M B, King A, Rosswong S and Wynn G 2002 *Astrophys. J.* **579** L63
[93] Davies M, Levan A and King A 2005 *Mon. Not. R. Astron. Soc.* **365** 54
[94] de Jager O C and Stecker F W 2002 *Astrophys. J.* **566** 738
[95] Della Valle M *et al* 2006 *Astrophys. J.* **642** L103
[96] Dermer C and Böttcher M 2000 *Astrophys. J.* **534** L155
[97] Derishev E V, Kocharovsky V V and Kocharovsky Vl V 1999 *Astrophys. J.* **521** 640
[98] Dermer C, Böttcher M and Chiang J 2000, *Astrophys. J.* **537** 255
[99] Dermer C, Chiang J and Mitman K 2000 *Astrophys. J.* **537** 785
[100] Derishev E V, Kocharovsky V V and Kocharovsky Vl V 2001 *Astron. Astrophys.* **372** 1071
[101] Derishev E V, Kocharovsky V V and Kocharovsky Vl V 1999 *Astrophys. J.* **521** 640
[102] Dermer C 2005 *Proc. Gamma Ray Bursts in the Swift Era (Washington, DC)* ed S Holt *et al AIP Conf. Proc.* at press
[103] Dermer C and Mitman K 1999 *Astrophys. J.* **513** L5

[104] Djorgovski S G *et al* 1998 *Astrophys. J.* **508** L17
[105] Drago A *et al* 2005 *Preprint* astro-ph/0512652
[106] Drenkhahn G and Spruit H 2002 *Astron. Astrophys.* **391** 1141
[107] Dyks J, Zhang B and Fan Y Z 2005 *Astrophys. J.* (*Preprint*) astro-ph/0511699 submitted
[108] Eichler D and Granot J 2006 *Astrophys. J.* (*Preprint*) astro-ph/0509857 submitted
[109] Eichler D, Livio M, Piran T and Schramm D 1989 *Nature* **340** 126
[110] Eichler D and Levinson A 2000 *Astrophys. J.* **529** 146
[111] Eichler D and Levinson A 2003 *Astrophys. J.* **596** L147
[112] Ellison D and Double G 2002 *Astropart. Phys.* **18** 213
[113] Faber J, Baumgarte T, Shapiro S and Taniguchi K 2006 *Astrophys. J.* **641** L93
[114] Fan Y Z, Dai Z G, Huang Y F and Lu T 2002 *Chin. J. Astron. Astrophys.* **2** 449
[115] Fan Y Z, Zhang B and Proga D 2005 *Preprint* astro-ph/0509019
[116] Fan Y Z, Zhang B and Wei D M 2005 *Astrophys. J.* **628** L25
[117] Fan Y Z, Zhang B, Kobayashi S and Mészáros P 2005 *Astrophys. J.* **628** 867
[118] Fan Y Z and Piran T 2006 *Preprint* astro-ph/0601054
[119] Fan Y Z and Piran T 2006 *Astrophys. J. Lett.* (*Preprint*) astro-ph/0604016 submitted
[120] Fargion D 1999 *Astron. Astrophys. Suppl.* **138** 507–8
[121] Fargion D 2004 *Astron. Soc. Pacific Conf. Series* **312** 423
[122] Fargion D and Grossi M 2005 *Nuovo Cimento* C **28** 809
[123] Fenimore E, Epstein R and Ho C 1993 *Astron. Astrophys. Suppl.* **97** 39
[124] Fenimore E *et al* 1993 *Nature* **366** 40–2
[125] Fenimore E and Ramirez-Ruiz E 2000 *Astrophys. J.* (*Preprint*) astro-ph/0004176
[126] Fenimore E, Madras C and Nayakshin S 1996 *Astrophys. J.* **473** 998
[127] Fenimore E, Ramirez-Ruiz E and Wu B 1999 *Astrophys. J.* **518** L73
[128] Fernandez E *et al* 2006 *Nucl. Phys. Proc. Suppl.* **151** 381–92
[129] Flanagan E and Hughes S 1998 *Phys. Rev.* D **57** 4535 (1998)
[130] Finn L S, Mohanty S D and Romano J D 1999 *Phys. Rev.* D **60** 121101
[131] Finn L S, Sutton P J and Krishnan B 2004 *Astrophys. J.* **607** 384
[132] Fishman G and Meegan C 1995 *Annu. Rev. Astron. Astrophys.* **33** 415
[133] Fox D *et al* 2003a *Nature* **422** 284
[134] Fox D *et al* 2003b *Astrophys. J.* **586** L5
[135] Fox D *et al* 2005 *Nature* **437** 845
[136] Fox D 2005 *Proc. Gamma Ray Bursts in the Swift Era (Washington, DC)* ed S Holt *et al AIP Conf. Proc.* at press
[137] Frail D *et al* 1997 *Nature* **389** 261
[138] Frail D *et al* 1998 *AIP Conf. Proc.* **428** 563
[139] Frail D *et al* 2000, *AIP Conf. Proc.* **526** 298
[140] Frail D *et al* 2001 *Astrophys. J.* **562** L55
[141] Frail D *et al* 2003 *Astron. J.* **125** 2299
[142] Fragile P *et al* 2004 *Astropart. Phys.* **20** 598
[143] Freedman D and Waxman E 2001 *Astrophys. J.* **547** 922
[144] Friedman A S and Bloom J S 2005 *Astrophys. J.* **627** 1
[145] Fruchter A *et al* 1999 *Astrophys. J.* **519** L13
[146] Fryer C, Woosley S and Hartmann D 1999 *Astrophys. J.* **526** 152
[147] Fryer C and Kalogera V 2001 *Astrophys. J.* **554** 548
[148] Fryer C, Woosley S and Heger A 2001 *Astrophys. J.* **550** 327
[149] Fryer C, Holz D and Hughes S 2002 *Astrophys. J.* **565** 430
[150] Fryer C and Mészáros P 2003, *Astrophys. J.* **588** L25
[151] Fryer C, Holz D and Hughes S 2004 *Astrophys. J.* **609** 288
[152] Fryer C L and Woosley S E 1998 *Astrophys. J.* **502** L9
[153] Fryer C, Woosley S and Hartmann D H 1999 *Astrophys. J.* **526** 152
[154] Fryer C L, Woosley S E, Herant M and Davies M B 1999 *Astrophys. J.* **520** 650
[155] Fuller G, Pruet J and Kevork A 2000 *Phys. Rev. Lett.* **85** 2673
[156] Galama T *et al* 1998 *Nature* **395** 670
[157] Galama T *et al* 2000 *Astrophys. J.* **536** 185
[158] Gal-Yam A *et al* 2006 *Astrophys. J.* (*Preprint*) astro-ph/0509891 submitted
[159] Garnavich P, Loeb A and Stanek K 2000 *Astrophys. J.* **544** L11
[160] Galama T and Wijers R 2000 *Astrophys. J. Lett.* **549** L209
[161] Gehrels N *et al* 2005 *Nature* **437** 851

[162] Gehrels N 2005 *Proc. Gamma Ray Bursts in the Swift Era (Santa Barbara, CA)* ed S Holt *et al AIP Conf. Proc.* at press
[163] Gehrels N 2006 *Talk at KITP GRB and Supernova 2006 Workshop* UCSB (http://online.kitp.ucsb.edu/online/grb06/gehrels2/oh/212.html)
[164] GEO-600 : http://www.geo600.uni-hannover.de/
[165] Ghirlanda G, Ghisellini G, Lazzati D and Firmani C 2004 *Astrophys. J.* **613** L13
[166] Ghirlanda G, Ghisellini G and Lazzati D 2004 *Astrophys. J.* **616** 331
[167] Ghirlanda G, Ghisellini G, Firmani C, Celotti A and Bosnjak Z 2005 *Mon. Not. R. Astron. Soc.* **360** L45
[168] Ghirlanda G, Ghisellini G, Nava L and Firmani C 2005 *AIP Conf. Proc.* **801** 123
[169] Ghirlanda G *et al* 2006 *Mon. Not. R. Astron. Soc.* (*Preprint*) astro-ph/0511795 submitted
[170] Ghisellini G and Celotti A 1999 *Astrophys. J.* **511** L93
[171] Ghisellini G and Lazzati D 1999 *Mon. Not. R. Astron. Soc.* **309** L13
[172] GLAST: http://glast.gsfc.nasa.gov/
[173] Goodman J 1986 *Astrophys. J.* **308** L47
[174] Goodman J 1997 *New Astron.* **2** 449
[175] Gou L J, Mészáros P, Abel T and Zhang B 2003 *Astrophys. J.* **604** 508
[176] Granot J 2003 *Astrophys. J.* **596** L17
[177] Granot J and Königl A 2001 *Astrophys. J.* **560** 145
[178] Granot J and Königl A 2003 *Astrophys. J.* **594** L83
[179] Granot J, Königl A and Piran T 2006 *Mon. Not. R. Astron. Soc.* (*Preprint*) astro-ph/0601056 submitted
[180] Granot J, Ramirez-Ruiz E and Perna R 2005 *Astrophys. J.* **630** 1003
[181] Granot J and Kumar P *Astrophys. J.* (*Preprint*) astro-ph/0511049 submitted
[182] Granot J, Nakar E and Piran T 2003 *Nature* **426** 138
[183] Granot J, Piran T and Sari R 1999a *Astrophys. J.* **513** 679
[184] Granot J, Piran T and Sari R 1999b *Astrophys. J.* **527** 236
[185] Granot J, Piran T and Sari R 2000 *Astrophys. J.* **534** L163
[186] Granot J and Loeb A 2001 *Astrophys. J.* **551** L63
[187] Granot J and Sari R 2002, *Astrophys. J.* **568** 820
[188] Granot J and Kumar P 2003, *Astrophys. J.* **591** 1086
[189] Grindlay J, Portegies Zwart S and McMillan S 2006 *Preprint* astro-ph/0512654
[190] Grupe D *et al* 2006 *Astrophys. J.* (*Preprint*) astro-ph/0603773 submitted
[191] Guetta D, Spada M and Waxman E 2001 *Astrophys. J.* **557** 399
[192] Guetta D, Spada M, Waxman E 2001 *Astrophys. J.* **557** 399
[193] Guetta D, Granot J and Begelman M 2005 *Astrophys. J.* **622** 482
[194] Guetta D and Piran T 2006 *Preprint* astro-ph/0602208
[195] Haislip J *et al* 2006 *Nature* **440** 181
[196] Halzen F 2006 *EPJC* (*Preprint*) astro-ph/0602132
[197] Halzen F 2006 *Eur. Phys. J.* C (*Preprint*) astro-ph/0602132 at press
[198] Harrison F *et al* 2001 *Astrophys. J.* **559** 123
[199] Harding A and Baring M 1994 *AIP Conf. Proc.* **307** 520
[200] Hededal C, Haugboelle T, Frederiksen J and Nordlund A 2004 *Astrophys. J.* **617** L107
[201] Heinz S and Begelman M 1999 *Astrophys. J.* **527** L35
[202] Heise J, Zand J, Kippen R and Woods P 2001 *Gamma-Ray Bursts in the Afterglow Era* ed E Costa *et al* (Berlin: Springer) p 16
[203] HETE http://space.mit.edu/HETE/
[204] Hjorth J *et al* 2003 *Nature* **423** 847
[205] Hjorth *et al* 2005 *Astrophys. J.* **630** L117
[206] Holder J *et al* 2005 *Proc. ICRC 2005 (Pune, India)* (*Preprint*) astro-ph/0507451
[207] Horváth I 1998 *Astrophys. J.* **508** 757
[208] Horváth I *et al* 2006 *Astron. Astrophys.* **447** 23
[209] Horns D *et al* 2006 *Nucl. Phys. Proc. Suppl.* **151** 373–80
[210] Huang KY *et al* 2005 *Astrophys. J.* **628** L93
[211] Hudec R 2004 *AIP Conf. Proc.* **727** 479
[212] Hulth P O 2006 *NO-VE 2006, Neutrino Oscillations in Venice (Italy)* (*Preprint*) astro-ph/0604374
[213] Hurley K *et al* 1994 *Nature* **372** 652
[214] Hurley K *et al* 2005 *Nature* **434** 1098
[215] IceCube: http://icecube.wisc.edu/
[216] Inoue S, Aharonian F and Sugiyama N 2005 *Astrophys. J.* **628** L9

[217] Ioka K, Kobayashi S and Meszaros P 2004 *Astrophys. J.* **613** L171
[218] Ioka K, Kobayashi S and Zhang B 2005 *Astrophys. J.* **631** 429
[219] Ioka K *et al Preprint* astro-ph/0511749
[220] Jakobsson P 2005 *GCN* **3940** 1
[221] Jakobsson P *et al* 2006 *Proc. Gamma Ray Bursts in the Swift Era (Washington, DC)* ed S Holt *et al AIP Conf. Proc.* at press *Preprint* astro-ph/0602071
[222] Janka H, Mazzali P, Aloy M and Pian E 2006 *Astrophys. J.* at press *Preprint* astro-ph/0509722
[223] Janka H T *et al* 1999 *Astrophys. J.* **527** L39
[224] Janka H T, Thomas E, Ruffert M and Fryer C L 1999 *Astrophys. J.* **527** L39
[225] Kann D, Klose S and Zeh A 2006 *Astrophys. J.* **641** 993
[226] Katz J 1994a *Astrophys. J.* **422** 248
[227] Katz J 1994b *Astrophys. J.* 432 L107
[228] Katz J, Piran T and Sari R 1998 *Phys. Rev. Lett.* **80** 1580
[229] Kawai N *et al* 2006 *Nature* **440** 184
[230] Keshet U and Waxman E 2005 *Phys. Rev. Lett.* **94** 111102
[231] Kifune T 2004 *Rome/Frascati 2004: Physics and astrophysics in space (Frascati physics series; 37)* ed A Morselli *et al* pp 351–8
[232] Kippen M *et al* 2003 *Astron. Soc. Pacific Conf.* **662** 244
[233] Klebesadel R, Strong I and Olson R 1973 *Astrophys. J.* **182** L85
[234] KM3NeT :http://km3net.org/
[235] Kumar P and Panaitescu A 2000 *Astrophys. J.* **541** L51
[236] Kobayashi S, Piran T and Sari R 1997 *Astrophys. J.* **490** 92
[237] Kobayashi S, Piran T and Sari R 1999, *Astrophys. J.* **513** 669
[238] Kobayashi S and Meszaros P 2002 *Astrophys. J.* **589** 861
[239] Kobayashi S and Meszaros P 2003b *Astrophys. J. Lett.* **585** L89
[240] Kobayashi S 2000 *Astrophys. J.* **545** 807
[241] Kobayashi S *et al* 2005 *Astrophys. J. Preprint* (astro-ph/0506157) submitted
[242] Kobayashi S and Sari R 2001 *Astrophys. J.* **551** 934
[243] Kobayashi S and Zhang B 2003a *Astrophys. J.* **582** L75
[244] Kobayashi S and Zhang B 2006 in preparation
[245] Königl A and Granot J 2002 *Astrophys. J.* **574** 134
[246] Kouveliotou C *et al* 1993 *Astrophys. J.* **413** L101
[247] Kouveliotou C 1998 *Review at the APS Spring Meeting (Indianapolis, IN)*
[248] Kochanek C and Piran T 1993 *Astrophys. J.* **417** L17
[249] Kulkarni S *et al* 1998a *Nature* **395** 663
[250] Kulkarni S *et al* 1998b *Nature* **395** 663
[251] Kulkarni S *et al* 1999 *Nature* **398** 389
[252] Kulkarni S *et al* 2000 Gamma ray bursts *Proc. 5th Huntsville Symp.* (New York: AIP) **526** 277
[253] Kulkarni S *et al* 1999 *Nature* **398** 389
[254] Kumar P 1999 *Astrophys. J.* **523** L113
[255] Kumar P 2000 *Astrophys. J.* **538** L125
[256] Kumar P and Piran T 2000 *Astrophys. J.* **532** 286
[257] Kumar P and Panaitescu A 2000, *Astrophys. J.* **541** L9
[258] Kumar P and Granot J 2003 *Astrophys. J.* **591** 1075
[259] Lamb D Q, Donaghy T and Graziani C 2005 *Nuovo Cimento* C **28** 365–72
[260] Lamb D Q *et al* 2005b *Preprint* astro-ph/0507362
[261] Lamb D Q and Reichart D 2000 *Astrophys. J.* 536 1L
[262] La Parola V *et al Astron. Astrophys.* (*Preprint*) astro-ph/0602541 submitted
[263] Lazzati D *et al* 2001 *Astron. Astrophys.* **378** 996
[264] Lazzati D, Rossi E, Ghisellini G and Rees M J 2004 *Mon. Not. R. Astron. Soc.* **347** L1
[265] Lazzati D and Begelman M 2005 *Astrophys. J.* **629** 903
[266] Lazzati D and Begelman M 2006 *Astrophys. J.* at press *Preprint* astro-ph/0511658
[267] Lee W H and Kluźniak W L 1999 *Astrophys. J.* **526** 178
[268] Lee W H, Ramirez-Ruiz E and Page D 2004 *Astrophys. J.* **608** L5
[269] Lee W H, Ramirez-Ruiz E and Granot J 2005 *Astrophys. J.* **630** L165
[270] Le Floc'h *et al* 2003 *Astron. Astrophys.* **400** 499
[271] Le Floc'h *et al Proc. Gamma Ray Bursts in the Swift Era (Washington, DC)* ed S Holt *et al AIP Conf. Proc.* (*Preprint*) astro-ph/0601252 at press

[272] Lemoine M 2002 *Astron. Astrophys.* **390** L31
[273] Lemoine M and Pelletier G 2003 *Astrophys. J. Lett.* **589** L73
[274] Li L-X 2000 *Astrophys. J.* **544** 375
[275] Li L-Zh and Chevalier R 2001 *Astrophys. J.* **551** 940
[276] Liang E W and Zhang B 2005 *Astrophys. J.* **633** 611
[277] Liang E W and Zhang B 2006 *Astrophys. J.* **638** L67 *Preprint* astro-ph/0508510
[278] Liang E W *et al* 2006 *Astrophys. J.* (*Preprint*) astro-ph/0602142 at press
[279] http://www.ligo.caltech.edu/
[280] Lithwick Y and Sari R 2001 *Astrophys. J.* **555** 540
[281] Livio M and Waxman E 2000 *Astrophys. J.* **538** 187
[282] Lloyd N and Petrosian V 2001a *Astrophys. J.* **543** 722
[283] Lloyd-Ronning N and Petrosian V 2002 *Astrophys. J.* **543** 722
[284] Lloyd-Ronning N and Ramirez-Ruiz E 2003 *Astrophys. J.* **576** 101
[285] Loeb A and Barkana R 2001 *Annu. Rev. Astron. Astrophys.* **39** 19
[286] Lee H, Wijers R and Brown G 2000 *Phys. Rep.* **325** 83
[287] Lyutikov M and Blandford R 2004 *Astron. Soc. Pacific Conf.* **312** 449
[288] Lyutikov M, Pariev V I and Blandford R 2003 *Astrophys. J.* **597** 998
[289] Malesani *et al* 2004 *Astrophys. J.* **609** L5
[290] MacFadyen A, Ramirez-Ruiz E and Zhang W Q 2005 *Proc. Gamma Ray Bursts in the Swift Era* ed S Holt *et al* (Washington, DC: AIPC) at press *Preprint* astro-ph/0510192
[291] MacFadyen A, Ramirez-Ruiz E and Zhang W Q 2005 *Proc. Gamma Ray Bursts in the Swift Era (Washington, DC)* ed S Holt *et al AIP Conf. Proc.* (*Preprint*) astro-ph/0510192 at press
[292] MacFadyen A and Woosley S 1999 *Astrophys. J.* **524** 262
[293] Mannheim K, Protheroe R and Rachen J 2001a *Phys. Rev.* D **63** 023003
[294] Mannheim K 2001b *AIP Conf. Proc.* **558** 417
[295] Mao S and Mo H J 1998 *Astron. Astrophys.* **339** L1
[296] Masetti N, Palazzi E, Pian E, Patat F 2006 *GRB Coordinates Network* 4803
[297] Matzner C D 2003 *Mon. Not. R. Astron. Soc.* **345** 575
[298] McEnery J, Moskalenko I and Ormes J 2004 *Cosmic Gamma-Ray Sources* ed K S Cheng and G E Romero (Dordrecht: Kluwer) ASSL **304** 361–95 (*Preprint*) astro-ph/0406250
[299] McMahon E *et al* 2006 *Mon. Not. R. Astron. Soc.* **366** 575
[300] Medvedev A and Loeb A 1999 *Astrophys. J.* **526** 697
[301] Medvedev A 2000 *Astrophys. J.* **540** 704
[302] Medvedev A 2006 *Astrophys. J.* **637** 869
[303] Medvedev A *et al* 2006 *J. Korean Astron. Soc.* **37** 533
[304] Metzger M *et al* 1997 *Nature* **387** 878
[305] Mészáros A *et al* 2000 *Astrophys. J.* **539** 98
[306] Mészáros P 1995 *17th Texas Symp. on Relat. Astrophys. (Munich)* ed H Boehringer *et al* (New York: Acad. Sci.) pp 440–10
[307] Mészáros P 2002 *Annu. Rev. Astron. Astrophys.* **40** 137
[308] Mészáros P, Laguna P and Rees M J 1993 *Astrophys. J.* **414** 181
[309] Mészáros P and Rees M J 1993a *Astrophys. J.* **405** 278
[310] Mészáros P and Rees M J 1993b *Astrophys. J.* **418** L59
[311] Mészáros P and Rees M J 1994 *Mon. Not. R. Astron. Soc.* **269** L41
[312] Mészáros P, Rees M J and Papathanassiou H 1994 *Astrophys. J.* **432** 181
[313] Mészáros P and Rees M J 1997 *Astrophys. J.* **476** 232
[314] Mészáros P and Rees M J 1997b *Astrophys. J.* **482** L29
[315] Mészáros P and Rees M J 1999 *Mon. Not. R. Astron. Soc.* **306** L39
[316] Mészáros P, Rees M J and Wijers R 1998 *Astrophys. J.* **499** 301
[317] Mészáros P, Rees M J and Wijers R 1999 *New Astron.* **4** 313 (*Preprint*) astro-ph/9808106
[318] Mészáros P and Rees M J 2000b *Astrophys. J.* **530** 292
[319] Mészáros P and Rees M J 2001 *Astrophys. J.* **556** L37
[320] Mészáros P and Rees M J 1992 *Astrophys. J.* **397** 570
[321] Mészáros P, Ramirez-Ruiz E and Rees M 2001 *Astrophys. J.* **554** 660
[322] Mészáros P, Ramirez-Ruiz E, Rees M J and Zhang B 2002 *Astrophys. J.* **578** 812
[323] Mészáros P and Waxman E 2001 *Phys. Rev. Lett.* **87** 171102
[324] Milgrom M and Usov V 1995 *Astrophys. J.* **449** L37
[325] Miller M C 2005 *Astrophys. J.* **626** L41

[326] Mirabal N *et al* 2006 *Astrophys. J. Lett.* (*Preprint*) astro-ph/0603686 submitted
[327] Modjaz M *et al* 2006 *Astrophys. J. Lett* (*Preprint*) astro-ph/0603377 submitted
[328] Dimmelmeier H, Font J and Mueller E 2001 *Astrophys. J.* **560** L163
[329] MacFadyen A and Woosley S 1999 *Astrophys. J.* **524** 262
[330] Mukerjee S *et al* 1998 *Astrophys. J.* **508** 314
[331] Nakamura T 2000 *Astrophys. J.* **534** L159
[332] Nakar E, Piran T and Waxman E 2003 *J. Cosmol. Astropart. Phys.* **10** 005
[333] Nakar E and Piran T 2003 *Astrophys. J.* **598** 400
[334] Nakar E, Granot J and Guetta D 2004, *Astrophys. J.* **606** L37
[335] Nakar E and Piran T 2005 *Mon. Not. R. Astron. Soc.* **360** L73
[336] Nakar E and Piran T 2004 *Mon. Not. R. Astron. Soc.* **353** 647
[337] Nakar E and Piran T 2005 *Astrophys. J.* **619** L147
[338] Nakar E, Gal-Yam A and Fox D 2006 *Astrophys. J.* (*Preprint*) astro-ph/0511254 at press
[339] Nakar E, Gal-Yam A, Piran T and Fox D 2006 *Astrophys. J.* **640** 849
[340] Nava L, Ghisellini G, Ghirlanda G, Tavecchio F and Firmani C 2006 *Astron. Astrophys.* (*Preprint*) astro-ph/0511499 at press
[341] Narayan R, Paczyński B and Piran T 1992 *Astrophys. J.* **395** L8
[342] Narayan R, Piran T and Kumar P 2001 *Astrophys. J.* **557** 949
[343] Nardini M, Ghisellini G, Ghirlanda G, Tavecchio F, Firmani C and Lazzati D 2005 *Preprint* astro-ph/0508447
[344] Natarajan P *et al* 2005 *Mon. Not. R. Astron. Soc.* **364** L8
[345] Haugboelle T, Hededal C and Nordlund A 2005 (*Preprint*) astro-ph/0503332
[346] Norris J, Marani G and Bonnell J 2000 *Astrophys. J.* **534** 248
[347] Norris J *et al* 2005 *Astrophys. J.* **627** 324
[348] Nousek J *et al* 2006 *Astrophys. J.* (*Preprint*) astro-ph/0508332 at press
[349] Narayan R, Piran T and Kumar P 2001 *Astrophys. J.* **557** 949
[350] O'Brien P *et al* 2006 *Astrophys. J.* (*Preprint*) astro-ph/0601125 submitted
[351] Odewahn S *et al* 1998, *Astrophys. J.* **509** L5
[352] Ong R 2005 *Proc. ICRC 2005, Pune, India, June 2005, Preprint* astro ph/0605191
[353] Paczyński B 1986 *Astrophys. J.* **308** L43
[354] Paczyński B 1990 *Astrophys. J.* **363** 218
[355] Paczyński B 1991 *Acta Astron.* **41** 257
[356] Paczyński B 1998 *Astrophys. J.* **494** L45
[357] Paczyński B and Rhoads J 1993 *Astrophys. J.* **418** L5
[358] Paczyński B and Haensel P 2005 *Mon. Not. R. Astron. Soc.* **636** L4
[359] Palmer D *et al* 2005 *Nature* **434** 1107
[360] Panaitescu A 2006 *Mon. Not. R. Astron. Soc.* **367** L42
[361] Panaitescu A and Kumar P 2000 *Astrophys. J.* **543** 66
[362] Panaitescu A and Kumar P 2001 *Astrophys. J.* **560** L49
[363] Panaitescu A and Kumar P 2002 *Astrophys. J.* **571** 779
[364] Panaitescu A and Mészáros P 2000 *Astrophys. J.* **544** L17
[365] Panaitescu A and Mészáros P 1998a *Astrophys. J.* **492** 683
[366] Panaitescu A and Mészáros P 1998b *Astrophys. J.* **501** 772
[367] Panaitescu A and Mészáros P 1998c *Astrophys. J.* **493** L31
[368] Panaitescu A and Mészáros P 1999 *Astrophys. J.* **526** 707
[369] Panaitescu A, Mészáros P and Rees M J 1998 *Astrophys. J.* **503** 314
[370] Panaitescu A, Mészáros P, Gehrels N, Burrows D and Nousek J 2006a *Mon. Not. R. Astron. Soc.* **336** 1357
[371] Panaitescu A *et al* 2006b *Mon. Not. R. Astron. Soc.* (*Preprint*) astro-ph/0604105 submitted
[372] Papathanassiou H and Mészáros P *Astrophys. J.* **471** L91
[373] Pedersen H *et al* 1998 *Astrophys. J.* **496** 311
[374] Pe'er A., Mészáros P and Rees M J 2005 *Astrophys. J.* **635** 476
[375] Pe'er A, Mészáros P and Rees M J 2006a *Astrophys. J.* (*Preprint*) astro-ph/0510114 at press
[376] Pe'er A, Mészáros P and Rees M J 2006 *Astrophys. J.* (*Preprint*) astro-ph/0603343 submitted
[377] Pendleton G *et al* 1996 *Astrophys. J.* **464** 606
[378] Peng F, Königl A and Granot J 2005 *Astrophys. J.* **626** 966
[379] Perna R, Armitage P and Zhang B *Astrophys. J.* **636** L29
[380] Phinney E S 1991 *Astrophys. J.* **380** L17
[381] Pian E *et al* 2006 *Nature* (*Preprint*) astro-ph/0603530 submitted
[382] Pilla R and Loeb A 1998 *Astrophys. J.* **494** L167

[383] Piran T and Narayan R 1996, *AIP Conf. Proc.* **384** 233
[384] Piran T 1999 *Phys. Rep.* **314** 575
[385] Piran T 2005 *Rev. Mod. Phys.* **76** 1143
[386] Piro L *et al* 1998 *Astron. Astrophys.* **331** L41
[387] Piro L *et al* 2000 *Science* **290** 955
[388] Poirier *et al* 2003 *Phys. Rev.* D **67** 2001
[389] Popham R *et al* 1999 BH accretion *Astrophys. J.* **518** 356
[390] Preece R, Briggs M, Mallozzi R, Pendleton G, Paciesas W and Band D 2000 *Astrophys. J.* (Suppl.) **126** 19
[391] Price, P *et al* 2003, *Astrophys. J.* **589** 838
[392] Prochaska J *et al* 2006 *Astrophys. J.* (*Preprint*) astro-ph/0510022 at press
[393] Proga D and Begelman M 2003 *Astrophys. J.* **592** 767
[394] Proga D 2005 *Astrophys. J.* **629** 397
[395] Proga D and Zhang B 2006 *Mon. Not. R. Astron. Soc.* (*Preprint*) astro-ph/0601272 at press
[396] Pruet J 2003 *Astrophys. J.* **591** 1104
[397] Pe'er A and Waxman E 2004 *Astrophys. J.* **613** 448
[398] Pe'er A and Waxman E 2004 *Astrophys. J.* **628** 857
[399] Paczyński B and Xu G 1994 *Astrophys. J.* **427** 708
[400] Rachen J and Mészáros P 1998 *Phys. Rev.* D **58** 123005
[401] Ramirez-Ruiz E 2004 *Mon. Not. R. Astron. Soc.* **349** L38
[402] Ramirez-Ruiz E 2005 *Mon. Not. R. Astron. Soc.* **363** L61
[403] Ramirez-Ruiz E, Celotti A and Rees M J 2002 *Mon. Not. R. Astron. Soc.* **337** 1349
[404] Ramirez-Ruiz E and Lloyd-Ronning N M 2002 *New Astron.* **7** 197
[405] Ramirez-Ruiz E, MacFadyen A I and Lazzati D 2002 *Mon. Not. R. Astron. Soc.* **331** 197
[406] Rau A, Greiner J and Schwartz R 2006 *Astron. Astrophys.* **449** 79–88
[407] Razzaque S, Mészáros P and Waxman E 2003 *Phys. Rev.* D **68** 3001
[408] Razzaque S, Mészáros P and Waxman E 2004 *Phys. Rev.* D **69** 3001
[409] Razzaque S, Meszaros P and Zhang B 2004 *Astrophys. J.* **613** 1072
[410] Reichart D, Lamb D Q, Fenimore E E, Ramirez-Ruiz E, Cline T and Hurley K 2000 *Astrophys. J.* **552** 557
[411] Reichart D 1997 *Astrophys. J.* **485** L57
[412] Reichart D 1999 *Astrophys. J.* **521** L111
[413] Rhoads J 1997 *Astrophys. J.* **487** L1
[414] Rhoads J 1999 *Astrophys. J.* **525** 737
[415] Rees M J 1966 *Nature* **211** 468
[416] Rees M J and Mészáros P 1992 *Mon. Not. R. Astron. Soc.* **258** P41
[417] Rees M J and Mészáros P 1994 *Astrophys. J.* **430** L93
[418] Rees M J and Mészáros P 1998 *Astrophys. J.* **496** L1
[419] Rees M J and Meszaros P 2005 *Astrophys. J.* **628** 847
[420] Rampp M, Müller E and Ruffert M 1998 *Astron. Astrophys.* **332** 969
[421] Retter A *et al* 2005 *GCN* p 3788
[422] Rieger F and Duffy P 2005 *Astrophys. J.* **632** L21
[423] Roming P and Mason K 2005 *Proc. Gamma Ray Bursts in the Swift Era (Washington, DC)* ed S Holt *et al AIP Conf. Proc.* (*Preprint*) astro-ph/0605108 at press
[424] Rossi E, Lazzati D and Rees M J 2002 *Mon. Not. R. Astron. Soc.* **332** 945
[425] Rossi E *et al* 2004 *Mon. Not. R. Astron. Soc.* **354** 86
[426] Rossi E, Beloborodov A, Rees M J 2005 *Mon. Not. R. Astron. Soc.* (*Preprint*) astro-ph/0512495 submitted
[427] Rosswog S, Ramirez-Ruiz E and Davies M B 2003 *Mon. Not. R. Astron. Soc.* **345** 1077
[428] Ruderman M 1975 *Ann. N. Y. Acad. Sci.* **262** 164
[429] Ruderman M, Tao L and Kluzniak W 2000 *Astrophys. J.* **542** 243
[430] Ruffert M, Janka H T, Takahashi K and Schaefer G 1997 *Astron. Astrophys.* **319** 122
[431] Ruffert M and Janka H T 1998 *Astron. Astrophys.* **338** 53
[432] Ruffini R, Bianco C, Fraschetti F, Xue S-Sh and Chardonnet P 2001 *Astrophys. J.* **551** L107
[433] Ruffini R *et al* 2003 *AIP Conf. Proc.* **668** 16
[434] Rutledge R and Fox D 2004 *Mon. Not. R. Astron. Soc.* **350** L288
[435] Rybicki G and Lightman A 1979 *Radiative Processes in Astrophysics* (Wiley: New York)
[436] Ryde F 2004 *Astrophys. J.* **614** 827
[437] Ryde F 2005 *Astrophys. J.* **625** L95
[438] Ryde F and Petrosian V 2002 *Astrophys. J.* **578** 290
[439] Rykoff E S *et al Astrophys. J.* **631** L121

[440] Rykoff E S *et al Preprint* astro-ph./0601350
[441] Sahu K *et al* 1997 *Nature* **387** 476
[442] Sahu K *et al* 2000 *Astrophys. J.* **540** 74
[443] Salmonson J and Wilson J 2001b *Astrophys. J.* **544** L11
[444] Sari R 1997 *Astrophys. J.* **489** L37
[445] Sari R 1998 *Astrophys. J.* **494** L49
[446] Sari R 1999 *Astrophys. J.* **524** L43
[447] Sari R and Esin A A 2001 *Astrophys. J.* **548** 787
[448] Sari R and Mészáros P 2000 *Astrophys. J.* **535** L33
[449] Sari R and Piran T 1995 *Astrophys. J.* **455** L143
[450] Sari R and Piran T 1997 *Astrophys. J.* **485** 270
[451] Sari R, Piran T and Narayan R 1998 *Astrophys. J.* **497** L17
[452] Sari R and Piran T 1999 *Astrophys. J.* **517** L109
[453] Sari R, Piran T and Halpern J 1999 *Astrophys. J.* **519** L17
[454] Sato G *et al* 2005 *GCN* p 3793
[455] Savaglio S, Glazebrook K, Le Borgne D 2005 *Proc. on Gamma Ray Bursts in the Swift Era (Washington, DC)* ed S Holt *et al AIP Conf. Proc.* (*Preprint*) astro-ph/0601528 at press
[456] Scully S and Stecker F 2000 *Astropart. Phys.* **16** 271
[457] Shemi A and Piran T 1990 *Astrophys. J.* **365** L55
[458] Soderberg A *et al* 2004 *Astrophys. J.* **606** 994
[459] Soderberg A and Berger E 2005 *GCN* p 4375
[460] Soderberg A *et al* 2006 *Astrophys. J.* **636** 391
[461] Soderberg A *et al* 2006 *Astrophys. J.* (*Preprint*) astro-ph/0601455 submitted
[462] Sokolov I V *et al* 2006 *Astrophys. J. Lett.* **642** L81
[463] Spada M, Panaitescu A and Mészáros P 2000 *Astrophys. J.* **537** 824
[464] Spitkovsky A 2006 *Preprint* astro-ph/0603211
[465] Spruit H C 1999 *Astron. Astrophys.* **341** L1
[466] Sollerman J *et al* 2006 *Astron. Astrophys.* (*Preprint*) astro-ph/0603495 submitted
[467] Stanek K *et al* 2003 *Astrophys. J.* **591** L17
[468] Stanek K 2006, *Astrophys. J.* (*Preprint*) astro-ph/0604113 submitted
[469] Stamatikos M *et al* 2004 *AIP Conf. Proc.* **727** 146
[470] Stamerra A 2005 *AIP Conf. Proc.* **794** 244–7
[471] Stecker F 2000 *Astropart. Phys.* **14** 207
[472] Swift http://swift.gsfc.nasa.gov/
[473] TAMA-300 http://tamago.mtk.nao.ac.jp/
[474] Tan J C, Matzner C D and McKee C F 2001 *Astrophys. J.* **551** 946
[475] Tavani M 1997 *Astrophys. J.* **483** L87
[476] Thompson C 2006 *Astrophys. J.* (*Preprint*) astro-ph/0507387 at press
[477] Thompson C 1994 *Mon. Not. R. Astron. Soc.* **270** 480
[478] Thorne K S 1987 *300 Years of Gravitation* ed S W Hawking and W Israel (Cambridge: Cambridge University Press) p 330
[479] Totani T 1999 *Astrophys. J.* **511** 41
[480] Usov V V 1994 *Mon. Not. R. Astron. Soc.* **267** 1035
[481] Vanderspek R *et al* 2004 *GCN* p 2735
[482] van der Horst A J 2005 *Mem. Soc. Astron. Ital.* **76** 635
[483] van Paradijs J, Kouveliotou C and Wijers R 2000 *Annu. Rev. Astron. Astrophys.* **38** 379
[484] van Paradijs J *et al* 1997 *Nature* **386** 686
[485] van Paradijs J 1999 *Science* **286** 693
[486] van Putten M 2001a *Phys. Rep.* **345** 1
[487] van Putten M 2001b *Astrophys. J.* **562** L51
[488] van Putten M 2002 *Astrophys. J.* **575** L71
[489] van Putten M 2003 *Astrophys. J.* **583** 374
[490] van Putten M and Ostriker A 2001 *Astrophys. J.* **552** L31
[491] van Putten M 2005 *Gravitational Radiation, Luminous Black Holes and Gamma-Ray burst supernovae* (Cambridge: Cambridge University Press)
[492] Vestrand W T *et al* 2005 *Nature* **438** 178
[493] Vietri M, de Marco D and Guetta D 2003 *Astrophys. J.* **592** 378
[494] Vietri M, Perola G, Piro L and Stella L 2000 *Mon. Not. R. Astron. Soc.* **308** L29

[495] Vietri M 1995 *Astrophys. J.* **453** 883
[496] Vietri M 1997a *Astrophys. J.* **478** L9
[497] Vietri M 1998a *Phys. Rev. Lett.* **80** 3690
[498] Vietri M and Stella L 1998 *Astrophys. J.* **507** L45
[499] Villasenor J S *et al* 2005 *Nature* **437** 855
[500] VIRGO: http://wwwcascina.virgo.infn.it/
[501] Wang X Y, Dai Z G and Lu T 2001a *Astrophys. J.* **556** 1010
[502] Wang X Y, Dai Z G and Lu T 2001b *Astrophys. J.* **546** L33
[503] Wang X Y, Li Z and Mészáros P 2006 *Astrophys. J.* **641** L89
[504] Wang X Y, Li Z and Mészáros P 2006 *Astrophys. J.* (*Preprint*) astro-ph/0601229 submitted
[505] Watson D *et al* 2005 *Astrophys. J.* **637** L69
[506] Waxman E 2004 *Astrophys. J.* **606** 988
[507] Waxman E 1995b *Astrophys. J.* **452** L1
[508] Waxman E 1995 *Phys. Rev. Lett.* **75** 386
[509] Waxman E 1997a *Astrophys. J.* **485** L5
[510] Waxman E 1997b *Astrophys. J.* **489** L33
[511] Waxman E 1997c *Astrophys. J.* **491** L19
[512] Waxman E, Frail D and Kulkarni S 1998 *Astrophys. J.* **497** 288
[513] Waxman E 2003 *Nature* **423** 388
[514] Waxman E 1995 *Phys. Rev. Lett.* **75** 386
[515] Waxman E and Bahcall J N 1997 *Phys. Rev. Lett.* **78** 2292
[516] Waxman E and Bahcall J N 2000 *Astrophys. J.* **541** 707
[517] Waxman E and Bahcall J N 1999b *Phys. Rev.* D **59** 023002
[518] Waxman E and Bahcall J N 1999 *Phys. Rev.* D **59** 023002
[519] Waxman E and Mészáros P 2003 *Astrophys. J.* **584** 390
[520] Weekes T 2000 *AIP Conf. Proc.* **558** 15
[521] Wei D M 2003 *Astron. Astrophys.* **402** L9
[522] Wei D M, Yan T and Fan Y Z 2006 *Astrophys. J.* **636** L69
[523] Wheeler J C, Yi I, Höfflich P and Wang L 2000 *Astrophys. J.* **537** 810
[524] Wijers R, Bloom J, Bagla J and Natarajan P 1998 *Mon. Not. R. Astron. Soc.* **294** L13
[525] Wijers R and Galama T 1999 *Astrophys. J.* **523** 177
[526] Wigger C *et al* 2004 *Astrophys. J.* **613** 1088
[527] Wick S, Dermer C and Atoyan A 2004 *Astropart. Phys.* **21** 125
[528] Woosley S 2005 *Proc. on Gamma Ray Bursts in the Swift Era* ed S Holt *et al AIP Conf. Proc.* at press
[529] Woosley S 1993 *Astrophys. J.* **405** 273
[530] Wijers R, Rees M J and Mészáros P 1997 *Mon. Not. R. Astron. Soc.* **288** L51
[531] Wu X F *et al Astrophys. J.* (*Preprint*) astro-ph/0512555 submitted
[532] Woosley S, Zhang W and Heger A 2002 *Proc. Woods Hole GRB Meeting* ed R Vanderspek (*Preprint*) astro-ph/0206004
[533] Yamazaki R, Ioka K and Nakamura T 2004 *Astrophys. J.* **607** L103
[534] Zeh A, Klose S and Kann D 2006 *Astrophys. J.* **637** 889
[535] Zeh A, Klose S and Hartmann D 2004 *Astron. Astrophys.* **422** 113
[536] Zhang B *et al Proc. on Gamma Ray Bursts in the Swift Era (Washington, DC)* ed S Holt *et al AIP Conf. Proc.* at press
[537] Zhang B, Dai X Y, Lloyd-Roning N and Mészáros P 2004 *Astrophys. J.* **601** L119
[538] Zhang B and Mészáros P 2001a *Astrophys. J.* **552** L35
[539] Zhang B, Mészáros P 2001b *Astrophys. J.* **559** 110
[540] Zhang B and Mészáros P 2002 *Astrophys. J.* **571** 876
[541] Zhang B and Mészáros P 2004 *Int. J. Mod. Phys.* A **19** 2385
[542] Zhang B, Kobayashi S and Mészáros P 2003 *Astrophys. J.*, **589** 861
[543] Zhang B and Kobayashi S 2005 *Astrophys. J.* **628** 315
[544] Zhang B, Fan Y Z, Dyks J, Kobayashi S, Mészáros P, Burrows D, Nousek J and Gehrels N 2006 *Astrophys. J.* (*Preprint*) astro-ph/0508321 at press
[545] Zhang W and Fryer C L 2001 *Astrophys. J.* **550** 357
[546] Zhang W, Woosley S E, MacFadyen A 2003 *Astrophys. J.* **586** 356
[547] Zheng Zh and Ramirez-Ruiz E 2006 *Astrophys. J.* (*Preprint*) astro-ph/0601622 submitted
[548] Zou Y Z, Wu X F and Dai Z G 2006 *Preprint* astro-ph/0601292